OFFICE OF CIVILIAN RADIOACTIVE WASTE MANAGEMENT
ANALYSIS/MODEL COVER SHEET

Complete Only Applicable Items

1. QA: QA

2. ☒ Analysis — Check all that apply

Type of Analysis	☐ Engineering ☒ Performance Assessment ☐ Scientific
Intended Use of Analysis	☐ Input to Calculation ☒ Input to another Analysis or Model ☐ Input to Technical Document ☐ Input to other Technical Products

Describe use:

Rod failure fraction that is available for unzipping.

Rod stress distribution used for creep and SCC failure.

3. ☐ Model — Check all that apply

Type of Model	☐ Conceptual Model ☐ Abstraction Model ☐ Mathematical Model ☐ System Model ☐ Process Model
Intended Use of Model	☐ Input to Calculation ☐ Input to another Model or Analysis ☐ Input to Technical Document ☐ Input to other Technical Products

Describe use:

4. Title:

Initial Cladding Condition

5. Document Identifier (including Rev. No. and Change No., if applicable):

ANL-EBS-MD-000048 REV 00

6. Total Attachments:

3

7. Attachment Numbers - No. of Pages in Each:

I-5, II-19, III-4

	Printed Name	Signature	Date
8. Originator	E. Siegmann	Eric R. Siegmann	3/31/00
9. Checker	H. Anderson	A. L. Anderson	3/31/00
10. Lead/Supervisor	R. Rechard	R W for R.P. Rechard	3/31/00
11. Responsible Manager	R. MacKinnon	R W for R.J. MacKinnon	3/31/00

12. Remarks:

This document is associated with AMR F0045

OFFICE OF CIVILIAN RADIOACTIVE WASTE MANAGEMENT
ANALYSIS/MODEL REVISION RECORD
Complete Only Applicable Items

2. Analysis or Model Title:

Initial Cladding Condition

3. Document Identifier (including Rev. No. and Change No., if applicable):

ANL-EBS-MD-000048 REV 00

4. Revision/Change No.	5. Description of Revision/Change
REV 00	Initial Issue

CONTENTS

Page

FIGURES

Page

TABLES

Page

ACRONYMS

AMR	Analysis and Model Report
ANS	American Nuclear Society
ASTM	American Society for Testing and Materials
ATM	Approved Testing Material
B&W	Babcock & Wilcox
BU	Burnup
BWR	Boiling Water Reactor
CCDF	Complementary Cumulative Distribution Function
CE	Combustion Engineering
CFR	Code of Federal Regulations
CPU	Central Processing Unit
CRWMS	Civilian Radioactive Waste Management System
DCCG	Diffusion Controlled Cavity Growth
DHC	Delayed Hydride Cracking
DIRS	Document Input Reference System
DOE	U.S. Department of Energy
DTN	Data Tracking Number
EPRI	Electric Power Research Institute
FGR	Fission Gas Release
IAEA	International Atomic Energy Agency
ID	Inside Diameter
INEEL	Idaho National Engineering and Environmental Laboratory
INPO	Institute of Nuclear Power Operations
IRSR	Issue Resolution Status Report
KTI	Key Technical Issue
ISG	Interim Staff Guidance
LOCA	Loss of Coolant Accident
LWR	Light Water Reactor
M&O	Management and Operating Contractor
MGR	Monitored Geologic Repository
NRC	U.S. Nuclear Regulatory Commission
PCI	Pellet Clad Interaction
PWR	Pressurized Water Reactor
SAR	Safety Analysis Report
SCC	Stress Corrosion Cracking
SR	Site Recommendation
STP	Standard Temperature and Pressure
TBV	To Be Verified
TSPA	Total System Performance Assessment
TSPA&I	Total System Performance Assessment and Integration
TSPA-SR	Total System Performance Assessment-Site Recommendation
U.S.	United States of America
WP	Waste Package
YMP	Yucca Mountain Project

1. PURPOSE

The purpose of this analysis is to describe the condition of commercial Zircaloy clad fuel as it is received at the Yucca Mountain Project (YMP) site. Most commercial nuclear fuel is encased in Zircaloy cladding. This analysis is developed to describe cladding degradation from the expected failure modes. This includes reactor operation impacts including incipient failures, potential degradation after reactor operation during spent fuel storage in pool and dry storage and impacts due to transportation. Degradation modes include cladding creep, and delayed hydride cracking during dry storage and transportation. Mechanical stresses from fuel handling and transportation vibrations are also included. This Analysis and Model Report (AMR) does not address any potential damage to assemblies that might occur at the YMP surface facilities. Ranges and uncertainties have been defined. This analysis will be the initial boundary condition for the analysis of cladding degradation inside the repository. In accordance with AP-2.13Q, *Technical Product Development Planning*, a work plan (CRWMS M&O 1999a) was developed, issued, and utilized in the preparation of this document.

There are constraints, caveats and limitations to this analysis. This cladding degradation analysis is based on commercial Pressurized Water Reactor (PWR) fuel with Zircaloy cladding but is applicable to Boiling Water Reactor (BWR) fuel. Reactor operating experience for both PWRs and BWRs is used to establish fuel reliability from reactor operation. It is limited to fuel exposed to normal operation and anticipated operational occurrences (i.e. events which are anticipated to occur within a reactor lifetime), and not to fuel that has been exposed to severe accidents. Fuel burnup projections have been limited to the current commercial reactor licensing environment with restrictions on fuel enrichment, oxide coating thickness and rod plenum pressures. The information provided in this analysis will be used in evaluating the post-closure performance of the Monitored Geologic Repository (MGR) in relation to waste form degradation.

2. QUALITY ASSURANCE

The Quality Assurance program applies to the development of this analysis documentation. The Performance Assessment Operations responsible manager has evaluated the technical document development activity in accordance with QAP-2-0, *Conduct of Activities*. The QAP-2-0 activity evaluation, *Conduct of Performance Assessment* (CRWMS M&O 1999b), has determined that the preparation and review of this technical document is subject to *Quality Assurance Requirements and Description* DOE/RW-0333P (DOE 2000) requirements. Note that the activity evaluation (CRWMS M&O 1999b) remains in effect even though QAP-2-0 has been superseded by AP-2.16Q, *Activity Evaluation*. Preparation of this analysis did not require the classification of items in accordance with QAP-2-3, *Classification of Permanent Items*. This activity is not a field activity. Therefore, an evaluation in accordance with NLP-2-0, *Determination of Importance Evaluations* was not required.

3. COMPUTER SOFTWARE AND MODEL USAGE

Microsoft Excel for Windows Version 4.0 was used in the analysis to develop a software routine. Excel is commercially available software, and no macros was used. The software routine was run on a Dell Pentium personal computer (CPU number 111920) with a Windows 95 operating system. The software routine is documented in Attachment I and II of this AMR in accordance with AP-SI.1Q Section 5.1.1. The software routine is contained in file "Rod-Initial-C.xls" and the version number is the file date, 1/25/00. This file is contained in Data Tracking Number (DTN: MO0001SPAICC48.037).

There were no models used in support of this analysis activity.

This AMR was documented using only commercially available software (Microsoft Word 97-SR2) for word processing, which is exempt from qualification requirements in accordance with AP-SI.1Q, Software Management. There were no additional applications (Routines or Macros) developed using this commercial software.

SigmaPlot, Scientific Graphic Software, Version 2.0, Jandel Corporation is used to plot data from the analysis. No calculations are performed with this software.

4. INPUTS

4.1 DATA AND PARAMETERS

Most of the data used in this analysis is from the published literature for Pressurized Water Reactor (PWR) fuel performance and the respective reference is cited where the data are used. Table 1 shows the Data Tracking Numbers (DTN) for the input data. These data are appropriate for describing commercial nuclear fuel since they are published descriptions of commercial fuels. The data extend over many years of reactor operations and also are from many different reactor vendors.

Table 1. DTN Table for Input Data

DTN No.	Data	Source	Where Used in AMR
MO9912SPA FSDR1.002	W1717 Dimensions & fill pressure	DOE 1992, P2A-30 ACC: HQO.19920827.0001, p2A-30	Table 2, Section 6.3.1
MO9912SPA FGP72.003	Fission gas production 31 cm^3/MWd (@ STP)	Rothman p.21, Table 6, References ANS 5.4 (Garde references same #) ACC: NNA.19870903.0039	6.3.2
MO9912SPA FGR11.004	Fission Gas Release Fractions	A.M. Garde, 1986 TIC 237128, Figure 4, p. 26	6.3.3; Table 3; Figure 4
MO9912SPA FGR00.005	Fission Gas Release Fractions	Manzel, R. and Coquerelle, M. 1997 TIC: 232556; Figure 1, P. 465	6.3.3; Table 3; Figure 5
MO9912SPA FGR00.006	Fission Gas Release Fractions	Morel, M.; Melin, P.; and Dumont, A. 1994 TIC: 243043, Figures 3 & 4, p. 18	6.3.3; Table 3
MO9912SPA FGF00.007	Fission Gas Release Fractions	Van Swam, L.F.; Bain, G.W., Dey, W.C.; Davis, D.D.; and Hickermann, H. 1997a TIC: 232556, Figure 9, p. 459	6.3.3; Table 3

DTN No.	Data	Source	Where Used in AMR
MO9912SPAFGR00.008	Fission Gas Release Fractions	Bain, G.M.; McInteer, W.A.; Papazoglou, T.P. 1985 TIC: 226810, Figure 4, p. 4-13	6.3.3; Table 3; Figure 4
MO9912SPAFGR06.009	Fission Gas Release Fractions	Guenther, R.J.; Blahnik, D.E.; Campbell, T.K.; Jenquin, U.P.; Mendel, J. 1988b TIC: 223978, p. 2.1	high gas release, 6.3.3; Table 3
MO9912SPAFGR34.010	Fission Gas Release Fractions	Lanning, D.D.; Beyer, C.E.; and Painter, C.L. 1997 TIC: 238923, Table 2.2, p. 2.6	6.3.3; Table 3
MO0001SPAPRA00.035	Frequencies of Events for Secondary Line Breaks Inside containment and Large Break LOCA	Duke Power 1997, pp. 3-6 & 3-7	6.3.3
MO9912SPAHEL06.012	He Production	Manaktala, H.K. 1993 TIC: 208034, Figure 3-4, p. 3-12	6.3.4; Figure 6
MO9912SPAFRV23.013	Free volume	Smith, G.P., Jr.; Pirek, R.C.; Freeburn, H.R.; and Schrire, D. 1994 TIC: 245407, Figure 4.2.4, p. 4-23	6.3.5; Figure 7
MO9912SPAFRT00.014	Surface oxidation vs. Burnup	Van Swam, L.F. Bain, G.W., Dey, W.C.; Davis, D.D.; and Hickermann, H.; 1997a TIC: 232556, Figure 8, p. 459	Basis for Surface Corrosion Analysis, 6.4; Figure 11
MO9912SPASOX00.015	Pilling-Bedworth Factor	Van Swam, L.F.; Strasser, A.A.; Cook, J.D.; and Burger, J.M. 1997b TIC: 232556, p. 426	Pilling-Bedworth factor used for cladding loss, 6.4
MO9912SPAHPM34.016	Hydrogen Absorption Fraction	Lanning, D.D.; Beyer, C.E.; and Painter, C.L. 1997 TIC: 238923, p. 8.4, Figure 8.2, 8.10	6.5
MO9912SPACSD06.017	Critical Crack Depth	Sanders, T.L.; Seager, K.D.; Rashid, Y.R.; Barret, P.R.; Malinauskas, A.P.; Einziger, R.E.; Jordan, H.; Duffey, T.A.; Sutherland, S.H.; and Reardon, P.C. 1992 TIC: 232162, p. I-52, III-60	6.6
MO9912SPAROD00.019	Rod Failure Data	Yang, R.L. 1997 TIC: 232556, Table 1 (PWR) p. 10, Table 1	Data 1989 to 1995 Frequencies & types of failures, # assemblies discharged; 6.6;6.8.2; Table 8; 6.8.3
MO9912SPAFFD37.021	Rod Failure Data	EPRI (Electric Power Research Institute) 1997 (Jones)TIC: 236839, p. 4-1	Average of 2.2 rods failed/failed assembly, 6.6; 6.8.1; 6.8.2; 6.8.5
MO9912SPAASF01.020	Rod Failure Data	DOE (EIA), 1996 TIC: 232923, Table 5, p. 21	Assemblies discharged 1969 – 1988, 6.8.1; 6.8.2

DTN No.	Data	Source	Where Used in AMR
MO9912SPA BWR50.022	BWR Fuel Reliability	Bailey, W.J. and Wu, S. 1990 TIC: 245644, Table 30, data on p. 6.23	6.8.1; 6.8.2
MO9912SPA GE800.023	BWR Fuel Reliability	Potts, G.A. and Proebstle, R.A. 1994 TIC: 243043, Table 2, p. 92	1986 – 1988, 6.8.1
MO9912SPA CFF00.024	BWR Fuel Reliability	Yang, R.L. 1997 TIC: 232556, Table 2, p. 10	6.8.1; 6.8.3
MO9912SPA BWRR1.025	GE BWR fuel Design Data	DOE (U.S. Department of Energy) 1992 ACC: HQO.19920827.0001, p. 2A-15, 2A-21	Number of rods in 7×7 and 8×8 assem. 6.1; 6.8.1
MO9912SPA PWR50.026	PWR Fuel Reliability	Bailey, W.J. and Wu, S. 1990 TIC: 245644, Table 30, data on p.6.23	6.8.1; 6.8.2
MO9912SPA PFR01.027	PWR Fuel Reliability	DOE (EIA), 1996 TIC: 232923 Table 5, p. 21	Assem. Discharged, 6.8.1; 6.8.2
MO9912SPA PFR00.028	PWR Fuel Reliability	Yang, R.L. 1997 TIC: 232556, Table 1, p. 10	Assemblies discharged and failure rates, 6.8.2; Table 8; 6.8.3; 6.6
MO9912SPA FFR76.029	Fuel Failure Rate in Dry Storage	MacKinnon, M.A. and Doherty, A.L. 1997 TIC: 237126, P. 2.1 & 5.16	Observed failure rate = 0.045%, 6.10
MO9912SPA SFC01.032	Creep failure criteria	Chung et al. 1987, Table 1,2 TIC: 238255, p. 780-781	Failure criteria, 6.10.1
MO9912SPA THD00.031	Dry Storage Temperatures	Peehs 1998, Fig. 13a TIC: 245171	Temperature History for Dry Storage Cask, 6.10.1; Figure 24
MO0001SPA FGR06.036	Fission Gas Release for Unpressurized Fuel	Manaklala, H.K., 1993 TIC: 208034, Figure 3-5, p.3-13	6.3.3, Table 3

4.2 CRITERIA

The U.S. Nuclear Regulatory Commission's (NRC's) Total System Performance Assessment and Integration (TSPA&I) Issue Resolution Status Report (IRSR) (NRC 1998) establishes generic technical acceptance criteria considered by the NRC staff to be essential to a defensible, transparent, and comprehensive assessment methodology for the repository system. These regulatory acceptance criteria address five fundamental elements of the DOE TSPA analysis for the Yucca Mountain site, namely:

Data and analysis justification (focusing on sufficiency of data to support the conceptual basis of the process analysis and abstractions)

1. Data uncertainty and verification (focusing on technical basis for bounding assumptions and statistical representations of uncertainties and parameter variabilities)

2. Analysis uncertainty (focusing on alternative conceptual analysis consistent with available site data)

3. Analysis verification (focusing on testing of analysis abstractions using detailed process-level analysis and empirical observations)

4. Integration (focusing on appropriate and consistent coupling of analysis abstractions).

Relevant to the topic of this AMR, elements (1) through (4) of the acceptance criteria are addressed herein. Element (5) of the acceptance criteria, which strictly applies to the completed synthesis of process-level analysis and abstractions, will be addressed separately in the Total System Performance Assessment-Site Recommendation (TSPA-SR).

In addition, a second NRC IRSR Key Technical Issue: Container Life and Source Term (NRC 1999) establishes generic technical acceptance criteria used by the NRC staff for the waste form, with the cladding degradation analysis being part of this Key Technical Issues (KTI). Attachment III describes how this AMR addresses the IRSR issues and criteria.

4.3 CODES AND STANDARDS

American Society for Testing and Materials (ASTM) Standard C1174-97–*Standard Practice for the Long-Term Behavior of Materials, Including Waste Forms, Used in Engineered Barrier Systems (EBS) for Geologic Disposal of High-Level Radioactive Waste* (ASTM 1997) is used to support the degradation analysis development methodology, categorize the analysis developed with respect to their usage for long-term TSPA, and relate the information/data used to develop the analysis to the requirements of the standard.

This AMR was prepared to comply with the above NRC TSPA&I acceptance criteria, as well as the DOE interim guidance (Dyer 1999) which requires the use of specified Subparts/Sections of the proposed NRC high-level waste rule, 10 Code of Federal Register (CFR) Part 63 (64 FR 8640). Subparts of this proposed rule that are particularly applicable to data include Subpart B, Section 15 (Site Characterization) and Subpart E, Section 114 (*Requirements for Performance Assessment*). Subparts applicable to analysis are outlined in Subpart E, Sections 114 (*Requirements for Performance Assessment*) and 115 (*Characteristics of the Reference Biosphere and Critical Group*).

5. ASSUMPTIONS

5.1 ASSUMPTIONS FOR CLADDING TYPES

5.1.1 The commercial nuclear fuel with stainless steel cladding (approximately 1.15% of commercial fuel inventory) is considered as a separate type of clad fuel. Stainless steel cladding represents a design of cladding that was abandoned in the early years of commercial reactor operation. It is assumed to be failed (perforated) at emplacement and available to unzip when the Waste Package (WP) has failed. The basis for this assumption is that fuel with stainless steel cladding represents a very small population of the fuel assemblies but this type of cladding has a faster corrosion rate than Zircaloy. This assumption is conservative since most of the stainless steel cladding would be unfailed and would offer some protection for many years (Section 6.1).

5.1.2 The Westinghouse 17 by 17 Lopar design (called W1717WL) fuel assembly was selected to analyze all fuel cladding. The basis for this assumption is that this design is the most commonly used assembly, constituting 21 percent of the discharged Pressurized Water Reactor (PWR) assemblies (DOE 1996, Table B8, pp. 151-154). The W1717WL is the largest fraction of the more general W1717 type design that constitutes 33 percent of the discharged PWR fuel (DOE 1996, Table B8, pp. 151-154). The W1717 design is the thinnest Zircaloy clad fuel (570 microns cladding thickness) (DOE 1992, pp. 2A-3 to 2A-47) (Section 6.1).

5.1.3 It is assumed that the PWR fuel is more limiting than the BWR fuel in terms of stress and other failure mechanisms analyzed. Rothman (1984, pp. 18-20) summarizes internal rod pressures and concludes that measured BWR pressures are lower after irradiation than PWRs (1.4 to 2.0 MPa for BWRs vs. 3.8 to 5.8 MPa for PWRs). Rothman (1984, p. 20) concludes that the stresses in BWR cladding are about one third of that in PWR cladding (34 MPa for BWRs vs. 95 MPa for PWRs at 325°C). The one-third stresses produce an approximate one third lower creep strain. Chung et al. (1986, pp. 780, 781) performed slow burst tests and mandrel tests on PWR and BWR irradiated cladding. Failures were inspected and most failures were attributed to small cracks on the outer surface. This was not expected since failure would have been expected from cracks that would have originated on the inner surface from Pellet Cladding Interaction (PCI). PCI was very common in the early BWR fuel and the BWR test samples were from Big Rock Point, one of the earliest plants. Chung et al. showed that the maximum strain for the irradiated BWR cladding averaged 0.8%, smaller than the PWR average of 4%. In the PWR creep analysis presented in Section 6.10.1, BWR data are included with the PWR data to reduce the mean failure limit to 3.3%. This reduction in failure criteria partially addresses the weaker BWR cladding. The upper limit for the failure criterion is based on the lowest BWR creep failure limit observed, 0.4%.

5.1.4 Typical BWR cladding is thicker than PWR cladding (813 microns for BWRs (DOE 1992, p. 2A-21) vs. 570 microns for PWRs (DOE 1992, pp. 2A-3 to 2A-47)). Most BWR fuel is also enclosed in solid flow channels while the PWR assemblies are an open lattice

design. This flow channel would divert water away from the fuel after the WP fails and would offer the fuel additional protection from mechanical damage. The BWR fuel operates at an approximate 20% lower burnup (discussed in Section 6.2 and shown in Figure 1). It also has a thinner oxide thickness (30 μm for an average BWR vs. 45 μm for a PWR, from Van Swam et al. (1997a, pp. 457, 459)). Potts (1997, p. 270, Figure 3) shows a range of oxide thickness for BWR fuel. This oxide thickness range can be compared with the PWR oxide thickness discussed in Section 6.4 and shows that the BWR oxide layer is generally thinner. Furthermore, it is also concluded that cases of nodular oxide corrosion, which have occurred in BWR reactor coolant corrosion environments, are also bounded by the PWR maximum oxide thickness analysis. Nodular corrosion in BWR cladding has been observed in only limited areas of BWR fuel rods and has been mitigated in more contemporary fuel by additional controls in the cladding heat treatment and the use of hydrogen additions to the BWR water chemistry (IAEA 1998, p. 90).

5.1.5 Because the PWR fuel cladding operates under higher stress, is thinner, and is not enclosed in a flow channel, PWR fuel was selected for the cladding degradation analysis. It is conservatively assumed that all the cladding behaves as the PWR cladding because the BWR cladding is much thicker and experiences lower stresses. Separate in-reactor failure data is used for the PWR and BWR fuel types.

5.2 ASSUMPTIONS FOR ROD INTERNAL PRESSURE

5.2.1 Fission gas production is assumed to be linearly proportional to the fuel burnup. The basis for this assumption is that Rothman (1984, p.21, Table 6) found the correlation of 31 cm3/MWd (at standard temperature and pressure) for the production of fission gas (Section 6.3.2).

5.2.2 The Complementary Cumulative Distribution Function (CCDF) for the fraction of fission gas released from the fuel structure into the rod free volume can be estimated by fitting a CCDF to observed fission gas releases under various operational and experimental conditions and burnups (Section 6.3.3). The basis of this assumption is the general structure of a CCDF itself. The probabilities are determined from estimated frequencies and the gas release fractions are the observed values.

5.2.3 Helium production by alpha decay can be approximated by a correlation originally reported by Johnson and Gilbert (1983, p. B.5) and reproduced in Manaktala (1993, Figure 3-4, p. 3-12). The basis for this assumption is the corroboration by two other sources, Rothman (1984), and Berggren (1980). The effect of helium production only becomes important in time periods exceeding 1000 years (Section 6.3.4, Table 7). The helium release fraction is evenly distributed between 50% and 100%. This is conservative because little or none of the helium generated when the fuel is cool would be released (Section 6.3.4).

5.2.4 The initial fill pressure is assumed to be 2 to 3.5 MPa at 27ºC for determination of total internal rod pressure. (DOE 1992, p. 2A-30)

5.2.5 After an initial period of in-reactor irradiation during which the fuel pellet contracts due to an initial densification, the fuel pellet will swell linearly with burnup. The basis for this assumption is that the change in free volume as a function of burnup is linear as shown on Figure 7, which is taken from Smith et al. (1994, p. 4-23, Figure 4.2.4) (Section 6.3.5).

5.3 ASSUMPTIONS FOR SURFACE CORROSION

5.3.1 The oxide thickness is assumed to follow a burnup dependency described by Van Swam et al. (1997a, p. 459, P5a power history) and is uniformly sampled inside the range of ±28μm from the peak oxide thickness. The basis for this assumption is that the data is for Zircaloy cladded PWR fuel and the corrosion rates are similar to others, such as Garde (1991). The amount of metal loss from the cladding is approximately 57% of the thickness of the oxide layer. The basis for this assumption is the reduced density of the zirconium oxide (ZrO_2) and the voids in the oxide layer. This is the inverse of the Pilling-Bedworth factor of 1.75 given by Van Swam et al. (1997b, p. 426). Calculations of volume changes in this AMR support this value (Section 6.4).

5.4 ASSUMPTIONS FOR CRACK SIZE DISTRIBUTION

5.4.1 The crack size distribution is needed to calculate a stress distribution and stress intensity factor. The crack size distribution is assumed to be exponentially distributed. (Sanders et al. 1992, p. I-56.) The basis for this is the statement by Sanders et al. that this shape has been experimentally verified (Sanders et al. 1992, p. I-52, I-54). Tasooji et al. (1984, p.602) also uses an exponential distribution. It is also assumed that rod failure is caused by initial cladding cracks in rods that were at least 28 percent through wall. The basis for this assumption is analysis referenced by Sanders et al. (1992, p. I-52). For the analysis, any rod failures observed in reactor operation that are not directly attributable to external causes were deemed to have been caused by cracks. It is also assumed that the rod failure data reported by Yang (1997, p. 10, Table 1) is representative of PWR failure distribution for most fuel. This assumption is valid because PWR fuel reliability has been quite uniform (Section 6.8.2). Details of the crack size distribution analysis are presented in Section 6.6.

5.4.2 The sharp-tipped crack is the limiting case for evaluating the Delayed Hydride Cracking (DHC). The shape and depth of the crack determine the stress intensity at the crack tip. The sharp-tipped crack presents the highest stress at the tip of the crack making this the limiting case (Section 6.6).

5.5 ASSUMPTIONS FOR ROD FAILURE DURING REACTOR OPERATION

5.5.1 Fuel will be loaded into waste packages in the chronological order that it was discharged from the reactors. This assumption places the fuel from periods with poor fuel performance into the same waste package and therefore increases the range for rod failure probabilities inside the waste package. This assumption also produces a spread in the distribution of the failures in the waste packages over time. It is also assumed that there is no thermal blending, i.e. no mixing of assemblies to reach an optimum thermal loading.

Thermal blending would reduce the variation in WP rod failures by putting cooler fuels, which tend to be older and have large failure rates, with hotter fuels, which tend to be newer and have lower failure rates. (Section 6.8 and Section 6.8.5).

5.5.2 BWR fuel assemblies typically had 49 rods per assembly in the period of 1969 through 1976. This assumption is based on the fact that the early design was a 7×7 array with 49 fuel rods in the array. Although the newer 8×8 design was beginning to be introduced late in this period, the number of 8×8 assemblies is insignificant during this period (Sasaki and Kuwabara, 1997, Figure 3, p. 17) (Section 6.8.1).

5.5.3 BWR fuel assemblies had an average of approximately 56 rods per assembly in the period between 1977 and 1980. Half of the assemblies during this period were the new 8×8 design (62 rods per fuel assembly) and half were the older 7×7 design (49 rods per assembly) (Sasaki and Kuwabara 1997, Figure 3, p. 17) (Section 6.8.1).

5.5.4 Fretting wear damage to cladding is assumed in this analysis to contribute to incipient rod failures (McDonald and Kaiser, 1985, Figure 2, p. 2-15). In addition, the damage fraction from all causes is multiplied by a factor of 4 to account for potential failure of the four adjacent rods in a square fuel rod array. This conservatively bounds the expected damage due to fretting wear in reactor operations (Section 6.8.3).

5.6 ASSUMPTIONS FOR ROD FAILURE DURING DRY STORAGE

5.6.1 It is assumed that all rods are stored for 20 years in a dry storage container and are exposed to a temperature profile reported by Peehs (1998, Figure 13a). These temperatures are maximum temperatures for a Castor V dry storage cask, and it is conservative to use them for actual temperatures (Section 6.10.1). These temperatures are comparable to cask temperatures reviewed by Eble (1999) as discussed in Section 6.11. This dry storage period could be at the utility's facilities or at a regional storage facility.

5.6.2 For all mechanical evaluations of the cladding stresses, only the Zircaloy metal is assumed to be load bearing. Therefore, no credit is taken for the Zircaloy lost due to outer diameter fuel rod corrosion. Oxidation on the cladding inner diameter in intact fuel rods has been observed for higher burnups, but it is typically only 10% of the total oxide thickness, and has been ignored for this analysis.

5.6.3 It is assumed that no additional cladding creep occurs during the fuel drying stage of emplacement in the dry storage cask. This assumption is valid because of the short time periods and low temperatures. During 10 hours of drying, the fuel could heat up to a maximum of 217°C (Nuclear Assurance Corporation 1999, p. 4.4-42). The combination of short pump-down times and low fuel temperatures means that little cladding creep will occur during the drying stage compared to the higher temperatures and longer times from other periods.

5.6.4 K_{IH} is the critical stress intensity factor and K_I is the stress intensity factor (Section 6.10.2). If $K_I > K_{IH}$, then the crack tip at an existing crack will start to propagate and, it is

assumed, because of long repository times, crack velocities are not important and failure will occur.

5.6.5 Finally, it has been assumed that the distribution of flaw sizes that exists immediately after irradiation is unaffected by cyclic mechanical loads during fuel storage in spent fuel pools or dry storage. This assumption is justified due to the absence of any significant cyclic mechanical loads on the fuel rods due to vibration or pressurization / depressurization cycles.

5.7 ASSUMPTIONS FOR ROD FAILURE DURING FUEL SHIPMENT

5.7.1 All fuel is assumed to be shipped for three weeks with the cladding temperature of 350ºC for that interval. The basis for this assumption is that reasonable shipments across the country should be completed in three weeks and that the temperature is conservatively set at a maximum of 350ºC for the analysis to evaluate the worst case of time at temperature. As corroborating evidence, this is 28º C above the mean of the design basis maximum cladding temperature reported by shipping vendors in their Safety Analysis Reports (SARs) as reviewed by Eble (1999) (Section 6.11).

6. ANALYSIS

The numbers reported in this section are reported to 3 figures to assist in making the numbers more traceable. This analysis is considered accurate to only the first significant figure, that is, accurate to approximate 80% to 90%. The remaining figures are only reported for traceability.

6.1 CLADDING TYPES

Commercial reactor fuel design has been evolving over the last 30 to 40 years. Eight of the earlier United States (U.S.) reactors used stainless steel cladding (tubing), but no operating U.S. reactor currently uses this type of cladding. A total of 723 metric tons of uranium is contained in stainless steel clad fuel, which is approximately 1.15 percent of the estimated 63,000 metric tons of commercial fuel to be placed in the repository. All of the stainless steel cladding is assumed to be failed at emplacement and it is assumed that this fuel is immediately subject to dissolution and unzipping when water or water vapor enters the failed waste package (WP). This fuel is grouped separately in the TSPA.

Since the mid-1980s, U.S. practice during refueling outages has been to remove the failed fuel rods from assemblies that are to be returned to the core. The failed rods are replaced with dummy rods that contain no fuel. Those assemblies that have undergone this process are said to have been “reconstituted.” The failed rods are put in a canister with similar failed rods. This practice produces an assembly-size canister where approximately 25 to 60 failed rods are stored. Such canisters are to be analyzed with the group of WPs containing stainless steel assemblies where, again, it is assumed that all the rods are failed and available for immediate dissolution and unzipping when the WP fails.

Zirconium first became available in industrial quantities in 1946 when a commercially viable process to refine it was developed. The metal was first used in the chemical industry for corrosion control applications such as boiling hydrochloric acid (HCl). Because of its high cost

(about $10/lb for commercial grade tubing), its use tends to be limited in most industrial applications.

Zirconium-based alloys were introduced as a fuel cladding material (tubing) in the early 1950s because of its consistently high resistance to corrosion in high temperature water, its relatively high mechanical strength and low thermal neutron absorption cross-section. The low thermal neutron capture cross-section is about 30 times less than that of stainless steel, which gives zirconium and its alloys improved neutron efficiency in light water reactors. Nuclear grade zirconium differs from commercial grades in that the hafnium, which naturally occurs with zirconium and has a large neutron cross-section, is removed. Using materials with low neutron absorption cross-sections reduces fuel cost because more neutrons are available for neutron fission and energy production. The behavior of these materials in reactor operation has been extensively researched. Such work is reported in the proceedings of meetings sponsored by the American Society for Testing and Materials, "Zirconium in the Nuclear Industry." The American Nuclear Society topical meetings, "International Topical Meeting on Light Water Reactor Fuel Performance," also publish the results of this work in its proceedings. Other technical publications are also available on this topic. The distinguishing characteristics of zirconium metallurgy come from its high reactivity with oxygen, its affinity for hydrogen, the different types of chemical interactions with the alloying elements, and from its anisotropic physical and mechanical properties which result from its hexagonal crystal structure.

There are two types of light water reactors: Boiling Water Reactors (BWRs) and Pressurized Water Reactors (PWRs). In a BWR, the reactor coolant is permitted to boil in the reactor core and the steam is piped to a steam turbine to make electricity. In a PWR, the reactor coolant is pressurized so that it does not boil and is piped to a steam generator where a second coolant is permitted to boil, generating steam to be piped to the steam turbine. Both types of reactors are fueled by zirconium alloy rods containing pellets of uranium oxide (UO_2) ceramic material.

Two different alloys of zirconium are currently used: Zircaloy-2 and Zircaloy-4. These alloys were developed to reduce the general corrosion rate in steam and water, respectively. Zircaloy-2 tends to be used in BWRs (i.e. steam environment) and Zircaloy-4 in PWRs (i.e. water environment). The primary difference in the two alloys is the nickel content. As the length of reactor fuel cycles is extended, advanced alloys are being developed. New alloys such as M4, M5, and ZIRLO have been developed for reduced corrosion and reduced hydrogen pickup. McCoy (CRWMS M&O 1998a, pp. 6 to 11) summarizes the various fuel element designs that have been used in the United States. The fuel element design integrates the cladding thickness with other features such as cladding material, rod linear power, gas plenum volume, expected burnup, and rod center line temperatures so that fuel rod pressures and stresses are controlled.

For this initial cladding condition analysis, the Westinghouse W1717WL (17 × 17 Lopar) fuel assembly was selected as the design basis fuel assembly. This is the most commonly used fuel assembly, constituting 21 percent of the discharged PWR assemblies to date (DOE 1996, Table B8, pp. 151-154). The W1717WL is the largest fraction of the more general W1717 type design that constitutes 33 percent of the discharged PWR fuel to date. The W1717 design is the thinnest Zircaloy clad fuel at 570 microns cladding thickness (DOE 1992, pp. 2A-3 to 2A-47). Table 2 gives typical characteristics of the Westinghouse W1717WL design (DOE 1992, p. 2A-30 for assembly dimensions used in later calculations).

Table 2. Design Characteristics of Base Case Fuel Assembly

(Westinghouse W1717WL)

Characteristic	Numerical Value	Characteristic	Numerical Value
Cladding OD[a]	0.950 cm	Irradiation time[e]	4.5 yrs[e]
Cladding thickness[a]	0.05715 cm	Reactor Coolant Pressure[c]	14-16 MPa
Cladding ID[a]	0.836 cm	Reactor Coolant Temperature[c]	300–330°C
Rod length[a]	385 cm	Clad ID Temperature[c]	340–370°C
Active core length[a]	366 cm	Burnup (mean)[b]	44 MWd/kgU
Plenum length[a]	16.00 cm	Oxide thickness[b]	50 µm
Plenum volume/Rod[b]	8.77 cc	Fission Gas Rel.[b]	2.5%
Effective gas volume/Rod[b]	23.3 cc	Plenum P.(27°C)[b]	4.4 MPa
Active fuel volume/Rod[b]	201 cc	Stress (27°C)[b]	29 MPa
Initial fill pressure[a]	2.0 - 3.5 MPa	Stress(350°C)[b]	59 MPa
Rods/Assembly[a]	264	Fuel Volume/WP[b, d]	1.112 m^3

[a] DOE (1992, p. 2A-30)
[b] from this analysis, DTN: MO0001SPAICC48.037
[c] Pescatore et al. 1990, p. 7
[d] 21 PWR assemblies per waste package
[e] 18 month cycle, 1/3 core per cycle change-out

6.2 BURNUP

The fuel assembly burnup strongly affects the condition of the cladding. The burnup has a strong effect on the amount of cladding surface oxidation, absorbed hydrogen, fission gas production and release, increased internal rod pressure, and resultant fuel pellet swelling and the corresponding free volume reduction. Figure 1 shows the trend for PWR and BWR burnup over the past several decades (DOE 1996, p.23). It also shows that the PWRs tend to achieve higher burnups. The expected inventory of PWR fuel assemblies was estimated in CRWMS M&O (2000b, Attachment III, file = Bin.dat, Case A84kMTU). This file contains an estimate of all the fuel that YMP is expected to receive including PWR and BWR fuel types. This input has been modified for this analysis. The first modification was the removal of BWR deliveries since the analysis presented here is for PWR fuel. The second modification was to order the deliveries of assemblies by increasing burnup. The resulting file is sheet "WP-BU-A" in the software routine "Rod-Initial-C.xls" presented in DTN: MO0001SPAICC48.037. The number of assemblies in each burnup (BU) grouping is added. As a check, the sum of the assemblies in the groups is compared to the total number of assemblies. Figure 2 shows the expected burnup distribution for PWR fuel assemblies, including expected future higher burnup fuels. The practical limit for batch average discharge burnup is approximately 62 MWd/kgU. This is because shipping of UO_2 is limited to 5% enrichment and most fabrication facilities are licensed for no more than that enrichment. There is also a Nuclear Regulatory Commission (NRC) limit for oxide thickness, and vendor-specific hydrogen content, which limit the residence time in the reactor. The rod

fission gas pressures are also limited to slightly above reactor coolant pressure to prevent cladding from creeping away from the fuel pellets. All of these restrictions mean that the burnup distribution developed in this analysis is not very sensitive to the data presented in CRWMS M&O 2000b. The NRC limit on oxide thickness, and/or the fuel vendor specific hydrogen content limit, will force fuel vendors to introduce more advanced alloys. With the higher burnups, more of the cladding will be advanced alloys such as M4, M5 and ZIRLO. These have about one half the oxidation rate of Zircaloy-2 (Z-2) or Zircaloy-4 (Z-4) and therefore approximately half the hydrides, if the hydrogen pickup fraction remains constant. Mardon et al. (1997, p. 408, Figure 3) gives a comparison of Zircaloy-4 to M4 and M5. Charquet et al. (1994, p. 80) discusses hydrogen pickup and its dependency on oxidation rate. The analysis presented in this report is based on Zircaloy-4, and no effort was made to account for how advanced alloys might improve these results which is an additional conservatism in the analysis.

Figure 3 gives the Complementary Cumulative Distribution Function (CCDF) for the burnup distribution used in this analysis. The mean of this distribution is 44.1 MWd/kgU and the median is 44.7 MWd/kgU. The range is from 5 to 73 MWd/kgU.

In this work, the unit used for burnup is MWd/kgU. Some of the figures that are scanned from other sources are in GWd/MTU and these two units are equivalent. One scanned figure, Figure 14, is in MWd/MTU and the abscissa are expanded in thousands (i.e. 40,000 MWD/MTU is equivalent to 40 MWd/kgU).

6.3 ROD INTERNAL PRESSURE

The internal pressure of the rod influences the possibility of rod failure from cladding creep, hydride reorientation, delayed hydride cracking and stress corrosion cracking as stress and temperature drive each of these failure mechanisms. The internal pressure determines the cladding hoop stress. The internal pressure is determined by the initial fill pressure, fission gas pressure, and, for extended time duration, helium gas pressure from alpha decay. These partial pressures may be summed. The purpose of this section is to establish a mean, median, range, and distribution of internal pressures for later statistical analysis.

6.3.1. Helium Fill Pressure

The objective of this analysis is to establish an initial helium fill pressure in a fuel rod. Early in the history of fuel rod development, helium gas was inserted into the fuel rods to improve the heat transfer across the pellet/cladding gap. DOE (1992) gives the fill pressure for many fuel designs. The W1717WL (17×17 Lopar) uses a range of 2 to 3.5 MPa (DOE 1992, p. 2A-30). The Combustion Engineering (CE) C1616C design uses a fill pressure of 2.1 to 3.2 MPa (DOE 1992, p. 2A-13). Pati and Garde (1985, p. 4-28) state that the CE rods for the Calvert Cliffs reactor used initial fill pressures of 3.2 MPa. Manzel and Coquerelle (1997, p. 463) report using 2.25 MPa fill pressure in the Siemens PWR rods. For the analysis presented here, the W1717WL design will be used, and the fill pressure will be assumed to be uniformly distributed between 2 to 3.5 MPa.

The fill gas follows the Ideal Gas Law (Castellan 1971, p.9, eq. 2-13):

$$P_f(i) = P_f(0) * (FVol(0)/FVol(i)) * (T_k(i)/T_k(0)) \quad \text{(Eq. 6.3-1)}$$

where

$P_f(i)$ = Fill pressure at time i, MPa
$P_f(0)$ = Initial fill pressure, MPa, uniformly distributed $2 < P_f(0) < 3.5$ MPa
$FVol(0)$ = Initial free volume, cm^3
$FVol(i)$ = Free volume at time i, cm^3
$T_k(0)$ = Initial fill temperature, 300 K
$T_k(i)$ = Temperature at time i, K

6.3.2. Fission Gas Pressure

The objective of this analysis is to estimate a probability distribution for fission gas pressure in a fuel rod. The fission gas pressure is determined by a combination of the fission gas production rate in the fuel rod, fission gas release rate from the fuel pellets into the "gap", free volume for the gas to occupy, and temperature. The fission gas production is linearly proportional to the fuel burnup, 31 cm3 (STP) /MWd (Rothman 1984, p. 21, Table 6). Standard temperature and pressure (STP) are 273 K and 0.1 MPa. The equation to calculate the pressure from fission gas is then derived from this input along with the Ideal Gas Law (Castellan 1971, p.9, eq. 2-13) to be:

$$P_{fg}(i) = 31* BU * Mkg * 0.1MPa* T_k(i) * FGR / (Fvol(i)*273\ K) \quad \text{(Eq. 6.3-2)}$$

where

$P_{fg}(i)$ = Fission gas pressure at time i, MPa
BU = Burnup, MWd/kgU
Mkg = Mass of U in one rod, 1.76 kg (W1717WL)
$T_k(i)$ = Temperature at time i, K
FGR = Fission gas release fraction, dimensionless (described below)
Fvol(i) = Free volume at time i, cm^3 (see Section 6.3.5)

The factors of 0.1 MPa and 273 K reflect the standard conditions used in measuring the volume of gas produced. Equation 6.3-2 is used to calculate internal pressure in the fuel rod due to fission gasses in the gap and gas plenum. This is fully developed in Attachment II where this equation is used to calculate the fission gas pressure.

6.3.3. Fission Gas Release Fraction

Most of the fission gas that is produced is held in the fuel matrix and is not available to pressurize the cladding. The fraction of gas that is released from the fuel matrix into the "gap" and free volume depends on the fuel pellet temperature history. The fuel pellet temperature history is dependent on the reactor design, fuel rod design, burnup, and power history. The fuel

rod design is especially dependent on the linear heat generation rate for the fraction of gas that is released. The fraction of the gas that is released that depends on the power history is related to the occurrence of reactor power transients.

Garde (1986, Figure 4, p. 26, which is reproduced in this analysis as Figure 4) shows the percentage of fission gas release (FGR) for various nuclear power plant sources and PWR designs as a function of burnup. The figure shows that the FGR increases with burnup and has scatter. Rows 1 and 2 of Table 3 give the best estimate and high values for FGR as a function of burnup based on this figure. These FGRs represent various PWR sources and are below 5%. In the same report, Garde (1986, Table 4, p. 19) gives the measured FGR for 12 rods with burnups of approximately 50 MWd/kgU, and these tests averaged 0.94% (Row 3 of Table 3). These rods were an earlier Combustion Engineering 14 × 14 design with an initial helium fill gas pressure of 2.8 MPa and linear power of 19 kW/m (Garde 1986, p. b-2, c-1).

Manzel and Coquerelle (1997, pp. 464 and 465, Figure 1) measured FGR for rods with burnups of approximately 80 MWd/kgU (their Figure 1 is reproduced here as Figure 5). These Siemens-designed rods had an initial fill gas pressure of 2.25 MPa. The rods operated at 27 to 31 kW/m in the first cycle (much higher than the rods in Garde's study) and, by the seventh cycle, the rods were operating at 13 to 16 kW/m. The FGR best estimate and high values are summarized in Rows 4 and 5 of Table 3 and are high compared to values reported by others. This could be because of the higher linear power.

Morel et al. (1994, Figure 4, p. 18) reports FGR for fuel of Framatome design that was operated in either regular or load-following (varying power to match demand) generation. Morel et al. show FGR increasing to approximately 3% at burnups of approximately 60 MWd/kgU, results that are similar to that of Garde. Morel's data is summarized on Row 6 and does not give any ranges. Load-following generation is not considered in this analysis as a factor that would tend to increase FGR. Morel et al. (1994, Figure 3, p. 18) also show that fuel rod power spikes rising from a steady state of approximately 15 kW/m to a peak of approximately 25 kW/m increase the FGR, with about seven power spikes. Over time the spikes result in a total release of approximately 8% FGR with "bursts" evident after each transient.

Van Swam et al. (1997a, p. 459) describes the Siemens high burnup fuel program and, in their Figure 9, they give FGRs for fuel approaching 75 MWd/kgU. Their results were extrapolated to 80 MWd/kgU and best estimate and high values are shown on Rows 7 and 8 of Table 3.

Bain et al. (1985, Figure 4, p. 4-13) give FGR including approximate ranges for 32, 40, and 50 MWd/kgU burnups for Babcock and Wilcox (B&W) designed rods. These rods operated at about 15 kW/m. The authors attribute the large FGR ranges to the location of the rod in the assembly and small differences in the rod power histories. Their data were included in Garde's summary (Figure 4 of this analysis) as the Oconee-1 data and are shown in Rows 9 and 10 of Table 3.

Table 3. Observed Fission Gas Releases (Percentages)

Row No.	Fuel Vendor	Reference	Burnup (MWD/kgU)				
			20	40	50	60	80
			Fraction of Fission Gas Released (%)				
1	CE	Garde (1986), Fig. 4 Best Est.	0.5	0.8	1	2	N/A
2	CE	Garde (1986, Fig.4) High Value	1	3.3	3.8	4.5	N/A
3	CE	Garde (1986, Table 4) Average of 12 measurements	N/A	N/A	0.94	N/A	N/A
4	Siemens	Manzel et al. (1997, Fig. 1) Best Est.	6	6.6	7.5	8.6	14
5	Siemens	Manzel et al. (1997) High Value	N/A	8	9	10	N/A
6	Framatome	Morel et al. (1994, Fig. 4) Best Est.	0.3	0.8	1.8	3	N/A
7	Siemens	Van Swam et al. (1997a, Fig. 9) Best Est.	N/A	1	3	4.5	8
8	Siemens	Van Swam et al. (1997a, Fig. 9 High Value	N/A	N/A	3.2	5	9
9	B&W	Bain et al. (1985, Fig. 4), Best Est.	N/A	1.5	1.6	N/A	N/A
10	B&W	Bain et al. (1985, Fig. 4) High Value	N/A	3.4	3.8	N/A	N/A
11	N/A	Median for CCDF	1.69	2.14	2.98	4.53	11.00
12	N/A	Average High Values	N/A	4.90	4.95	6.50	N/A
13	N/A	Average High/Median	N/A	2.29	1.64	1.44	N/A
14	CE	Manaktala (1993, Fig. 3-5) Maine Yankee	12 to 15	N/A	N/A	N/A	N/A
15	Westing-house	Barner (1985, ATM-101, p. 4.9) (10 rods)	0.15 to 0.27	N/A	N/A	N/A	N/A
16	CE	Guenther et al. (1988a ATM-103, p. 4.15)	0.25 (@ 30 MWd/kgU)		N/A	N/A	N/A
17	CE	Guenther et al. (1991 ATM-104, p. 8.9) (3 rods measured)	N/A	0.38, 0.62, 1.10	N/A	N/A	N/A
18	CE	Guenther et al. (1988b, ATM-106, p.2.1) (3 rods measured)	N/A	1.4, 7.4, 11.2	N/A	N/A	N/A
19	GE	Lanning et al. (1997, Transients, Tbl. 2.2)	3.5-38	3.5-44.1	13-14.4	22-34	N/A

DTN: MO0001SPAICC48.037

The data cited above and summarized in Table 3 represent FGR for fuel from six different manufacturers and for various burnups. For the purpose of building a CCDF, the best estimates of the reported FGR have been averaged and used as the median (50%) value (see Row 11 of Table 3). These values are conservative because they are high when compared to the release rates reported by U.S. fuel manufacturers (Garde for Combustion Engineering fuel, Bain for Babcock and Wilcox fuel, and Barner for Westinghouse fuel). The median values have been added to Garde's (1986) Figure 4 (also Figure 4 of this analysis) and are well above most of Garde's data. This is because of the high releases reported by Manzel and Coquerelle (1997). The high values were also averaged and were considered the upper 5% values since these values encompass almost all the data (see Figure 4 for the plot of 5% values). The ratio of upper 5% to the median was approximately 2.3 for the 40 MWd/kgU burnup. The 2.3 multiplication factor times the median is conservatively used to calculate the FGR for the 5% CCDF for all burnup groups. The median value for 20 MWd/kgU was calculated by averaging the slopes of the burnup dependencies for Garde (Row 1, 20 and 40 MWd/kgU values) and Manzel and

Coquerelle (Row 4, 20 and 40 MWd/kgU values) and calculating the value from the 40 MWd/kgU median value. This procedure was necessary because just averaging values at the 20 MWd/kgU group would have produced FGRs higher than the next burnup group.

Evaluating other FGR measurements for off-normal fuel types or fuel exposed to transient tests generated more extreme values of the CCDF. Manaktala (1993, Figure 3-5) shows Maine Yankee fuel at approximately 15 MWd/kgU with FGRs in the 12% to 15% range. Rothman (1984, p. 19) notes that this fuel was manufactured with defects, including no helium backfill and low fuel pellet densities. The pellets contracted away from the cladding, producing high fuel temperatures and high FGR. Rothman notes that such fuel constitutes less than 1% of all spent fuel anticipated from all sources.

A group of fuels has been characterized for YMP testing. These fuels, termed Approved Testing Materials (ATMs), are also included in Table 3. Fuels ATM-101 (Barner 1985, p. 4.9, Table 4.4 – 10 rods measured), ATM-103 (Guenther et al. 1988a, p. 4.15, 2 rods measured) and ATM-104 (Guenther et al. 1991, p. 8.9, Table 8.7 – 3 rods measured) all show releases in the range reported by Garde (1986). ATM 106 (Guenther et al. 1988b, p. 2.1) showed FGRs measured in 3 rods of 1.4%, 7.4%, and 11.2%, respectively, two of which are much higher than measured in other Combustion Engineering designed fuel rods as reported by Garde. No explanation for these high releases was identified in this review. As noted earlier, Morel et al. (1994, Figure 3, p. 18) report FGR for power spikes in fuel of Framatome design. They show that power spikes from 15 kW/m to 25 kW/m increased the FGR with about seven power spikes producing a total release of about 8% FGR with bursts after each transient. From these observations, it was assumed that there was a 1% chance of having either manufacturing defects, or fuel exposed to repetitive transients, or other unspecified causes that produce FGRs that would be six times the median values. The factor of six is the multiplier used to bring the median at 40 MWd/kgU to the release observed in the Maine Yankee fuel (12 – 15%) (approximately 13%) and ATM-106 (11.6%). For the 1-% CCDF for the FGR, the median values of the gas release fractions are multiplied by a factor of 6 for all burnup groups. For lower burnup fuels, this results in FGRs in approximately the 10.1% to 17.9% ranges. At a burnup of 80 MWd/kgU, the releases were limited to 50%, a limit above the highest observed releases in tests discussed in the next paragraph.

The statistical tail of the CCDF represents fuel that was exposed to transients more severe than those considered in Morel et al. (1994, p. 18, Figure 3) but not so severe as to disrupt the core (cause fuel rod failure). Lanning et al. (1997, Table 2.2) show FGR from 3.5% to 44.1% for power transients. The results, summarized in Row 19 of Table 3, show little burnup dependency. The ratio of the median FGR at a burnup of 50 MWd/kgU (2.98%) to the higher release reported by Lanning (44.1%) is 15. Therefore, the median FGRs for each burnup class were increased by a factor of 15 to represent this CCDF class. The CCDF of 0.22% represents the sum of initiating event frequencies given in the McGuire Nuclear Station Probabilistic Risk Assessment (PRA) for large break Loss of Coolant Accident (LOCA, LL event) and steam line breaks (T6 event) (Duke Power 1997, pp. 3-6, 3-7). Fission gas release for probabilities less than 0.22% were set to the value for 0.22%. Table 4 gives the CCDFs for fission gas release percent for various burnups. The FGRs were limited to 50%, which is approximately 6% higher than measured releases in transient tests reported in Table 3. Since the higher releases are of interest in this analysis, the lower half of the CCDF was set by Garde's releases. The first column of Table 4 gives the CCDF in terms of percent. The second column gives the multiplication factor, which is applied

to the median values to produce the other values in the table. When performing calculations for a rod with a specified burnup, the median FGR is calculated by linear interpolation of the median FGRs in Table 4. The distribution is then calculated by selecting a random number between 0 and 100 (CCDF value) and calculating a FGR multiplier by linear interpolation on the column labeled "FGR Multiplier" in Table 4. This multiplier is applied to the median value to obtain the FGR for the rod with the specified burnup.

Table 4. CCDFs for Fission Gas Release vs. Burnup

CCDF	FGR Multiplier	Burnup (MWd/kgU)				
		2-20	40	50	60	80
		Fission Gas Release (%)				
100	0.4	0.68	0.86	1.19	1.81	4.40
50 (median)	1	1.69	2.14	2.98	4.53	11.00
5	2.3	3.89	4.92	6.85	10.41	25.30
1	6	10.14	12.84	17.88	27.15	50.00
0.22	15	25.35	32.10	44.70	50.00	50.00
0	15	25.35	32.10	44.70	50.00	50.00

DTN: MO0001SPAICC48.037

When the FGR analysis is integrated with the burnup distribution described in Section 6.2, the resulting FGR distribution as shown in Table 5 is generated. The distribution is slightly skewed to the higher FGRs with the mean FGR higher than the median.

Fission gas inventory is expected to stay constant with time in the repository. Peehs (1998, pp. 4 and 5) demonstrates that the fission gas release rate is near zero at repository temperatures because the diffusion coefficients become small. Using the equation presented in Lanning et al. (1997, p. A.4) that is applicable for temperatures of 27°C (300 K), the diffusion coefficient is approximately $3x10^{-31}$ m^2/sec at room temperature, suggesting little diffusion during most repository times.

Table 5. Statistical Summary for FGR Distribution

Measure	Value
Mean	4.20
Standard Error	0.100
Median	3.08
Mode	50
Standard Deviation	4.47
Sample Variance	20.0
Kurtosis	30.9
Skewness	4.62
Range	49.3
Minimum	0.696
Maximum	50
Count	2000
5% CCDF value	10.8
95% CCDF value.	1.09
Confidence Level(95.0%)	0.196

DTN: MO0001SPAICC48.037

The quantity of fission gas will not decrease significantly from nuclear decay. Table 6 below gives the composition of krypton (Kr) and xenon (Xe) fission gas release as element volume percentages for Fort Calhoun rods. Table 6 also gives the element volume percentages of the components and their respective half lives (Lide and Frederikse 1997, pp. 11-58 to 11-59 and 11-84 through 11-86). The table shows that only about 5% of the krypton will decay.

Table 6. Composition of Fission Gas and half-lives, Fort Calhoun Fuel Rods

Fission Gas Isotope	Element Volume %[a]	Half Life, Years
Kr83	9.22	Stable
Kr84	35.48	Stable
Kr85	4.61	10
Kr86	50.69	Stable
Total Kr	100.00	N/A
Xe130	0.22	Stable
Xe131	5.69	Stable
Xe132	23.97	Stable
Xe134	27.76	Stable
Xe136	42.36	Stable
Total Xe	100.00	N/A

[a] Rod KJE006 values reported as representative, Garde 1986, p. 21, Table 6.

6.3.4. Helium Production

Both Delayed Hydride Cracking (DHC) and strain failures are driven by the cladding stress which may be caused by the internal gas (including initial fill gas, fission product gases, and helium gas from alpha (α) decay) pressure buildup. The gas pressure will slowly increase over time by the production of helium (He) which is produced in nuclear decay as an alpha particle. Manaktala (1993, Figure 3-4, p. 3-12) presents the helium pressure buildup for 100°C as a function of time for a PWR fuel rod with 36 MWd/kgU burnup and an assumed 100% helium release from the fuel into the fuel rod gap. This figure was originally reported by Johnson and Gilbert 1983, p. B.5 and reproduced in Manaktala's report. The figure has been reproduced as Figure 6 and two straight-line fits were included. The pressure change profile (after adjustment for temperature) is used in this analysis. The pressure change curve (in log-log space) was approximated in this AMR by two linear equations, one for less than or equal to 1,000 years and one for above that time.

$$P_{He}(MPa) = 0.019953 * t^{0.65} \quad \text{for } t \leq 1{,}000 \text{ years}$$
$$P_{He}(MPa) = 0.17783 * t^{0.3333} \quad \text{for } t > 1{,}000 \text{ years} \qquad \text{(Eq. 6.3-3)}$$

where

P_{He} = Increase in pressure due to He production, MPa, at 100°C and release fraction = 1.0 (i.e., 100% He release)
t = Time from reactor discharge of fuel, years

Table 7, below, gives the temperature and pressure history for a typical rod in the repository. For periods of high temperatures, such as during the first 100 years, the helium will contribute approximately 7% of the total pressure. This table represents an upper limit since it assumes 100% helium release. As noted in the previous section, the diffusion coefficients for fission gasses become very small at lower temperatures and 100% helium release is unlikely. For this analysis, the helium release fraction will be assumed evenly distributed between 50% and 100%. This is conservative because little or none of the helium generated when the fuel is cool would be released. The correlation was developed in this AMR for a burnup of 36 MWd/kgU and is adjusted for other burnups assuming a linear correlation.

The final equations are:

$$P_{He}(MPa) = 1.4859\ 10^{-6} * BU * T_k * HGR * t^{0.65} \quad t \le 1{,}000 \text{ years:} \qquad \text{(Eq. 6.3-4)}$$
$$P_{He}(MPa) = 1.3243\ 10^{-5} * BU * T_k * HGR * t^{0.3333} \quad t > 1{,}000 \text{ years:}$$

where

P_{He} = Increase in pressure due to He production, MPa, at 100°C
Bu = Burnup, MWd/kgU
T_k = Temperature, K
HGR = Helium release fraction, uniformly distributed, 0.5<HGR<1.0
t = Time from reactor discharge of fuel, years

Table 7. Effect of Helium Production on Rod Pressure

Time (yr.)	Temperature (°C)	Helium Pressure (MPa)	Fission Gas Pressure (MPa)[a]	Total Pressure (MPa)	He % of total Pres.
1	210	0.03	6.44	6.5	0.40
10	240	0.12	6.84	7.0	1.76
100	150	0.45	5.64	6.1	7.41
1,000	104	1.80	5.03	6.8	26.34
10,000	79	3.62	4.69	8.3	43.51
100,000	27	6.64	4.00	10.6	62.40
1,000,000	27	14.30	4.00	18.3	78.15

a: Initial fill and fission gas pressure assumed to be 4 MPa at 27°C.
DTN: MO0001SPAICC48.037

For corroborating data, Rothman (1984, p. 21, Table 6) also considered helium production in a Calvert Cliffs reactor PWR rod with a burnup of 36 MWd/kgU. This helium source term was evaluated to produce a helium partial pressure of 4.7 MPa at 10,000 years, close to the 3.6 MPa using Manaktala (1993) and calculated above. Berggren (1980, p. 4) predicts approximately 15 MPa of helium pressure in one million years for a BWR rod assuming 100% helium release. This is in good agreement with the estimate in Table 7.

6.3.5. Free Volume

The free volume is the plenum volume plus the volumes in the rod available for the fission gas and helium to occupy. This volume decreases with burnup. Figure 7, taken from Smith et al. (1994, p. 4-23, Figure 4.2.4), shows the change in free volume as a function of burnup. An initial positive change (i.e., free volume increase) is also reported by Lanning et al. (1997, Figure 4.4, p. 4.4) and is attributed to an initial pellet densification. After this initial period of pellet contraction (densification), the pellet swelling is linear with burnup. The free volume decrease was estimated by Smith et al. (1994, Figure 4.2.4 p. 4-23) by the equation (but with uncertainty added):

$$FVol = FVol_0 - [\ Unc * (\ 0.15 * BU - 1.0)\ ] \qquad \text{(Eq. 6.3-5)}$$

where

FVol = Free volume, cm^3
$FVol_0$ = Initial free volume, cm^3
Unc = Uncertainty distribution, uniform from 0.75 to 1.25
BU = Burnup, MWd/kgU

The uncertainty distribution was selected to cover the range observed from various designs shown in Figure 7 at a burnup of approximately 58 MWd/kgU. It was introduced as a multiplication term so that it approaches zero as the volume change approaches zero. A uniform distribution was used.

The free volume for the W1717WL (or Lopar) design was estimated based on the dimensions of the W1717WL (DOE 1992, p. 2A-30) to be 23.3 cm^3. This free volume decreases with burnup based on Equation 6.3-5.

6.3.6. Rod Pressure Distribution

Having generated correlations for fill pressure (Equation 6.3-1), fission gas pressure (Equation 6.3-2), helium pressure (Equation 6.3-4), and free volume (Equation 6.3-5), a probability distribution for the rod pressure buildup can now be generated. Figure 8 shows the fuel rod internal pressure as a function of burnup. This curve is for 27°C and helium buildup for 100 years. Also shown are the minimum and maximum pressures after 2000 statistical samplings. The mean pressures are consistent with or slightly higher than reported measurements. Einziger et al. (1982, p. 66, Section II.C) measured pressures of 2.28 and 2.8 MPa after 2 cycles. Garde (1986, Table 7, p.28) reported pressures for 12 fuel rods in the range of 3.51 to 4.04 MPa with a mean of 3.80 MPa, for rods with a burnup in the range of 50-56 MWd/kgU. Figure 8 shows a mean pressure of 5 MPa at 50 MWd/kgU, slightly higher than Garde's measurement because of the higher fission gas release predicted including the data from Manzel et al. (1997).

A desirable upper limit for plenum pressure at end of life is the pressure that exceeds the reactor system pressure (about 15 MPa at 320°C or 7.5 MPa at 27°C). High burnup designs are starting to approach internal pressures that slightly exceed reactor system pressure but are sufficiently low as to ensure that the cladding does not creep away from the pellets (lift-off) during reactor

operation. Figure 8 shows that the mean rod internal pressure approaches reactor systems pressure at about 65 MWd/kgU at 25ºC (pressure 7.5 MPa). Rothman (1984, pp. 18-20) summarizes end of life rod pressures and concludes that pressures at 25ºC in PWR fuel rods of 3.8 to 5.8 MPa are typical and maximum values of 7.7 to 8.3 MPa are rare. He also notes that measured BWR pressures are lower, 1.4 to 2.0 MPa, and concludes (Rothman 1984, p.20) that the stresses in BWR cladding at the end of reactor life are about one third of that in PWR cladding (34 MPa vs. 95 MPa at 325°C). It is conservatively assumed in this calculation that all the cladding behaves as the PWR cladding because the BWR cladding has much lower stresses.

The rod pressurization analysis is integrated with the expected burnup distribution analysis summarized in Section 6.2 to produce a rod internal pressure CCDF as depicted in Figure 9. Again, this CCDF is for 27°C and helium inventory for 100 years of alpha decay. Data are rounded to three significant figures. The mean pressure is 4.8 MPa and the median is 4.5 MPa. The range is 2.1 MPa to 17.6 MPa. The 5% - 95% range is 7.34 MPa to 3.03 MPa. Approximately 4.5% of the rods have internal pressure approaching the reactor system pressure (7.5 MPa at 27°C, 15 MPa at a reactor temperature of approximately 320ºC).

6.4 SURFACE CORROSION

As the fuel is irradiated in the reactor, the outer surface oxidizes, thus thinning the cladding and producing hydrogen, some of which is absorbed into the cladding. Figure 10, taken from Garde (1991, p. 583) shows the maximum oxide thickness increases as a function of rod average burnup for CE fuel. The oxide thickness is at a maximum near the upper end of the fuel rod where there are both high coolant temperatures and high linear powers. The figure also shows the scatter in the data. Figure 11, taken from Van Swam et al. (1997a, p. 459, Figure 8), shows the peak oxide thickness for burnups up to approximately 75 MWd/kgU and shows ranges for the data. The authors (i.e., Van Swam et al. (1997a)) suggest linear fits intersecting at 37 MWd/kgU with two different equations for two different power histories. An oxide thickness analysis was developed using the power history P5a (denoting the higher linear generation rate) of Figure 11. This data was fitted in this AMR with two linear equations:

$$\begin{aligned} Ox\ (\mu m) &= 0.81081*Bu + Unc., \text{ for } Bu \le 37 \text{ MWd/kgU} \\ Ox\ (\mu m) &= 2.7907*Bu - 73.256 + Unc., \text{ for } Bu > 37 \text{ MWd/kgU} \end{aligned} \qquad \text{(Eq. 6.4-1)}$$

where

Ox = Oxide thickness in µm, ≤ 120 µm
Bu = Burnup, in MWd/kgU
Unc. = Uncertainty Range, = -28 µm to +28 µm, uniformly distributed

Figure 12 shows the corrosion analysis with the ranges of plus or minus 28 microns above or below the P5a analysis. This range captures most of the scatter for each of the three-(3) power histories (P5a, P5b, and P7). The lower oxide thickness observed in the P7 power history at 70 MWd/kgU has been neglected since it represents a minimum oxide thickness. It was assumed that the oxide thickness was uniformly sampled inside that range. The oxide thickness was limited to 120 microns. This is 20 microns above an NRC limit of 100 microns (Essig 1999, Enclosure 1, p. 2) for normal operation and Anticipated Operational Occurrences (AOOs),

transients that might occur at least once in the plant lifetime. When this corrosion analysis is integrated with the burnup distribution given in Section 6.2, the CCDF for peak rod oxide thickness shown in Figure 13 is generated. Some of the statistical results of this analysis rounded to three significant figures are:

Mean oxide thickness:	54.2 µm
Median thickness:	52.0 µm
5% - 95% range:	112 µm to 5.28 µm
% at 120 µm limit:	2.55%

Equation 6.4-1 gives the oxide thickness on the cladding for various burnups. Cladding metal loss is approximately 57 percent of the oxide thickness because of the reduced density and voids in the zirconium oxide (ZrO_2). This percent of the oxide thickness is the inverse of the Pilling-Bedworth factor of 1.75 given by Van Swam et al. (1997b, p. 426). Calculations, found in this AMR (DTN MO0001SPAICC48.037, file rod-initial-C.xls, sheet = "Corrosion," cells = "G11 through L15"), of volume changes support this number.

As noted above, the analysis restricted the cladding oxide thickness to 120 microns, 20 microns above the current NRC limit. Figure 14 (Wilson et al. 1997, p.28, Figure 8) shows the evolution of Westinghouse cladding to ZIRLO to stay below such limits. Framatome has developed M4 and M5 cladding with approximately one half the corrosion rate of the standard Zircaloy-4 (Mardon et al. 1997, p. 407, Figures 1 and 2).

This analysis only addresses general surface corrosion. Microbially induced corrosion, crevice corrosion and pitting have not been observed in reactor operation or pool storage.

6.5 HYDRIDE FORMATION

As the cladding oxidizes, hydrogen is absorbed and forms hydrides in the cladding. The hydride content affects the material properties of the cladding and contributes to the potential for delayed hydride cracking and cladding embrittlement. Charquet et al. (1994, p. 80) show that the amount of hydrides in the fuel cladding depends on the amount of oxidation of the cladding. Cladding oxidation is discussed in Section 6.4. As the cladding oxidizes, the water is the source of the oxygen and hydrogen is released through the chemical reaction: $Zr + 2H_2O \Rightarrow ZrO_2 + 4H$. For each atom of zirconium consumed, four atoms of hydrogen are produced. Some of this hydrogen is absorbed in the cladding. Lanning et al. (1997) recommends a value of 15% for the hydrogen absorption fraction for the NRC's FRAPCON-3 fuel performance code. This value is based on experimental observations shown in Figure 8.2 of Lanning et al. (1997, p. 8.4 and p. 8.10).

Figure 13 gives the percentage of rods that have a peak oxide thickness greater than some value for the rod burnup distribution in Section 6.2. The location of the peak oxide thickness is typically near the top of the core where the coolant temperature and cladding outer surface temperature are at the maximum value. Figure 15 gives the CCDF for the average hydrogen concentration at the point or location of the peak cladding oxide thickness. It is based on the peak oxide thickness and 15% of the hydrogen that is produced from oxidation is absorbed. Values are rounded to three significant figures. The mean value is approximately 358 ppm and the median value is approximately 343 ppm with a 95% to 5% range of 34.9 ppm to 738 ppm.

These values represent averages across the cladding. The hydrogen content is highest at the outer surface and decreases toward the center. Figure 16, reproduced from Schrire and Pearce (1994, p. 107, Figure 4), gives the normalized distribution of hydrogen across the cladding, including a profile for the location of peak oxide thickness. This figure shows that most of the hydrides are in the outer 100 microns of cladding. The hydrogen content is near its minimum on the inside surface, where cracks exist from potential pellet cladding interaction.

This analysis is for today's most commonly used cladding material in PWRs, Zircaloy-4. Zircaloy-2 and Zircaloy-4 are very similar. Today's advanced fuels are being discharged with burnups of 45 - 50 MWd/kgU, with a few test assemblies being discharged as high as 60 MWd/kgU. As higher burnup fuels are developed, designers will be forced to use special alloys such as ZIRLO, M4 or M5. Figure 14 demonstrates that these types of alloys would be expected to reduce the degree of cladding oxidation and, therefore, also reduce the amount of hydrogen in the cladding.

6.6 CRACK SIZE DISTRIBUTION

Delayed Hydride Cracking (DHC) starts with an existing crack. The shape and depth of the crack determine the stress intensity factor at the crack tip. For this analysis, a sharp-tipped crack shape is assumed as the limiting case. Sanders et al. (1992, p. I-56) present a method for developing a crack-size distribution and recommend a maximum initial crack size for fuel that has not failed during reactor operation to be 28 percent of original cladding thickness. This is based on two different analyses (Sanders et al. 1992, p. I-52 and p. III-60). Cladding with larger initial cracks would be expected to fail during reactor operation as the cracks propagate through the cladding. This analysis uses both Sanders' methodology and maximum crack size. It is assumed that the crack size distribution is exponentially shaped (discussed in Section 5):

$$P(w) = B\, e^{-Bw} \qquad \text{(Eq. 6.6-1)}$$

where

$P(w)$ = Probability of having a crack of depth w in a rod
w = Crack depth, μm
B = Constant, 0.0550 μm^{-1}

This equation is integrated for crack depth from w to ∞, giving the probability of having a crack of depth w or larger:

$$F(w) = e^{-Bw} \qquad \text{(Eq. 6.6-2)}$$

where

$F(w)$ = Probability of having a crack of depth w or larger
w = Crack depth, μm
B = Constant, 0.0550 μm^{-1}

The variable B can be evaluated by reviewing fuel performance and calculating the probability of rod failure from cracks. Yang (1997, p. 10, Table 1) reviewed PWR fuel performance and reported 485 fuel assembly failures in 16,153 assemblies over the period 1991 through 1995, the last five (5) years for which data are available (the table has been reproduced as Table 8 and is discussed in Section 6.8.2). Yang reports the causes of the failures and reports that 240 fuel assembly failures were caused by external events (handling, debris, and grid fretting). It is assumed that the remaining failures (245) were all caused by initial cladding cracks in rods that were at least 28 percent through wall (approximately 160 µm for the W1717WL). This is conservative, since some if not most of these failures were not caused by cracks. Considering the mixture of the different types of PWR assemblies, an average assembly has 221 rods. It is also assumed that each failed assembly has 2.2 failed rods (EPRI 1997, p. 4-1). The probability of having a crack equal to or greater than 160 µm is:

$$F(160\ \mu m) = 2.2*245/(221*16153) = 1.51E\text{-}4 = e^{-B*160} \qquad \text{(Eq. 6.6-3)}$$

This equation is used to evaluate B ($B = 0.0550\ \mu m^{-1}$). Figure 17 gives the crack size distribution for PWR rods based on recent fuel failure rates as discussed above. The analytical median (50 percent) crack is about 13.0 µm (2.2% of clad thickness) deep. A maximum crack size for fuel not failing during irradiation is calculated to be 28 percent (160 µm) of cladding thickness (Sanders et al. 1992, p. I-52) and has a probability of 1.51E-4 per rod. The mean crack is approximately 18.6 µm deep.

Figure 17 shows the CCDF for crack size goes to zero crack size at a CCDF of 1.0. This may not be the actual case. Manufacturing defects could produce small defects (1 to 2 microns). Many of these are removed in the pickling (soaking in acid) stage of fuel manufacturing. The presence of these small defects would not affect the probability distribution for the larger cracks because this distribution is determined by observed rod failure rates, including manufacturing surface defects.

Chung et al. (1987, p. 775) reported 20 experiments where irradiated cladding was exposed to hoop stress until failure. In 11 of the tests, the failures were found to have pseudo-cleavage features associated with failures at cracks. These tests corroborate the existence of cracks on the inside of the fuel cladding.

Einzinger et al. (1982, p.72) have reported the formation of oxygen-stabilized alpha zirconium phases in irradiated cladding samples annealed between 482°C and 571°C. The presence of this phase was noted on both the exterior and interior of fuel rod cladding. When significant cladding creep occurred during the annealing, small micro-cracks were observed to form on both the inside and outside surfaces of the cladding in this phase. This behavior is not expected in Light Water Reactor (LWR) fuel rods in repository conditions because the maximum storage temperature of 350°C reduces the diffusion coefficient of oxygen in zirconium by a factor of 100 compared to the 482°C experiment. Furthermore, no micro-cracks were observed on the same cladding after oxidation during reactor exposure up to 340°C. In a storage environment of temperatures decaying from a maximum temperature of 350°C, the formation of an oxygen-rich alpha zirconium phase would not be anticipated, nor would significant creep-out occur to cause cracking.

When performing the statistical sampling, Equation 6.6-2 is rearranged to express the crack depth, given a random number between 1 and zero:

$$w(\mu m) = -\ln(rand()) /B \quad \text{(Eq. 6.6-4)}$$

where

$w(\mu m)$ = Crack depth
rand() = Random number between 0 and 1
B = $0.0550\ \mu m^{-1}$

6.7 CLADDING STRESS

The total cladding internal pressure is developed in Section 6.3.6. The loss of cladding thickness from surface corrosion is developed in Section 6.4. The size distribution of the cracks is developed in Section 6.6. Hence, a distribution for the hoop stress in the cladding can be calculated. The thin wall approximation from Roark (1989, p. 519, equation 1c) for hoop stress is used. The equation used is:

$$St = P * ID /[(2 * (Th-Ox-W)] \quad \text{(Eq. 6.7-1)}$$

where

St = Cladding stress, MPa
P = Total rod gas pressure, MPa
Th = Initial cladding thickness, cm
Ox = Metal loss from oxide layer, cm
W = Crack depth, cm
ID = Cladding inside diameter, cm

The thin wall approximation underestimates the stress at the inside of the cladding by approximately 7 percent. When compared with the thick wall approximation from Roark (1989, p. 638, equation 1b), this results in an error that is small compared with the other uncertainties in this analysis. Stress concentration at a crack tip is discussed in Section 6.10.2.

The rod internal pressure and cladding oxide metal loss are functions of burnup. The initial clad thickness is 0.057 cm for a W1717WL design. When integrating the above equation with the burnup distribution discussed in Section 6.2, the CCDF for stress (room temperature, 100 years of alpha decay) is shown in Figure 18. The statistical parameters for stress for the distribution of 2000 samplings rounded to three significant figures are:

mean = 38.4 MPa

median = 35.8 MPa

minimum =15.6 MPa

95%=23.2 MPa

5% = 61.8 MPa

maximum = 146 MPa

The long tail in the CCDF is caused by the low probability occurrences of high pressures for the high burnup rods as shown in Figures 8 and 9. Rothman (1984, p. 20) reports a "worst-case" stress of 95 MPa at 325°C (47.5 MPa at 27°C). Because of the higher burnup distribution as described in Section 6.2 and the high fission gas release analysis developed in Section 6.3.3, 17.5% of the rods in this analysis exceed Rothman's "worst-case" value.

Pescatore et al. (1990, p.67, Table 9) tabulate both average and maximum hoop stresses for PWR fuels from many other sources. For 320°C, Pescatore's average values vary from 24 to 62 MPa and his maximum values are up to 134 MPa. He also notes that rods with maximum stresses represent less than 1 percent of the total rods.

The stress-distribution in the cladding includes only hoop stresses caused by the differential pressure between the interior and the exterior of the rod. This is an essential requirement for the application of both continuum and fracture mechanics, and the use of uniform mechanical properties of the material under load. There are two locations in the fuel rod cladding in which these requirements apply, in the tubing end-plug weld regions and in a thin region of the cladding near the oxidizing surface.

With respect to the end-plug weld region, rather than applying a 3D finite element stress model, it is assumed that yield criteria or fracture stresses in the cladding will be exceeded before these criteria are exceeded near the end-plug weld.

In the case of cladding near the oxidizing surface, the Zircaloy material in contact with the oxide attempts to maintain an epitaxial relationship with the growing zirconium oxide. This results in a high tensile stress region in the Zircaloy and a corresponding high compressive stress region in the oxide. The consequences of these stresses are implicitly modeled in the "transitioning" of the oxidization kinetics, and are incorporated into the oxidation model. The tensile stress in the Zircaloy material immediately below the oxide is not incorporated into the mechanical model because it represents a thin boundary layer (about 0.1 microns) in which continuity of the material is maintained. Furthermore, "transitioning" in the oxidation kinetics is not accompanied by the initiation of a crack.

6.8 RODS FAILURES DURING REACTOR OPERATION

The objective of this analysis is to calculate a possible rod failure probability distribution for fuel rods that failed during reactor operation (or that would be incipient failures) that might be contained in a WP. The assumption is that the fuel is loaded into the WP in the chronological order that it was discharged from the reactor. This assumption places the fuel from periods with poor fuel performance (many known rod failures) into the same WP and therefore increases the range of rod failure probabilities inside the WP. In the mid 1970s, there were years where core designs had poor fuel performance. For example, in 1973 almost 60% of the BWR assemblies that were discharged had some failed rods in them. These older and cooler assemblies would probably be blended in a WP with newer and hotter assemblies to have a more even thermal load

of the WPs. For the calculation of rod failure distribution, it is assumed that no blending occurs and the assemblies are loaded into WPs in the chronological order of discharge from the reactor.

6.8.1. BWR Rod Failure Distribution

Page 1 of Attachment I gives the historic reliability of BWR fuel. Column A gives the calendar year, and Column B gives the number of discharged assemblies for each year (DOE (EIA) 1996, p.21, Table 5 for 1969 – 1988; and Yang 1997, Table 2, p. 10 for the later years). Column C gives the number of assemblies with failed rods. The data for 1969 through 1985 are from Bailey and Wu (1990, p. 6.23, Table 30). Assembly failure data from 1986 through 1988 were taken from Potts and Proebstle (1994, Table 2, p. 92). Bailey and Wu's (1990) data were not used during this period because the reported failure rates appeared to be too low, suggesting incomplete data. Data for years 1989 through 1995 are taken from Yang (1997, Table 2, p. 10). Column D gives the percent of assemblies that were discharged each year with failed rods. In 1970, all 29 assemblies that were discharged were reported to have failed rods. In the period 1973 through 1976, the damaged assemblies peaked at approximately 57% and then decreased to approximately 18%. These were pellet-clad-interaction (PCI) failures and led to design changes. Assembly failure rates dropped off after this period. Column G gives the total number of rods discharged each year, and Column H gives the number of failed rods, assuming 2.2 rods failed per damaged assembly (EPRI 1997, p. 4-1). Column E gives the percent of the total number of assemblies over all years considered that has failed or were damaged in a particular year, with the worst year being 1974 where approximately 1% of the total number failed. Columns G and H are individually summed and then the average rod failure rate was determined to be approximately 0.17%. This rod failure rate is higher than reported by Electric Power Research Institute (EPRI), (1997, p. 4-1). This indicates that the actual ratio of failed rods per failed assembly may be less than 2.2. This analysis is therefore considered to be conservative.

For the TSPA, it is desired to know what percent of the rods are defective. The above paragraph discusses assemblies with failed rods. EPRI (1997, p. 4-1) reports that, on average, there are 2.2 rods failed per failed assembly. The BWR fuel assemblies were originally 7 by 7-rod designs with 49 rods per assembly. These were replaced in the period of 1977 through 1980 with 8 × 8-rod designs with 62 rods per assembly. (See Sasaki and Kuwabara (1997, Figure 3, p. 17) for an approximate evolution of BWR design.) DOE (1992, p 2A-15 and 2A-21) gives the number of rods per assembly and the most commonly used design was selected. For this analysis, it is assumed that the assemblies have 49 rods through 1976. In the period 1977 through 1980, it was assumed that half the assemblies are new designs and the average is approximately 56 rods per assembly. Starting in 1981, the assemblies contain 62 rods. This evolution is shown in Column F. Column I gives the percent of rods that have failed in each calendar year. The worst year was 1970 when approximately 4.5% of the rods discharged were estimated to have failed. In 1973, approximately 2.6% of the rods discharged were estimated to have failed.

To estimate the range of failed rods in a WP, it was assumed that each year's discharged fuel assemblies were placed, chronologically, into WPs. This means that blending does not occur and the period of high rod failure rates (1970, and 1973 through 1976) produces WPs with higher failure rates than the average. Column J gives the number of WPs that contain rods with failure rates given in Column I. Column K gives the percent of all BWR WPs that contain rods with the failure rates in Column I. Columns I and K are reproduced in page 2 of Attachment I as Columns

A and B but are ordered in ascending order of rod failure rates. A Complementary Cumulative Distribution Function (CCDF) is calculated (Column C) and plotted as Figure 19. Column C shows the percent of WPs that contain more failed rods than given in Column A. This figure shows that the range for rods failed in the BWR WP varies from 0.003% to approximately 4.5% with a median of 0.055% and mean of 0.196%.

6.8.2. PWR Rod Failure Distribution

Page 3 of Attachment I contains the calculation of the historic reliability of PWR fuel. The same procedure was used to analyze the PWR data as was used for the BWR data as described above. Column A gives the calendar year, and Column B gives the number of discharged assemblies for each year (DOE (EIA) 1996, Table 5 for 1970 – 1988; and Yang 1997, Table 1, p. 10 for 1989 - 1995). Column C gives the number of assemblies with failed rods. The data for 1970 through 1985 is from Bailey and Wu (1990, p. 6.23, Table 30). The rod failure rate for the period 1986 through 1988 was calculated as an average of the previous and later three years (1983 – 1985, 1989 – 1991). This rate is 4.1% and is larger than the 0.006% reported by Westinghouse for their fuel in 1987 and 1988 (Preble et al. 1993, p. B.5). Bailey and Wu's (1990) data for this interval were not used because the reported failure rates appeared to be too low, suggesting incomplete data. Data for years 1989 through 1995 is taken from Yang (1997, Table 1, p. 10. A portion of this table has been reproduced as Table 8 in this report. Table 8 gives the various causes of rod failure as a function of calendar year and gives the total number of discharged assemblies. Column D of Attachment I, p. 3 gives the percent of assemblies that were discharged each year with failed rods. The worst year was 1972 when approximately 13% of the assemblies were damaged. Column E gives the percent of the total number of assemblies over all years considered that have failed in a particular year, with the worst year being 1989 with 0.43% of the total number being damaged. This column also shows that the PWR fuel reliability is more consistent than the BWR fuel reliability by approximately a factor of two.

Column F gives the average number of rods per PWR assembly. This number is calculated on Page 4 of Attachment I. Except for La Crosse (a 48-megawatt BWR designed by Allis Chalmers), all of the commercial U.S. BWR reactors were designed by General Electric, and the evolution of the fuel designs was simpler than that of PWRs. Three different reactor vendors designed the U.S. PWRs, and the fuel varied from Combustion Engineering 14 by 14 designs (164 rods) to Westinghouse 17 by 17 designs (264 rods). The average is based on the most common six PWR fuel designs. The number of assemblies discharged is from CRWMS M&O (1998a, Table 4.1.1-1). The number of rods for each design is taken from DOE (1992, pp. 2A-7, 12, 13, 26, 28, and 30). The most common six (6) PWR fuel designs, weighted by the number of assemblies discharged, averaged 221.4 rods per assembly. This number was used in Column F for all years.

Column G gives the total number of rods discharged each year, and Column H gives the number of failed rods assuming that 2.2 rods (EPRI 1997, p. 4-1) fail per failed assembly (Column C). To estimate the range of failed rods in a WP, it was assumed that each year's discharged fuel assemblies were placed, chronologically, into WPs. This means that blending does not occur and the period of high rod failure rates (1972 and 1989) produces WPs with higher rod failure rates than the average. Column I gives the rod failure rate for each year, and Column J gives the number of WPs that are required for the number of assemblies discharged that year. These WPs

will have rod failure rates given in Column I. Column K gives the percent of all PWR WPs that contain rods with the failure rates in Column I. Columns I and K are reproduced in page 2 of Attachment I as Columns D and E, but are ordered in ascending order of rod failure rates. A Complementary Cumulative Distribution Function (CCDF) is calculated (Column F) and plotted as Figure 20. Column F shows the percent of WPs that contain more failed rods than given in Column D. This figure shows that the range for rods failed in the PWR WP varies from 0% to approximately 0.127% with a median of 0.032% and mean of 0.030%. For the PWR WPs, the mean and median are very close suggesting a more normal distribution when compared to the BWR WPs.

Table 8. Causes of Fuel Failures in PWRs

	Number of Assemblies							
Failure Cause	**1989**	**1990**	**1991**	**1992**	**1993**	**1994**	**1995**	**1996 (Partial)**
Handling Damage		6	2			1	1	1
Debris	146	11	67	20	13	6	10	1
Baffle Jetting								
Grid Fretting	14	18	9	33	36	9	33	19
Primary Hydriding		1		4				
Crudding/Corrosion							4	1
Cladding Creep Collapse							1	
Other Fabrication	1	15	1	5	3	1	15	3
Other Hydraulic					1			
Inspected/Unknown					36	36	13	2
Uninspected	43	58	35	61	14	3	12	1
Totals	204	109	114	123	103	56	89	27
Total Discharged	2196	3461	2937	3302	3612	2636	3666	

Yang (1997), DTN: MO9912SPAROD00.019

6.8.3. Incipient Failures

Incipient failures refer to rods that did not fail in the reactor but are sufficiently damaged such that they would be expected to fail prematurely in the WP. One type of incipient failure is cracks in the cladding that were discussed in Section 6.6. Most causes of rod failure are attributed to specific design or operational related problems such as baffle jetting or grid fretting, and tend to occur early in the assembly life. Andrews and Matzie (1985, Table 2, p. 2-42) showed that the rod failure rate decreases with cycle of exposure (see Table 9). This shows that the cladding is not deteriorating significantly and that a large incipient failure rate is not expected. Most fuel today resides in the core for 3 cycles (1/3 core replacement approximately every 18 months). If it is assumed that the incipient failure rate is comparable to a fourth cycle, then the incipient failure rate would be 0.00064% (Table 9), which is negligible compared to other failure rates.

Dry storage conditions are very similar to WP conditions. The Idaho National Engineering and Environmental Laboratory (INEEL) dry storage program results are that the failure rate in dry storage was approximately 0.01% for unconsolidated rods and approximately 0.045% for all rods (MacKinnon and Doherty 1997, p. 2.1, 5.16). This further shows that incipient failures are unlikely.

Another way to estimate an incipient failure rate is to consider fretting by debris. McDonald and Kaiser (1985, Figure 2, p. 2-15) show the location of 82 rods in a core that were damaged during reactor operation after a steam generator replacement. These failures were attributed to debris fretting. This type of fretting tends to occur early in the cycle, before the fuel builds up a hard oxide layer. Inspection of the referenced figure shows that 39 failed rods (approximately 50% of the 82 total failed rods) are adjacent to other failed rods. This could be interpreted as there is an approximately 50% chance that the debris is of sufficient size or in a specific location to damage adjacent rods. Yang (1997, Tables 1 and 2, p. 10) shows that debris fretting was the cause of failure in 33% of the damaged assemblies. This analysis will assume that 50% of the failed rods have adjacent rods with incipient failures, and the total failure distributions are increased by approximately 16.5% (33% × 0.50). As pointed out in the first paragraph of this section, rod failure rates decrease with time and incipient failure rates could be many orders of magnitude smaller.

Table 9. Fuel Reliability Vs Burnup

Cycles of Exposure	1	2	3	4, 5, 6	Totals
Range of Assembly Burnup Gwd/Mtu	0 - 20	12 – 32	20 - 32	32 – 52	N/A
Total Number of Fuel Rods in Burnup Range	799,500	620,100	450,100	109,000	1,978,700
Total Number of Leaking Rods	140	50	25	0	215
Percent of Leaking Rods	0.0175	0.0081	0.0056	0.00064 [b]	0.011

[a] Table reproduced form Andrews and Matzie (1985, Table 2, p. 2-42)
[b] Rod failure rate estimated using Chi Squared approximation with two degrees of freedom.

6.8.4. Combined CCDF

A single CCDF for the number of rods failed in either PWR or BWR WPs may be estimated. The BWR and PWR CCDFs may be combined to give a distribution of rod failures for all WPs. Columns J on pages 1 and 3 of Attachment I shows that approximately 60% of the WPs contain PWR fuel and 40% contain BWR fuel. The single CCDF is generated by summing the two individual CCDFs after weighing by 60% (PWR) and 40% (BWR). The total CCDF was then increased by 16.5% to account for the potential for incipient failures from debris fretting. This calculation is shown on page 2 and 5 of Attachment I and plotted as Figure 21. The tail of the combined CCDF is dominated by the higher failure rates of the early designed BWR fuels. The median of the combined CCDF is 0.0346% and the mean is 0.109%.

6.8.5. Corroborating Data

The objective of this analysis is to estimate the distribution of rods that failed during reactor operation (or that would be incipient failures) that might be contained in a WP. The assumption that produces the spread in the distribution was that the poorly performing fuels of the mid-1970s were placed, chronologically, into a group of WPs. Figure 22 gives the BWR and PWR fuel rod reliability as a function of calendar year based on this analysis. Assembly failure rates were converted to rod failure rates using a conversion of 2.2 failed rods per failed assembly. EPRI (1997, p. 4-1) states that this conversion factor applies for the early years and the number of failed rods per failed assembly has decreased to be closer to one (1) today. The use of the conversion factor of 2.2 failed rods per failed assembly for each year over-predicts the rod failure rate in later years. Manaktala (1993, p.3-3 Figure 3-1) shows the failure rate at BWR plants with older designed fuel rods peaking at about 2% in the 1970s and then falling off as hydriding and PCI problems were reduced with shaped pellets and cladding design changes. The PWR fuel failures peaked in the early 1970s with five (5) plants having Pellet Cladding Interaction (PCI) failure rates of approximately 5%. Sanders et al. (1992, Figure I-11, p. I-37 and reproduced here as Figure 23) show very similar shapes of the reliability curves of both fuel types to those presented in Figure 22 but with lower peaks for the BWRs in the 1970s. Table 10 gives the rod and/or assembly failure rates from 15 sources and makes a total of 18 comparisons to rates from this AMR. In 16 of 18 comparisons, the other authors report lower fuel failure rates. Sanders et al. (1992, p. I-36) reports the high failure rates for the specific periods of time and when these failure rates are added as is reported in Table 10 (not actually averaged by number of discharged rods), their PWR failure rate is higher than reported in this study. This AMR conservatively bounds the expected conditions. In most cases, the analysis presented in this AMR over-predicts the failure rates and therefore is conservative.

Yang et al. (1991, p. 268) report an average of 1.4 failed rods per failed assembly for PWRs and 1.1 failed rods per failed assembly for BWRs for their most recent (1991) review. The use of these lower conversion factors would slightly change the means and medians but would not have a significant effect on the statistical tail of the CCDF because the tail is determined by the early fuels for which the conversion of 2.2 failed rods per failed assembly applies.

Both Figures 22 and 23 show a strong improvement in fuel performance as a function of calendar year. The PWR industry has been plagued with steam generator problems that require steam generator maintenance at most refuelings. This has put great pressure on the owners and/or operators to keep the primary system as clean as possible. The BWR design runs primary coolant steam through the steam turbine, so the BWR owners and/or operators also are under pressure to keep the primary coolant as clean as possible. Most fuel contracts require fuel manufacturers to replace any failed fuel rods from an assembly that is not fully utilized at the next refueling. The Institute of Nuclear Power Operations (INPO) collects and reports data on reactor performance in terms of fuel cycle, with or without failed fuel. Rod failures have led to sophisticated detection techniques (Sunderland et al. 1994, p. 73) to detect failed fuel and identify in which fuel cycle it is located. Sayles et al. (1994, p. 76) describe identifying individual failed rods in operating reactors and using the ratio of ^{134}Cs to ^{137}Cs to identify in which cycle the fuel rod failed. If the assembly is to be reinserted for the next operating cycle, the failed fuel rods are usually removed from the assembly and replaced with dummy rods.

The above analysis addresses the number of rods that have failed during reactor operation. The degree of rod damage in reactor operation (EPRI 1997, p. 4-2 and 4-3) is reported to be:

Pinhole and through wall hairline cracks 80% to 90%
Intermediate condition 10% to 20%
Severe damage 0.04% to 0.9%

This means that, for most of the failed fuel, the very limited failure of the cladding will still limit the degree to which the fission products will escape past the cladding when the fuel is in the reactor as well as during storage and later in the repository.

Table 10. Comparison of Fuel Reliability from Various Sources

Fuel	Period	Reference	Failure Rate[a], %	This AMR %
BWR	Through 1990	DOE (1992, p. 2.5-4, Table 2.5.2)	4.9- (Assembly)	6.5
W-PWR	Through 1990	DOE (1992, p. 2.5-5, Table 2.5.3)	1.6- (Assembly)	3.5. (all PWR)
PWR-all	Through 1990	DOE (1992, p. 2.5-3,Table 2.5.1)	4.2- (Assembly)	3.5
All	1988	Bailey & Wu (1990, p. 4.2)	0.0022	0.049
GE-8 × 8	1983	Bailey et al. (1985, p. 1-3)	0.007	0.034
PWR-French	1979 –1984 1984	Dehon et al. (1985, p. 2-24)	0.001 - 0.01 0.005	0.006 – 0.048 0.018
BWR-Japan PWR-Japan	To 1997	Sasaki & Kuwabara (1997, p. 13, 14)	0.01 0.002	0.17 0.033
GE-BWR, 8 × 8	4/74 – 8/1993	Potts & Proebstle (1994, p. 92, Table 1)	0.016	0.4, all BWRs
PWR-CE	To 11/1984	Andrews and Matzie (1985, Table 2, p. 2-42)	0.011	0.027
All	Through 1984	EPRI (1997, p. 4-1)	0.02–.07	0.14
All	After 1984	EPRI (1997, p. 4-2)	0.006-0.03	0.036
BWR PWR	To 1986	Sanders et al. (1992, p. I-36)	0.15-0.68 0.035-0.44	0.06 – 4.4 0.006 – 0.13
PWR-Westinghouse	1 core, after SG replacement	McDonald and Kaiser (1985, pp. 2-5)	0.26	Within CCDF 0.004 – 5.3
All	1969 – 1976	Manaktala (1993, p. 3-2 and 3-3, Fig 3-1)	0.01-2+	0.004-5.3
PWR-Mark B-B&W	1986–1996	Ravier et al. (1997, p. 34, Fig. 4)	0 - 0.055	0 – 0.127

[a] Failure rates are on a rod basis unless noted as assembly-based.

DTN: MO0001SPAICC48.037

6.8.6. Future Fuels

As noted above, the trend has been for higher fuel reliability. Most current fuel contracts require the vendors to replace any failed fuel, and this is expensive. There is also a trend to increase burnup. Section 6.2 of this report discusses burnup. Today, because burnup is limited to a batch average discharge burnup of about 62 MWd/kgU for licensing considerations, both material shipping and manufacturing are limited to 5% enriched uranium. The average burnup in future cores might be expected to approach the mid-50s MWd/kgU. The NRC limits oxide thickness to 100 microns (Essig 1999, Encl. 1, and p.2), that either limits the burnup with standard Zircaloy cladding or requires advanced alloys. Vendors have introduced advanced alloys such as ZIRLO (Westinghouse, see Figure 14), M4, and M5 (Framatome). It is expected that fuel reliability will be maintained at least at current levels because of the introduction of new materials and economic pressures.

6.9 ROD FAILURE DURING SPENT FUEL POOL STORAGE

After discharge from the reactor, the fuel assemblies typically are stored in spent fuel storage pools. An International Atomic Energy Agency (IAEA) survey (IAEA 1988, p. 104, Table XXVI) reported no evidence of fuel degradation in spent fuel pools and no evidence of further degradation in the spent fuel pool of fuel that had been damaged during reactor operation. The oldest fuel in the survey was Shippingport PWR fuel that has been in wet storage since 1959. Other fuels reported to have had no further degradation during storage have been in wet storage since 1962, 1966, 1968, and the 1970s.

Under the DOE Spent Fuel and Fuel Pool Component Inventory Program, the effect of storing both fuel with intact cladding and fuel with failed cladding has been studied. An international survey of in-water storage (Johnson et al. 1980, p. iii) reports no cases of fuel cladding degradation during pool storage.

Johnson (1977, p. 20) reports: "Operators at several reactors have discharged, stored, and/or shipped relatively large numbers of Zircaloy-clad fuel that developed defects during reactor exposures (e.g., Ginna, Oyster Creek, Nine Mile Point, and Dresden Units I and II). Several hundred Zircaloy-clad assemblies that developed one or more defects in a reactor are stored in the GE-Morris pool without needing special containment. Detailed analysis of the radioactivity in the pool water indicates that the defects are not releasing significant quantities of radioactivity."

The importance of the spent fuel pool storage experience is that fuel failure or degradation is not expected during pool storage, and the fuel failure rates observed from reactor operation are appropriate for the cladding degradation analysis.

6.10 ROD FAILURE DURING DRY STORAGE

Because some utilities are exhausting their spent fuel pool capacity, they are starting to build and operate dry storage facilities where the fuel is dried and placed in metal canisters filled with inert gasses.

The DOE has sponsored a Spent Nuclear Fuel Integrity During Dry Storage-Performance Tests Program at the INEEL since 1984 (MacKinnon and Doherty 1997, pp. 2.1, 5.16) Approximately 26,500 rods have been studied in various commercial dry storage casks. This program also demonstrates what can be expected to happen to fuel in repository WPs during early storage times when temperatures are elevated. The fill gas has been monitored and few rod failures have been observed during dry storage. During fuel consolidation, approximately 10 rods are believed to have developed small leaks. Consolidation removes the spacers from the assembly and permits the fuel rods from two assemblies to be stored in the location of one assembly. Some rods leaked, but the release was over a period of approximately two months, a very slow gas release. From the leaking rods, only 0.5 percent of ^{85}Kr was released. After shipment to the INEEL, the observed rod failure was similar to that after reactor operation. For the rods that were not consolidated, 2 rods leaked out of 16,700 rods producing a failure probability of 1.2E-4 per rod. Overall, including the consolidated rods as dry storage failures, the observed failure rate is 0.045%. This will be added to the creep failures predicted in Section 6.10.1.

Dry storage tests were performed at the Nevada Test Site (Johnson et al. 1987 p. iv) with 17 PWR spent fuel assemblies, each in an individual test. These tests contained 3,468 rods, and cladding temperatures varied from 168°C to 380°C. One of the fuel rods failed during these tests. This assembly was exposed to air at 275°C and had nine thermal cycles during the tests. The estimated hole size was 1 micron. No further degradation was observed in this one failed rod after the initial failure. No visible damage was observed in the other tests.

Accelerated high temperature tests were performed on 15 PWR fuel rods (Einziger et al. 1982, pp. 65, 69). PWR rods were exposed to cladding temperatures of 482°C, 510°C, and 571°C for up to a year in limited air and inert gas atmospheres. No cladding breaches occurred. The cladding had crept away from the pellets and showed a smoother profile. Strains from 1.7 percent to 7 percent were measured. One rod had a local creep as high as 12 percent. The extended lifetime is attributed to significant creep strain of the Zircaloy cladding, which decreases the internal rod pressure. The cladding creep also contributes to radial cracks through the external oxide layer and internal fuel-cladding chemical interaction layers (layer of a few microns thickness where some zirconium/UO_2 interaction occurs), which propagated into and arrested in an oxygen stabilized alpha-Zircaloy layer. Since cracks extended only for a few microns and were arrested, their significance was small. There were no signs of either additional cladding hydriding, stress corrosion cracking (SCC), or fuel pellet degradation.

A second series of creep tests (Einziger and Kohli 1984, p. 107 and p. 114, Table 3) was performed on five PWR spent fuel rods. They were pressurized to a hoop stress of about 145 MPa, for times up to 2101 hours at 323°C. The conditions were chosen for limited annealing of in-reactor irradiation hardening. With the stresses in the range of 145 MPa, creep of 0.004% to 0.16% was observed. No cladding breaches occurred, although significant hydride agglomeration and reorientation took place in one rod that cooled under stress. Einziger and Kohli (1984, p. 107 and p. 114, Table 3) state that these high-temperature tests based on creep rupture as the limiting mechanism indicate that storage at temperatures between 400 and 440°C may be feasible for annealed rods.

Schneider and Mitchell (1992, p. 2.7) summarized experience in the foreign dry storage programs. At that time, seven countries had some fuel in dry storage. They conclude that LWR

fuel can be stored for up to 100 years at temperatures of 320 to 400°C in an inert atmosphere and, if exposed to air, will last comparable times if the temperature is limited to 135 to 160°C. The Canadians have large quantities of irradiated fuel with Zircaloy cladding that has been exposed to air with favorable results. For over eight years, they tested the effects of exposing fuel with defective cladding to moist and dry air with favorable results (no observed strain from UO_2 oxidation or cladding failure propagation).

Peehs (1998, pp.1 to 9) reviewed the performance of higher burnup fuels in dry storage casks. He reviewed the numerous possible fuel failure mechanisms and concluded that none of the mechanisms will lead to fuel failure. His temperature profile is used for the analysis presented in Section 6.10.1.

The importance of the spent fuel dry storage experience (domestic and foreign) is that fuel failure or degradation is expected to be very small during dry storage for the current fuels (burnups up to 50 MWd/kgU). Section 6.10.1 will analyze the potential for creep failures of very high burnup fuels with high stresses. Section 6.10.2 will analyze the potential for Delayed Hydride Cracking (DHC) for fuels with high stresses. It is also important to note that, under repository conditions, most of the cladding creep or DHC failures would be expected to occur in the first 100 years after closure. This is the time period when the fuel temperatures are highest and conditions closer to dry storage conditions. Dry storage is considered to be a good representation of this period.

6.10.1. Creep Failures in Dry Storage and Transportation

As noted above, approximately 0.045% of the rods have been observed to have failed in dry storage tests. With the potential for higher burnups in future fuels producing higher pressures and higher strains, the potential for creep failure in dry storage was evaluated. The distribution of rod stresses was developed in Section 6.7 and summarized in Figure 18. As noted before, there is a tail where 5% of the rods have hoop stresses over 61.8 MPa (at 27°C). These rods will have higher stresses during the time of elevated dry storage temperatures.

Best estimate dry storage temperatures were not available at the time of this analysis, so the temperature history was conservatively chosen to be that of the center rod in a Castor V package with 55 MWd/kgU fuel (Peehs 1998, Figure 13a). These temperatures were given for the first ten years and have been extrapolated to 20 years. In addition, a three-week period of temperatures at 350°C has been added to represent design bases shipping temperatures. This temperature profile is given in Figure 24. It is conservative to use the peak design bases temperatures for all rods since most will actually see lower temperatures. Shipping will be discussed in Section 6.11 however the creep analysis is integrated so that the creep components are added. Creep failures during dry storage are combined with the creep failures during shipping because the damage is cumulative.

The creep correlation developed by Matsuo (1987, pp. 23, 26) was used and is given below:

$$Ec = 3.62E12*(E/T)*\exp(2400*stress/E)*\exp(-2.72E5/(RT)) \quad \text{(Eq. 6.10-1)}$$

$$Es = 1.57E13*(E/T)*[\sinh(1130*stress/E)]^{2.1}*\exp(-2.72E5/RT)$$

$$esp = 2.16E\text{-}2*Ec^{0.109}$$

$$Strain = esp *(1-exp(-52*(Es*t)^{0.5})) + Es * t$$

where

Strain	=	Total Creep Strain, %
Ec, Es, esp	=	Strain Components
Ec	=	Calculated creep rate component, % / hr
Es	=	Steady state creep rate, units = % / hr
esp	=	Saturated primary (transient) creep strain, units = %

Inputs:

stress	=	Stress, MPa
t	=	Time, hrs
T	=	Temperature, K
E	=	114800-59.9*T, Young's modulus, MPa
R	=	8.3169, gas constant, J/mole-K

Details of the analysis are given in Attachment II. Figure 25 gives the expected strain from dry storage alone and also for dry storage and transportation as a function of initial rod stress. Little creep occurs for rods with stresses less than 80 MPa and, above that stress, the creep strain grows exponentially. Most of the creep occurs during the dry storage and only a small additional amount occurs during shipping.

To estimate what percent of the rods will fail from creep, a creep failure criteria must be established. For this, data from Chung et al. (1987, pp. 780-781) will be used. Chung et al. (1987) conducted a series of 20 slow burst tests and mandrel tests with irradiated cladding. Approximately half of these tests extended for over 200 hours. Four tests were on BWR Zircaloy 2 cladding with a burnup of 22 MWd/kgU and the remaining tests were on PWR Zircaloy 4 cladding with a burnup of 28 MWd/kgU. They measured an average strain at failure was 3.3% with a range of 0.4% to 11.7%. They also conducted scanning electron microscope inspection of the failures and found evidence that, in 11 of the tests, the failures occurred at cracks formed in the cladding. The use of these results for a failure criteria addresses the potential for lower failure strains from pre-existing internal cracks and the situation that failure might not be from pure material creep. This failure criteria does not address potential changes in the strain failure criteria with strain rate. The strain rates in Chung's gas pressurization experiment varied from $3\ 10^{-6}\ s^{-1}$ to $5.4\ 10^{-9}\ s^{-1}$ with an average of $5.8\ 10^{-7}\ s^{-1}$. The mandrel tests were in the range of $5\ 10^{-5}$ to $7\ 10^{-8}\ s^{-1}$. While these strain rates are faster than expected in repository conditions, they are not rapid burst tests. The creep tests summarized in CRWMS M&O 2000a extend up to 10,000 hours (approximately 1.14 year) and show creep strains, without failure, in excess of the failure criteria being used in this AMR.

Modeling the cladding directly over the fuel rather than the end-plug welds represents a more conservative case for repository failures than a separate set of failure criteria at the welds. This is based on the fact that there are more cladding restraint (and less creep-out), lower storage temperatures, less irradiation damage, less total hydrogen, and no PCI in this region. Whereas high residual stresses occur in these weld areas, and there is a potential for larger incipient cracks, rods with faulty welds with large incipient cracks were either removed during rod

fabrication leak testing, discovered during non-destructive evaluation, or failed in reactor. Therefore failures in end plug welds are included in the overall database and are not treated as a separate, more-restrictive failure mode.

There is corroborating evidence for using this failure criteria. In the German (Peehs) analysis (Pescatore et al. 1990, p. 39), a conservative value for a strain at which cladding failure occurs, 1% strain, was selected. Sanders et al. (1992, p. III-53) recommend a median value of 6 percent for rupture strain and also report a series of experiments with irradiated cladding that had a median failure strain of 4% (Sanders et al. 1992, p. III-51). Van Swam et al. (1997b, p. 430) report 8 ring tensile tests on irradiated cladding with the resulting total elongation being 7.6% (1.5% to 15% range) at 27°C and 15.8% (5% to 21% range) at 350°C. These results suggest that the creep failure criteria being used are very conservative because of the effect of the elevated temperatures. The Technical Basis Document (CRWMS M&O 1998b, Table 6-19, p. 6-14) showed 54 tensile tests or high temperature rod creep tests. The average uniform elongation strain for these tests is 4%. A failure criteria of 3.3% is used in this AMR to predict creep failure and is more conservative (lower) than most other reported values, especially since no correction has been made for the elevated temperatures.

Using a strain limit of 3.3% (range 0.4% to 11.7%) in Figure 25, an initial room temperature stress of approximately 112 MPa is required for the rod to fail from creep. The CCDF for initial rod stress was presented in Figure 18 and has been redrawn as Figure 26 using a logarithmic scale to better define the tail of the distribution. About 0.24% (with a range of 0.1% to 4.6%) of the rods are expected to fail in dry storage and transportation from creep. Transportation contributed about 0.01% of that total 0.24%.

The strain depends strongly on the temperature (an Arrhenius relationship in Equation 6.10-1) and this analysis was performed using peak cladding temperatures. If actual dry storage and shipping temperatures were available and stayed below 300°C, the failure rate would have been closer to zero. This demonstrates the degree of conservatism in using peak temperatures.

A test case (CRWMS M&O 2000a) is included in Attachment II, Creep Sheet, and Row 47. This test case is an analysis of three experiments reported by Matsuo. The test conditions are: time duration = 960 hours, temperature = 360°C, stress at 360°C = 118 MPa (corresponding to 56 MPa at room temperature). The measured strains (three tests) were 0.33, 0.40, and 0.44%. CRWMS M&O 2000a reported a calculated creep of 0.38%, the same result as shown in Row 47 and Cell G47. This demonstrated that the equations were programmed correctly. Visual inspection and hand calculations were also performed.

The analysis presented in this section is based on an empirical creep model developed by Matsuo. Many of the alternative models are discussed by Pescatore et al. (1994, pp. 47-86). One model discussed is the Diffusion Controlled Cavity Growth (DCCG) model. Pescatore (1990, p. 83) concludes that the DCCG has never been validated against cavity data and voids or cavities are very infrequently seen in irradiated Zircaloys. He recommends (p. 85) a methodology similar to the approach used here. Dry storage licensees were once required by the NRC to use the DCCG model to evaluate dry storage designs. The current NRC Interim Staff Guidance (ISG) Number 11 (NRC 2000) recognizes the controversy with this conceptual model and permits

license applicants to use other creep models in their license application. The use of Masuo's correlation is consistent with this ISG.

For most rods, the stresses during dry storage are too low to produce Stress Corrosion Cracking (SCC). Tasooji et al. (1984, p. 600, their Figure 3) show that stresses need to be above 180 MPa for SCC to occur. Both creep and SCC will be addressed when creep during dry storage will again be analyzed and integrated with creep from repository conditions.

6.10.2. DHC Failures in Dry Storage and Transportation

During Delayed Hydride Cracking (DHC), hydrides slowly form at a crack tip until the crack propagates through the hydride region at the crack tip and the crack propagation stops. This sequence repeats itself and the crack propagates slowly through the metal. The hydrides preferentially precipitate at the crack tip because the tensile stress reduced the solubility of the hydride in that region. The critical stress intensity factor (K_{IH}) is the minimum stress intensity that will permit any DHC, regardless of velocity (velocity approaches 0). For this analysis, the stress intensities (K_I) will be calculated and compared to the K_{IH}. If $K_I > K_{IH}$, then the crack will start to propagate and, it is assumed, because of long repository times, failure will occur. DHC failure occurred in some zirconium coolant tubes in a Candu reactor where high temperature gradients caused excess hydride buildup in a specific location.

The stress intensity factor, K_I, is a measure of the increased stress at the tip of a crack. The stress intensity factor is proportional to the far-field stress times the square root of the crack length. For a sharp crack, a limiting case, the stress intensity factor is the Reed-Hill (1973, p. 800) equation, substituting w (the crack depth) for c (the crack length), where the relationship is the crack depth = ½ crack length from Dieter (1961, p. 194):

$$K_I = St * (\pi * w)^{0.5} \qquad \text{(Eq. 6.10-2)}$$

where

K_I = Stress intensity factor, MPa-$m^{0.5}$

St = Cladding stress, MPa

w = Crack depth, m

The calculated crack size distribution is discussed in Section 6.6 and given in Figure 17. The median (P = 50 percent) value was 13.0 µm, the mean was 18.6 µm, and the largest size crack in the 2000 samplings was 119 µm. The calculated stress distribution is given in Figures 18 and 26. DHC is unlikely at temperatures above 260°C (Mahmood et al. 1998, p.20), because of the plasticity of the material. Rothman (1984, p. 37) reports that DHC is unlikely above 250°C because of the plasticity of the material. For this calculation, the temperature of 260°C is used and the pressure is adjusted accordingly. The crack size distribution and stress distribution can be combined to give the distribution of stress intensity factors, K_I, in Figure 27. Some of the properties of this distribution of the stress intensity factor are:

Mean: 0.47 MPa-$m^{0.5}$

Median: 0.40 MPa-$m^{0.5}$

95%: 0.097 MPa-$m^{0.5}$

5%: 1.078 MPa-$m^{0.5}$

maximum: 2.7 MPa-$m^{0.5}$

minimum: 1.61E-03 MPa-$m^{0.5}$

The critical stress intensity factor (K_{IH}) is the minimum stress intensity that will permit any DHC, regardless of velocity (velocity approaches 0). The work of Shi and Puls (1994, p. 239, Fig. 7), shows experimental K_{IH} in the range of 5 to 12 MPa-$m^{0.5}$ for zirconium alloy containing 2.5% Nb. Rothman (1984, p. 37), reports a K_{IH} of 6 MPa-$m^{0.5}$ for Zircaloy-2. Pescatore et al. (1990, Table 6, p.50) report values of 5 and 14. Huang (1995, p. 188) shows K_{IH} for irradiated Zircaloy-2 approaching 6 MPa-$m^{0.5}$. For this AMR, Huang's and Rothman's value for irradiated cladding of 6 MPa-$m^{0.5}$ was used. Because the observed values of K_I are well below these values, exactly which value of K_{IH} is selected is not important. No K_I values in this AMRs sampling of rods are near the threshold stress intensity value. The maximum observed K_I was 2.7 MPa-$m^{0.5}$ and the mean value was 0.47 MPa-$m^{0.5}$.

Rothman (1984, pp. 33 - 39) reviewed DHC in Zircaloy cladding in a repository. Rothman concludes that DHC is unlikely unless the fuel rods have large existing cracks (exceeding approximately 50 percent of wall thickness) and very high stresses (exceeding approximately 137 MPa). He also concludes that hydride reorientation is also unlikely because of the lack of large temperature gradients in the repository and the cladding stresses are lower than needed for reorientation. Peehs (1998, pp. 5, 6) concluded that neither DHC nor hydride reorientation would occur in dry storage.

In conclusion, failure of the cladding by DHC in dry storage is unlikely and has not been included in the abstraction for the TSPA analysis. Stresses (and stress intensity factors) are too low for crack propagation. Since the threshold for embrittlement failure is always greater than the threshold for DHC ($K_{IC} > K_{IH}$), embrittlement failures are also not expected.

6.11 ROD FAILURE DURING FUEL SHIPMENT (VIBRATION AND IMPACT)

During normal shipping of fuel, no failures have been identified in the literature. Sanders et al. (1992) analyzed transportation accidents. Failure probabilities were calculated for a specific drop test height of nine meters (9 m), a 0.3-m drop, and normal transport (i.e., normal vibration) (Sanders et al. 1992, Table III-10, p. III-137). The 9-m drop was by far the most severe, with failure probabilities of the order of $2x10^{-4}$. The normal transport failure probability is $2x10^{-7}$ per rod. This reference generated acceleration versus frequency curves for truck and rail shipping. It then looked at structural damage from a union of the hazard curves and the structural analysis and concluded that no additional damage is done in shipping. This value is conservatively bounded in this AMR by a failure fraction of $1x10^{-4}$ to account for other transport accident conditions.

In "*Dynamic Impact Effects on Spent Fuel Assemblies*," Witte et al. (1989) performed an analytical evaluation of the potential impacts of all movements. They conclude (Witte et al. 1989, p. 5) that no yielding of the rods would occur below 63g's acceleration. Normal transport would result in accelerations far below these values.

IAEA (1988, p. 114) surveyed shipping worldwide and reported that "to date, there have been no major incidents during 30 years experience connected with irradiated fuel transport."

Table 11 (Eble 1999) summarizes the design basis maximum cladding temperatures reported by numerous shipping cask vendors in their Safety Analysis Reports (SARs). The design basis temperatures are upper limit temperatures and most, if not all, of the actual fuel should be below this temperature. The range of temperatures is 242°C to 378°C, with a mean peak temperature of 322°C. Creep failures during shipment are combined with the creep failures during dry storage because the damage is cumulative. This analysis is discussed in Section 6.10.1 and the analysis is presented in Attachment II. The creep analysis performed in Section 6.10.1 considered dry storage and shipping and used a peak cladding temperature for transportation of 350°C. This temperature is 28°C above the mean value discussed above. It is consistent with the initial dry storage temperature and the cladding temperature limit currently used at YMP. It was also assumed that the shipment took three weeks and the temperature was at the peak value for that interval. As noted in Section 6.10.1, shipping contributed approximately 0.01% of the total rod failure rate from creep of 0.24% during dry storage and transportation. As noted in Section 6.10.2, no Delayed Hydride Cracking (DHC) is expected, including during transportation.

Table 11. Comparison of Maximum Cladding Design Temperatures for Shipping Casks (Eble 1999)

Vendor	Type	Canister	Max. Cladding Temp. (°C)
NAC	STC	Yes	302
NAC	STC	No	309
Holtec International, Inc.	HI-STAR 100	Yes MPC-68 (BWR)	378
Holtec International, Inc.	HI-STAR 100	Yes MPC-24 (PWR)	372
Westinghouse	WESFLEX W21	Yes	321
Westinghouse	WESFLEX W44	Yes	321
Westinghouse	WESFLEX W74	Yes	330
Transnuclear West	NUHOMS MP187	Yes	354
Transnuclear	TN-68	N.A.	254
Chem Nuclear	IF-300	N.A.	363
GNB	GNS-16	N.A.	242

The importance of the fuel transportation analysis and experience (domestic and foreign) is in demonstrating that very little fuel failure or degradation is expected during transportation. The use of actual temperatures instead of design temperatures would reduce the estimate of the small fraction of fuel damaged during transportation.

7. CONCLUSIONS

The purpose of this analysis is to describe the condition of the commercial nuclear fuel as it is received at the YMP site. This analysis generates the initial boundary condition for the subsequent analysis of degradation of the fuel in the repository. Table 12 summarizes the distributions of the various properties developed in this analysis. These distributions are given in the software routine: Rod-Initial-C.xls and are accessible through data tracking number DTN MO0001SPAICC48.037. The CCDFs for the various parameters are not independent. They are generated using a single burnup distribution and must be used accordingly. Creep failures in the proposed repository must be coupled with the creep failures in dry storage since rods predisposed to fail during the repository thermal cycle have already received some creep (and possible failure) during dry storage.

Table 12. CCDFs Describing Expected Fuel Stream into YMP

Property	Report Section	Mean Value	5% CCDF Value	CCDF Figure
Burnup	6.2	44.1 MWd/kgU	63.3 MWd/kgU	3
Helium fill Pressure	6.3.1	3.71 MPa	4.99 MPa	None
Fission Gas Release	6.3.3	4.2%	10.8%	None
Free Volume	6.3.5	17.7 cc	14.1 cc	None
Internal Pressure	6.3.6	4.8 MPa	7.34 MPa	9
Oxide Thickness	6.4	54.2 μm	112 μm	13
Average Hydride Content at peak oxide location	6.5	358 ppm	738 ppm	15
Crack Size	6.6	19 μm	57.1 μm	17
Cladding Thickness	6.7	522 μm	475 μm	None
Stress	6.7	38.4 MPa	61.8 MPa	18, 26
Stress Intensity Factor, K_I	6.10.2	0.47 MPa-$m^{0.5}$	1.08 MPa-$m^{0.5}$	27

DTN: MO0001SPAICC48.037

Table 13 gives the percent of rods that are estimated to have failed cladding at emplacement. Failures from fuel handling are included in the reactor failures and dry storage failures. The data presented provide a range of expected conditions that significantly impact the effectiveness of LWR fuel cladding on the waste form performance. Fuel rods that are estimated to have failed cladding may also be susceptible to cladding unzipping and fuel dissolution when the WP fails. Additional rods are expected to fail during disposal and will be susceptible to dissolution depending on the repository and WP conditions.

Creep strain failure during dry storage and transportation was calculated in this AMR and the failure percent was estimated as 0.24%. This failure rate is not included in Table 13 or 14 because it is recalculated when rod creep damage is integrated for a temperature profile that includes dry storage, transportation and emplacement at YMP. This analysis must be integrated because the rod damage from one temperature period must be carried forward to the next temperature period to analyze the total creep strain damage.

Table 13. Percent and Cause of Rods Failed in a WP

Rod Failure Mode	Percent of Rods Failed/WP
Reactor Operation Failures (Mean)	0.109 Range: 0.0 to 5.23
Pool Storage	0.0
Dry Storage	0.045
Dry Storage & Transportation, DHC	0.0
Transportation (Vibration, Impact)	0.01
Fuel Handling	(Included above)
Total	0.164 Range: 0.055 to 5.28

DTN: MO0001SPAICC48.037

The shape of the distribution function for the percent of rods failed in a WP is based on the assumption that the WPs are loaded with fuel in the order of reactor discharge. This assumption means that fuel from periods with poor fuel performance is placed in one set of WPs and fuel from periods with good fuel performance is placed in another set. This approach increases the range of the distribution. The periods of poor fuel performance were in the 1970s. These fuels have lower burnups and are cooler than the newer fuels and in actuality would probably be blended with newer, hotter fuels to meet thermal loading goals. Assuming, however, that no blending occurs, the CCDF for failed cladding in a WP is given in Table 14. This CCDF is the sum of the reactor operations failure and the failures listed in Table 13 from dry storage and transportation. The upper limit of the CCDF in Table 14 for reactor operation and other causes (as given in Figure 21) was increased by a factor of four (4) to represent uncertainty associated with potential unknown damage of the 4 nearest rods to the damaged one (square fuel arrays).

S. Cohen & Associates (1999, p. 7-1) has provided independent confirmation of the fuel condition as received at YMP. Their results, summarized in Table 15, show smaller rod failure rates than reported in this AMR. This AMR is conservative, being larger than that projected in Table 15. They include failures associated with consolidation although the commercial power industry has abandoned this practice in favor of dry storage. The dry storage failure rate reported in Table 15 includes consolidation failures, so the sum of these two reported rates is higher than it should be. In addition, the reported reactor in-service failure rate also includes handling failures. Overall, their projected fuel rod failure rates are close to that projected in this AMR.

Alternative Conceptual Models: The analysis by S. Cohen & Associates is considered an alternative conceptual model and qualitatively agrees with this analysis. Thus it is concluded that this analysis is valid for its intended use. The earlier YMP TSPAs performed in 1993 and 1995 did not consider cladding, and as such are an alternative conceptual model that is extremely conservative because it permits all fuel to dissolve at the intrinsic dissolution rate. The TSPAs done for European sites also did not consider cladding. The European sites have saturated, reducing environments where the UO_2 dissolution rates are so slow that cladding degradation was not considered.

The input values (numerical input data that has been assigned DTNs) listed in Table 1 have been labeled “to be verified” (TBV) in the DIRS database. These reactor fuel parameters from the open literature have been submitted to the DOE for approval as accepted data. When acceptance is received, the TBVs will be removed from these parameters.

This document may be affected by technical product input information that requires confirmation. Any changes to the document that may occur as a result of completing the confirmation activities will be reflected in subsequent revisions. The status of the input

information quality may be confirmed by review of the Document Input Reference System database.

Table 14. CCDF for Rods with Failed Cladding in a WP

CCDF All CSNF	Lower Uncertainty	% Failure	Upper Uncertainty
1.0000	0.0138	0.0550	0.2200
0.9987	0.0146	0.0585	0.2341
0.9849	0.0155	0.0622	0.2486
0.8561	0.0179	0.0717	0.2869
0.6555	0.0212	0.0849	0.3397
0.5819	0.0224	0.0895	0.3582
0.5058	0.0237	0.0948	0.3793
0.2709	0.0284	0.1136	0.4545
0.1966	0.0361	0.1445	0.5780
0.1084	0.0507	0.2028	0.8111
0.0970	0.0522	0.2089	0.8357
0.0766	0.0741	0.2965	1.1859
0.0640	0.0746	0.2983	1.1930
0.0503	0.0803	0.3213	1.2853
0.0373	0.1248	0.4990	1.9962
0.0323	0.2469	0.9875	3.9499
0.0221	0.2892	1.1568	4.6274
0.0196	0.4496	1.7985	7.1941
0.0190	0.5088	2.0352	8.1408
0.0115	0.6939	2.7757	11.1029
0.0036	0.7626	3.0505	12.2022
0.0002	1.3214	5.2856	21.1424
0.0000	1.3214	5.2856	21.1424

Note: Data excludes damage due to rod creep.
DTN: MO0001SPAICC48.037

Table 15. Fuel Failure Rates Predicted by S. Cohen & Associates 1999

Fuel Service Period	Rod Failure Percents (%)
In-service	< 0.05
Pool Storage	0
Dry Storage	0.03
Consolidation	0.005
Other Handling	0.0003
Total	< 0.1

The following summary is prepared for the Waste Form PMR:

The Waste Packages (WPs) will be loaded in the order of discharge from the various reactors as a function of calendar years. This generates some variability in the fraction of rods failed within a WP. This loading sequence tends to place fuel with higher cladding failure rates into

consecutively loaded WPs and produces larger variations than would be expected from thermal blending. This is a credible and reasonable assumption because the current fuel owners will presumably use a systematic approach in deciding which fuel will be shipped first to the repository.

Each failed Pressurized Water Reactor (PWR) fuel assembly has an average of 221 rods and has 2.2 failed fuel rods. The basis for the average of 2.2 failed fuel rods per failed assembly is described in the Initial Cladding Condition AMR (this report, Section 6.8). This failure value applies for the early years. Current failure rates are between 1.1 and 1.4 rods per assembly. Integrating this with the initial rates shows that the number of failed rods per failed assembly has decreased to be closer to one (1) today. It is conservative to apply the value of 2.2 for all time.

All rods are exposed to the conditions of dry storage at the design temperature of the Castor Mark V waste package. The best estimate dry storage temperatures were not available at the time of this analysis, therefore the Castor Mark V package with 55 MWd/kgU burnup fuel was selected to be conservative.

All rods are exposed to the conditions of a shipping cask for 3 weeks at 350ºC. This is conservative since this is the peak shipping cask design basis temperature for all rods. Most rods will actually be exposed to lower temperatures for a shorter time frame.

The uncertainty value for the rod failure data is four. This is based on a square pitch array of fuel rods in the fuel assembly. The rods more likely to have damage are the rods near the damaged rod. There are four rods near the damaged rod in a square pitch.

BWR cladding degrades in a similar manner to the base case PWR fuel. This is conservative since BWR cladding is thicker, is discharged with lower burnups and stresses, and is enclosed in flow channels, which provide additional protection.

8. SOURCE OF INPUT

8.1 REFERENCES CITED:

Andrews, M.G. and Matzie, R.A. 1985. "A Report on the Reliability, Performance and Progress of Combustion Engineering's Fuel Assemblies toward Extended Burnup." *Proceedings, American Nuclear Society Topical Meeting on Light Water Reactor Fuel Performance, Orlando, Florida, April 21-24, 1985. DOE/NE/34130-1,* Vol. 1. La Grange Park, Illinois: American Nuclear Society. TIC: 226810.

Bailey, W.E.; Marlowe, M.O.; and Proebstle, R.A. 1985. "Trends in BWR Fuel Performance." *Proceedings, American Nuclear Society Topical Meeting on Light Water Reactor Fuel Performance, Orlando, Florida, April 21-24, 1985. DOE/NE34130-1,* Vol. 1. La Grange Park, Illinois: American Nuclear Society. TIC: 226810.

Bailey, W.J. and Wu, S. 1990. *Fuel Performance Annual Report for 1988.* NUREG/CR-3950. Washington, D.C.: U.S. Nuclear Regulatory Commission. TIC: 245644.

Bain, G.M.; McInteer, W.A.; and Papazoglou, T.P. 1985. "Release and Migration of Fission Products in High-Burnup Fuel." *Proceedings, American Nuclear Society Topical Meeting on Light Water Reactor Fuel Performance, Orlando, Florida, April 21-24, 1985. DOE/NE34130-1,* Vol. 2. La Grange Park, Illinois: American Nuclear Society. TIC: 226810.

Barner, J.O. 1985. *Characterization of LWR Spent Fuel MCC-Approved Testing Material-ATM-101.* PNL-5109, Rev. 1. Richland, Washington: Pacific Northwest Laboratory. TIC: 240883.

Berggren, G. 1980. *Helium Retention Summary of Reports and Memoranda.* KBS TR 80-04. Stockholm, Sweden: Svensk Kärnbränsleförsörjning AB. TIC: 205784.

Castellan, G.W. 1971. *Physical Chemistry.* 2nd Edition. Reading, Massachusetts: Addison-Wesley Publishing Company. TIC: 247158.

Charquet, D.; Rudling, P.; Mikes-Lindback, M.; and Barberis, P. 1994. "Hydrogen Absorption Kinetics During Zircaloy Oxidation in Steam." *Zirconium in the Nuclear Industry, Tenth International Symposium, Baltimore, Maryland, June 21-24, 1993.* Garde, A.M. and Bradley, E.R., eds. *ASTM-STP-1245,* 80-97. Philadelphia, Pennsylvania: American Society for Testing and Materials. TIC: 237257.

Chung, H.M.; Yaggee, F.L.; and Kassner, T.F. 1987. "Fracture Behavior and Microstructural Characteristics of Irradiated Zircaloy Cladding." *Zirconium in the Nuclear Industry, Seventh International Symposium Sponsored by ASTM Committee B-10 on Reactive and Refractory Metals, Strasbourg, France, 24-27 June 1985.* Adamson, R.B. and Van Swam, L.F.P., eds. Pages 775-801. Philadelphia, Pennsylvania: American Society for Testing and Materials. TIC: 238255.

CRWMS M&O 1998a. *Design Basis Cladding Analysis.* BBA000000-01717-0200-00054 REV 01. Las Vegas, Nevada: CRWMS M&O. ACC: MOL.19980325.0102.

CRWMS M&O 1998b. "Waste Form Degradation, Radionuclide Mobilization, and Transport Through the Engineered Barrier System." Chapter 6 of *Total System Performance Assessment-Viability Assessment (TSPA-VA) Analyses Technical Basis Document.* B00000000-01717-4301-00006 REV 01. Las Vegas, Nevada: CRWMS M&O. ACC: MOL.19981008.0006.

CRWMS M&O 1999a. *Clad Degradation - Initial Clad Condition.* TDP-WIS-MD-000021 REV 00. Las Vegas, Nevada: CRWMS M&O. ACC: MOL.19990902.0474.

CRWMS M&O 1999b. *Conduct of Performance Assessment.* Activity Evaluation, September 30, 1999. Las Vegas, Nevada: CRWMS M&O. ACC: MOL.19991028.0092.

CRWMS M&O 2000a. *Comparison of Creep Correlations.* Input Transmittal PA-WP-00048.Ta. Las Vegas, Nevada: CRWMS M&O. ACC: MOL.20000223.0002.

CRWMS M&O 2000b. *Waste Packages and Source Terms for the Commercial 1999 Design Basis Waste Stream.* CAL-MGR-MG-000001 REV 00. CRWMS M&O, Las Vegas: Nevada. ACC: MOL.20000214.0479.

Dehon, C.; Cambon, J.L.; Houdaille, B.; and Chagrot, M 1985. "Main Results from FRAGEMA Fuel Performance in Power Reactors." *Proceedings, American Nuclear Society Topical Meeting on Light Water Reactor Fuel Performance, Orlando, Florida, April 21-24, 1985. DOE/NE/34130-1,* Vol. 1. La Grange Park, Illinois: American Nuclear Society. TIC: 226810.

Dieter, G.E. 1961. *Mechanical Metallurgy.* 1st Edition. New York, New York: McGraw-Hill Book Company. TIC: 245037.

DOE (U.S. Department of Energy) 1992. *Characteristics of Potential Repository Wastes.* DOE/RW-0184-R1. Volume 1. Washington, D.C.: U.S. Department of Energy, Office of Civilian Radioactive Waste Management. ACC: HQO.19920827.0001.

DOE 1996. *Spent Nuclear Fuel Discharges from U.S. Reactors 1994.* SR/CNEAF/96-01. Washington, D.C.: U.S. Department of Energy. TIC: 232923.

DOE 2000. *Quality Assurance Requirements and Description.* DOE/RW-0333P, Rev. 9. Washington, D.C.: U.S. Department of Energy, Office of Civilian Radioactive Waste Management. ACC: MOL.19991028.0012.

Duke Power 1997. *McGuire Nuclear Station, PRA, Revision 2 Summary Report.* Charlotte, North Carolina: Duke Power. TIC: 246471.

Dyer, J.R. 1999. "Revised Interim Guidance Pending Issuance of New U.S. Nuclear Regulatory Commission (NRC) Regulations (Revision 01, July 22, 1999), for Yucca Mountain, Nevada." Letter from Dr. J.R. Dyer (DOE/YMSCO) to Dr. D.R. Wilkins (CRWMS M&O), September 3, 1999, OL&RC:SB-1714, with enclosure, "Interim Guidance Pending Issuance of New NRC Regulations for Yucca Mountain (Revision 01)." ACC: MOL.19990910.0079.

Eble, R.G. 1999. "MGR Transportation Temperatures Preliminary Information." Memo from R.G. Eble to Eric Seigmann, August 31, 1999, with attachments. ACC: MOL.19991105.0079.

Einziger, R.E. and Kohli, R. 1984. "Low-Temperature Rupture Behavior of Zircaloy-Clad Pressurized Water Reactor Spent Fuel Rods Under Dry Storage Conditions." *Nuclear Technology, 67,* (1), 107-123. Hinsdale, Illinois: American Nuclear Society. TIC: 216868.

Einziger, R.E.; Atkin, S.D.; Stellrecht, D.E.; and Pasupathi, V. 1982. "High Temperature Postirradiation Materials Performance of Spent Pressurized Water Reactor Fuel Rods Under Dry Storage Conditions." *Nuclear Technology, 57,* (1), 65-80. Hinsdale, Illinois: American Nuclear Society. TIC: 237142.

EPRI (Electric Power Research Institute) 1997. *The Technical Basis for the Classification of Failed Fuel in the Back-End of the Fuel Cycle.* EPRI TR-108237. Palo Alto, California: Electric Power Research Institute. TIC: 236839.

Essig, T.H. 1999. "Acceptance for Referencing of Framatome Cogema Fuels Topical Report BAW-10186P: 'Extended Burnup Evaluation' (TAC No. MA3705)." Letter from T.H. Essig (NRC) to J.H. Taylor (Framatome), January 25, 1999, with enclosure. ACC: MOL.19990927.0213.

Garde, A.M. 1986. *Hot Cell Examination of Extended Burnup Fuel from Fort Calhoun.* DOE/ET/34030-11. Windsor, Connecticut: Combustion Engineering. TIC: 237128.

Garde, A.M. 1991. "Enhancement of Aqueous Corrosion of Zircaloy-4 Due to Hydride Precipitation at the Metal-Oxide Interface." *Zirconium in the Nuclear Industry, Ninth International Symposium, Kobe, Japan, November 5-8, 1990.* Eucken, C.M. and Garde, A.M., eds. *ASTM-STP-1132,* 566-594. Philadelphia, Pennsylvania: American Society for Testing and Materials. TIC: 246113.

Guenther, R.J.; Blahnik, D.E.; Campbell, T.K.; Jenquin, U.P.; and Mendel, J. 1988. *Characterization of Spent Fuel Approved Testing Material–ATM-103.* PNL-5109-103. Richland, Washington: Pacific Northwest Laboratory. TIC: 223979.

Guenther, R.J.; Blahnik, D.E.; Campbell, T.K.; Jenquin, U.P.; Mendel, J.E.; and Thornhill, C.K. 1988. *Characterization of Spent Fuel Approved Testing Material –ATM-106.* PNL-5109-106. Richland, Washington: Pacific Northwest Laboratory. TIC: 223978.

Guenther, R.J.; Blahnik, D.E.; Jenquin, U.P.; Mendel, J.E.; Thomas, L.E.; and Thornhill, C.K. 1991. *Characterization of Spent Fuel Approved Testing Material –ATM-104.* PNL-5109-104. Richland, Washington: Pacific Northwest Laboratory. TIC: 203846.

Huang, F.H. 1995. *Fracture Properties of Irradiated Alloys.* 418 p. Richland, Washington: Avante Press. TIC: 224548.

IAEA (International Atomic Energy Agency) 1988. *Survey of Experience with Dry Storage of Spent Nuclear Fuel and Update of Wet Storage Experience.* Technical Report Series, No. 290. Vienna, Austria: International Atomic Energy Agency. TIC: 233246.

IAEA (International Atomic Energy Agency) 1998. "Generic Formulation for Semi-Empirical Models." Section 7.3.1 of *Waterside Corrosion of Zirconium Alloys in Nuclear Power Plants.* IAEA-TECDOC-996. p. 178. Vienna, Austria: International Atomic Energy Agency. TIC: 238879.

Johnson, A.B., Jr. 1977. *Behavior of Spent Nuclear Fuel in Water Pool Storage.* BNWL-2256. Richland, Washington: Pacific Northwest Laboratory. TIC: 234703.

Johnson, A.B., Jr., and Gilbert, E.R. 1983. *Technical Basis for Storage of Zircaloy-Clay Spent Fuel in Inert Gases.* PNL-4835. Richland, Washington: Pacific Northwest Laboratory. TIC: 9151.

Johnson, A.B., Jr.; Bailey, W.J.; Schreiber, R.E.; and Kustas, F.M. 1980. *Annual Report - FY 1979. Spent Fuel and Fuel Pool Component Integrity.* PNL-3171. Richland, Washington: Pacific Northwest Laboratory. TIC: 229623.

Johnson, A.B., Jr.; Dobbins, J.C.; Zaloudek, F.R.; Gilbert, E.R.; and Levy, I.S. 1987. *Assessment of the Integrity of Spent Fuel Assemblies Used in Dry Storage Demonstrations at the Nevada Test Site.* PNL-6207. Richland, Washington: Pacific Northwest Laboratory. TIC: 230135.

Lanning, D.D.; Beyer, C.E.; and Painter, C.L. 1997. *FRAPCON-3: Modifications to Fuel Rod Material Properties and Performance Models for High-Burnup Application.* NUREG/CR-6534. Volume 1. Richland, Washington: Pacific Northwest National Laboratory. TIC: 238923.

Lide, D.R. and Frederikse, H.P.R., eds. 1997. *CRC Handbook of Chemistry and Physics.* 78th Edition. Boca Raton, Florida: CRC Press. TIC: 243741.

Mahmood, S.T.; Farkas, D.M.; Adamson, R.B.; and Etoh, Y. 1998. "Post-Irradiation Characterization of Ultra High Fluence Zircaloy-2 Plate." *Zirconium in the Nuclear Industry, Twelfth International Symposium held in Toronto, Ontario, Canada, June 15-18, 1998.* 19-20. Philadelphia, Pennsylvania: American Society for Testing and Materials. TIC: 237270.

Manaktala, H.K. 1993. *Characteristics of Spent Nuclear Fuel and Cladding Relevant to High-Level Waste Source Term.* CNWRA 93-006. NRC-02-88-005. San Antonio, Texas: Center for Nuclear Waste Regulatory Analyses. TIC: 208034.

Manzel, R. and Coquerelle, M. 1997. "Fission Gas Release and Pellet Structure at Extended Burnup." *Proceedings of the 1997 International Topical Meeting on LWR Fuel Performance, Portland, Oregon, March 2-6, 1997.* 463-470. La Grange Park, Illinois: American Nuclear Society. TIC: 232556.

Mardon, J.P.; Garner, G.; Beslu, P.; Charquet, D.; and Senevat, J. 1997. "Update on the Development of Advanced Zirconium Alloys for PWR Fuel Rod Claddings." *Proceedings of the 1997 International Topical Meeting on Light Water Reactor Fuel Performance, Portland, Oregon, March 2-6.* 405-412. La Grange Park, Illinois: American Nuclear Society, Inc. TIC: 232556.

Matsuo, Y. 1987. "Thermal Creep of Zircaloy-4 Cladding Under Internal Pressure." *Journal of Nuclear Science and Technology, 24,* (2), 111-119. Tokyo, Japan: Atomic Energy Society of Japan. TIC: 237137.

McDonald, S.G. and Kaiser, R.S. 1985. "The Impact of Metallic Debris on Fuel Performance - A Case History." *Proceedings, American Nuclear Society Topical Meeting on Light Water Reactor Fuel Performance. Orlando, Florida, April 21-24, 1985. DOE/NE/34130-1,* Volume 1, 2-(3-19). La Grange Park, Illinois: American Nuclear Society. TIC: 226810.

McKinnon, M.A. and Doherty, A.L. 1997. *Spent Nuclear Fuel Integrity During Dry Storage - Performance Tests and Demonstrations.* PNNL-11576. Richland, Washington: Pacific Northwest Laboratory. TIC: 237126.

Morel, M.; Melin, P.; and and Dumont, A. 1994. "Updated Status of In Reactor Experience of Fragema Fuel Products." *Proceedings of the 1994 International Topical Meeting on Light Water Reactor Fuel Performance, West Palm Beach, Florida, April 17-21, 1994.* 15-21. La Grange Park, Illinois: American Nuclear Society. TIC: 243043.

NRC (U.S. Nuclear Regulatory Commission) 1998. *Issue Resolution Status Report Key Technical Issue: Total System Performance Assessment and Integration.* Rev. 1. Washington, D.C.: U.S. Nuclear Regulatory Commission. ACC: MOL.19990105.0083.

NRC 1999. *Issue Resolution Status Report Key Technical Issue: Container Life and Source Term.* Rev. 2. Washington, D.C.: U.S. Nuclear Regulatory Commission. TIC: 245538.

NRC 2000. *Interim Staff Guidance-11 — Storage of High Burnup Spent Fuel.* Washington, D.C.: U.S. Nuclear Regulatory Commission. TIC: 247227.

Nuclear Assurance Corporation. 1999. *NAC-MPC Safety Analysis Report for the NAC Multi-Purpose Canister System.* Norcross, Georgia: Nuclear Assurance Corporation. TIC: 245218.

Pati, S.R. and Garde, A.M. 1985. "Fission Gas Release from PWR Fuel Rods at Extended Burnups." *Proceedings, American Nuclear Society Topical Meeting on Light Water Reactor Fuel Performance, Orlando, Florida, April 21-24, 1985. DOE/NE/34130-1,* Vol. 2. La Grange Park, Illinois: American Nuclear Society. TIC: 226810.

Peehs, M. 1998. *Assessment of Dry Storage Performance of Spent LWR Fuel Assemblies with Increasing Burn-Up.* Erlangen, Germany: Bereich Energieerzeugung. TIC: 245171.

Pescatore, C.; Cowgill, M.G.; and Sullivan, T.M. 1990. *Zircaloy Cladding Performance under Spent Fuel Disposal Conditions Progress Report May 1 - October 31, 1989.* BNL 52235. Upton, New York: Brookhaven National Laboratory. ACC: NNA.19900710.0055.

Potts, G.A. 1997. "Recent GE BWR Fuel Experience." *Proceedings of the 1997 International Topical Meeting on LWR Fuel Performance, Portland, Oregon, March 2-6, 1997.* 261-271. La Grange Park, Illinois: American Nuclear Society. TIC: 232556.

Potts, G.A. and Proebstle, R.A. 1994. "Recent GE BWR Fuel Experience." *Proceedings of the 1994 International Topical Meeting on Light Water Reactor Fuel Performance, West Palm Beach, Florida, April 17-21, 1994.* 87-95. La Grange Park, Illinois: American Nuclear Society. TIC: 243043.

Preble, E.A.; Painter, C.L.; Alvis, J.A.; Berting, F.M.; Beyer, C.E.; Payne, G.A; Wu, S.L. 1993. *Fuel Performance Annual Report for 1990.* NUREG/CR-3950. Washington, D.C.: U.S. Nuclear Regulatory Commission. TIC: 245486.

Ravier, G.; Masuy, G.; and Willse, J.T. 1997. "Framatome and FCF Recent Operating Experience and Advanced Features to Increase Performance and Reliability." *Proceedings of the 1997 International Topical Meeting on Light Water Reactor Fuel Performance, Portland, Oregon, March 2-6, 1997.* 31-36. La Grange Park, Illinois: American Nuclear Society. TIC: 232556.

Reed-Hill, R.E. 1973. *Physical Metallurgy Principles.* Second Edition. 797-801. New York, New York: D. Van Nostrand Company. TIC: 237154.

Roark, R.J. 1989. *Roark's Formulas for Stress and Strain.* 6th Edition. New York, New York: McGraw-Hill. TIC: 10191.

Rothman, A.J. 1984. *Potential Corrosion and Degradation Mechanisms of Zircaloy Cladding on Spent Nuclear Fuel in a Tuff Repository.* UCID-20172. Livermore, California: Lawrence Livermore National Laboratory. ACC: NNA.19870903.0039.

S. Cohen & Associates 1999. *Effectiveness of Fuel Rod Cladding as an Engineered Barrier in the Yucca Mountain Repository.* McLean, Virginia: S. Cohen & Associates. TIC: 246541.

Sanders, T.L.; Seager, K.D.; Rashid, Y.R.; Barrett, P.R.; Malinauskas, A.P.; Einziger, R.E.; Jordan, H.; Duffey, T.A.; Sutherland, S.H.; and Reardon, P.C. 1992. *A Method for Determining the Spent-Fuel Contribution to Transport Cask Containment Requirements.* SAND90-2406. Volume 8. Albuquerque, New Mexico: Sandia National Laboratories. TIC: 232162.

Sasaki, S. and Kuwabara, S. 1997. "Utility Perspective on Commercial Light-Water Reactor Fuel in Japan." *1997 International Topical Meeting on Light Water Reactor Fuel Performance, Portland, Oregon, March 2-6, 1997.* 11-20. La Grange Park, Illinois: American Nuclear Society. TIC: 232556.

Sayles, C.W.; Chang, R.Y.; Thomsen, O.J.; and Swoope, S.C. 1994. "Use of Axial Cesium Distribution for Failure Identification in San Onofre Units." *Transactions of the American Nuclear Society, New Orleans, Louisiana, June 19-23, 1994, 70,* 76-77. La Grange Park, Illinois: American Nuclear Society. TIC: 236801.

Schneider, K.J. and Mitchell, S.J. 1992. *Foreign Experience on Effects of Extended Dry Storage on the Integrity of Spent Nuclear Fuel.* PNL-8072. Richland, Washington: Pacific Northwest Laboratory. TIC: 205836.

Schrire, D.I. and Pearce, J.H. 1994. "Scanning Electron Microscope Techniques for Studying Zircaloy Corrosion and Hydriding." *Zirconium in the Nuclear Industry, Tenth International Symposium, Baltimore, Maryland, June 21-24, 1993.* Garde, A.M. and Bradley, E.R., eds. *ASTM-STP-1245,* 98-115. Philadelphia, Pennsylvania: American Society for Testing and Materials. TIC: 237130.

Shi, S.Q. and Puls, M.P. 1994. "Criteria for Fracture Initiation at Hydrides in Zirconium Alloys I. Sharp Crack Tip." *Journal of Nuclear Materials, 208,* (3), 232-242. Amsterdam, The Netherlands: North-Holland Publishing Company. TIC: 237135.

Smith, G.P., Jr.; Pirek, R.C.; Freeburn, H.R.; and Schrire, D. 1994. *The Evaluation and Demonstration of Methods for Improved Nuclear Fuel Utilization.* DOE/ET/34013-15. Washington, D.C.: U.S. Department of Energy. TIC: 245407.

Sunderland, D.J.; Kennard, M.W.; and Harbottle, J.E. 1994. "Identification of Failed LWR Fuel in U.S. Reactors." *Transactions of the American Nuclear Society, New Orleans, Louisiana, June 19-23, 1994. 70,* 73-74. La Grange Park, Illinois: American Nuclear Society. TIC: 237153.

Tasooji, A.; Einziger, R.E.; and Miller, A.K. 1984. "Modeling of Zircaloy Stress-Corrosion Cracking: Texture Effects and Dry Storage Spent Fuel Behavior." *Zirconium in the Nuclear Industry, Sixth International Symposium, Vancouver, British Columbia, June 28- July 1, 1982.* Franklin, D.G. and Adamson, R.B., eds. *ASTM STP 824,* 595-626. Philadelphia, Pennsylvania: American Society for Testing and Materials. TIC: 241417.

Van Swam, L.F.; Bain, G.M.; Dey, W.C.; Davis, D.D.; and Heckermann, H. 1997a. "BWR and PWR Fuel Performance at High Burnup." *Proceedings of the 1997 International Topical Meeting on LWR Fuel Performance, Portland, Oregon, March 2-6, 1997.* 455-462. La Grange Park, Illinois: American Nuclear Society. TIC: 232556.

Van Swam, L.F.; Strasser, A.A.; Cook, J.D.; and Burger, J.M. 1997b. "Behavior of Zircaloy-4 and Zirconium Liner Zircaloy-4 Cladding at High Burnup." *Proceedings of the 1997 International Topical Meeting on LWR Fuel Performance, Portland, Oregon, March 2-6, 1997.* 421-431. LaGrange Park, Illinois: American Nuclear Society. TIC: 232556.

Wilson, H.W.; Menke, H.F.; Kunishi, H; Miller, R.S.; and Scherpereel, L.R. 1997. "Westinghouse Fuel Performance in Today's Aggressive Plant Operating Environment." *Proceedings of the 1997 International Topical Meeting on LWR Fuel Performance, Portland Oregon, March 2-6, 1997*. 23-30. La Grange Park, Illinois: American Nuclear Society. TIC: 232556.

Witte, M.C.; Chun, R.C.; and Schwartz, M.W. 1989. "Dynamic Impact Effects on Spent Fuel Assemblies." *9th International Symposium on the Packaging and Transportation of Radioactive Materials, Washington, D.C., June 11-16, 1989. 1,* 186-194. Oak Ridge, Tennessee: Oak Ridge National Laboratory. TIC: 240741.

Yang, R.L. 1997. "Meeting the Challenge of Managing Nuclear Fuel in a Competitive Environment." *Proceedings of the 1997 International Topical Meeting on LWR Fuel Performance, Portland, Oregon, March 2-6, 1997*. 3-10. La Grange Park, Illinois: American Nuclear Society. TIC: 232556.

Yang, R.L.; Ozer, O.; and Klepfer, H.H. 1991. "Fuel Performance Evaluation for EPRI Program Planning." Volume 1 of *International Topical Meeting on LWR Fuel Performance, Avignon (France), April 21-24, 1991, Proceedings, Fuel for the 90's.* 258-271. La Grange Park, Illinois: American Nuclear Society. TIC: 243519.

8.2 SOURCE DATA

MO0001SPAFGR06.036. Fission Gas Release for Unpressurized Prw Rod. Submittal date: 1/25/00.

MO0001SPAPRA00.035. Duke Energy, McGuire Nuclear Station PRA Revision 2 Summary Report. Submittal date: 1/18/00.

MO9912SPAASF01.020. Annual Spent Fuel Discharges. Submittal date: 12/13/99.

MO9912SPABWR50.022. BWR FUEL RELIABILITY. Submittal date: 12/13/99.

MO9912SPABWRR1.025. GE BWR Fuel Design Data. Submittal date: 12/13/99.

MO9912SPACFF00.024. Causes of Fuel Failures in BWRS. Submittal date: 12/23/99.

MO9912SPACSD06.017. Crack Size Distribution. Submittal date: 12/13/99.

MO9912SPAFFD37.021. Failed Fuel Demographics Based on In-Reactor Criteria. Submittal date: 12/13/99.

MO9912SPAFFR76.029. Fuel Failure Rate in Dry Storage. Submittal date: 12/13/99.

MO9912SPAFGF00.007. Fission Gas Fraction - Siemans Fuel. Submittal date: 12/13/99.

MO9912SPAFGP72.003. Pressure vs. Time in Fuel Rods. Submittal date: 12/13/99.

MO9912SPAFGR00.005. Fission Gas Release Fractions - Siemens Fuel. Submittal date:

12/13/99.

MO9912SPAFGR00.006. Fission Gas Release Fraction - FRAGEMA Fuel. Submittal date: 12/13/99.

MO9912SPAFGR00.008. Fission Gas Release Fraction - B&W Fuel. Submittal date: 12/13/99.

MO9912SPAFGR06.009. Fission Gas Release Fraction - CE Fuel. Submittal date: 12/13/99.

MO9912SPAFGR11.004. Fission Gas Release Fractions - CE Fuel. Submittal date: 12/13/99.

MO9912SPAFGR34.010. Fission Gas Release Fraction - GE Fuel. Submittal date: 12/13/99.

MO9912SPAFRT00.014. Pwr Fuel Rod Oxide Thickness. Submittal date: 12/13/99.

MO9912SPAFRV23.013. Fuel Rod Void Volume. Submittal date: 12/13/99.

MO9912SPAFSDR1.002. Westinghouse 17 x 17 Fuel Assembly Dimensions and Backfill Pressure. Submittal date: 12/13/99.

MO9912SPAGE800.023. GE 8x8 Fuel Experience. Submittal date: 12/13/99.

MO9912SPAHEL06.012. Helium Production. Submittal date: 12/13/99.

MO9912SPAHPM34.016. Hydrogen Pickup Model. Submittal date: 12/13/99.

MO9912SPAPFR00.028. PWR Fuel Reliability - Causes Fuel Failures in PWRS. Submittal date: 12/13/99.

MO9912SPAPFR01.027. PWR Fuel Reliability - Annual Spent Fuel Discharges and Burnups. Submittal date: 12/13/99.

MO9912SPAPWR50.026. Pwr Fuel Reliability. Submittal date: 12/13/99.

MO9912SPAROD00.019. Rod Failure. Submittal date: 12/13/99.

MO9912SPASFC01.032. Strain Failure Criteria. Submittal date: 12/15/99.

MO9912SPASOX00.015. Surface Oxidation Versus Burnup. Submittal date: 12/13/99.

MO9912SPATHD00.031. Temperature History for Dry Storage. Submittal date: 12/15/99.

8.3 CODES, STANDARDS, REGULATIONS AND PROCEDURES

64 FR 8640. Disposal of High-Level Radioactive Wastes in a Proposed Geologic Repository at Yucca Mountain, Nevada. Proposed rule 10 CFR 63. Readily Available

AP-2.13Q, Rev. 0, ICN 0. *Technical Product Development Planning.* Washington, D.C.: U.S. Department of Energy, Office of Civilian Radioactive Waste Management. ACC: MOL.19990701.0617.

AP-2.16Q, Rev. 0, ICN 0. *Activity Evaluation*. Washington, D.C.: U.S. Department of Energy, Office of Civilian Radioactive Waste Management. ACC: MOL.20000207.0716.

AP-3.10Q, Rev. 2, ICN 0. *Analyses and Models.* Washington, D.C.: U.S. Department of Energy, Office of Civilian Radioactive Waste Management. ACC: MOL.20000217.0246.

AP-SI.1Q, Rev. 2 ICN 4. *Software Management.* Washington, DC: U.S. Department of Energy, Office of Civilian Radioactive Waste Management. ACC: MOL.20000223.0508

ASTM C 1174-97 1997. *Standard Practice for Prediction of the Long-Term Behavior of Materials, Including Waste Forms, Used in Engineered Barrier Systems (EBS) for Geological Disposal of High-Level Radioactive Waste*. West Conshohocken, Pennsylvania: American Society for Testing and Materials. TIC: 246015.

DOE (U.S. Department of Energy) 2000. *Quality Assurance Requirements and Description*. DOE/RW-0333P, Rev. 9. Washington, D.C.: U.S. Department of Energy, Office of Civilian Radioactive Waste Management. ACC: MOL.19991028.0012.

NLP-2-0, Rev. 5. *Determination of Importance Evaluations.* Las Vegas, Nevada: CRWMS M&O. ACC: MOL.19981116.0120.

NRC (U.S. Nuclear Regulatory Commission) 1998. *Issue Resolution Status Report Key Technical Issue: Total System Performance Assessment and Integration.* Rev. 1. Washington, D.C.: U.S. Nuclear Regulatory Commission. ACC: MOL.19990105.0083.

NRC (U.S. Nuclear Regulatory Commission) 1999. *Issue Resolution Status Report Key Technical Issue: Container Life and Source Term.* Rev. 2. Washington, D.C.: U.S. Nuclear Regulatory Commission. TIC: 245538.

QAP-2-0, Rev. 5. *Conduct of Activities.* Las Vegas, Nevada: CRWMS M&O. ACC: MOL.19980826.0209.

QAP-2-3, Rev. 10. *Classification of Permanent Items.* Las Vegas, Nevada: CRWMS M&O. ACC: MOL.19990316.0006.

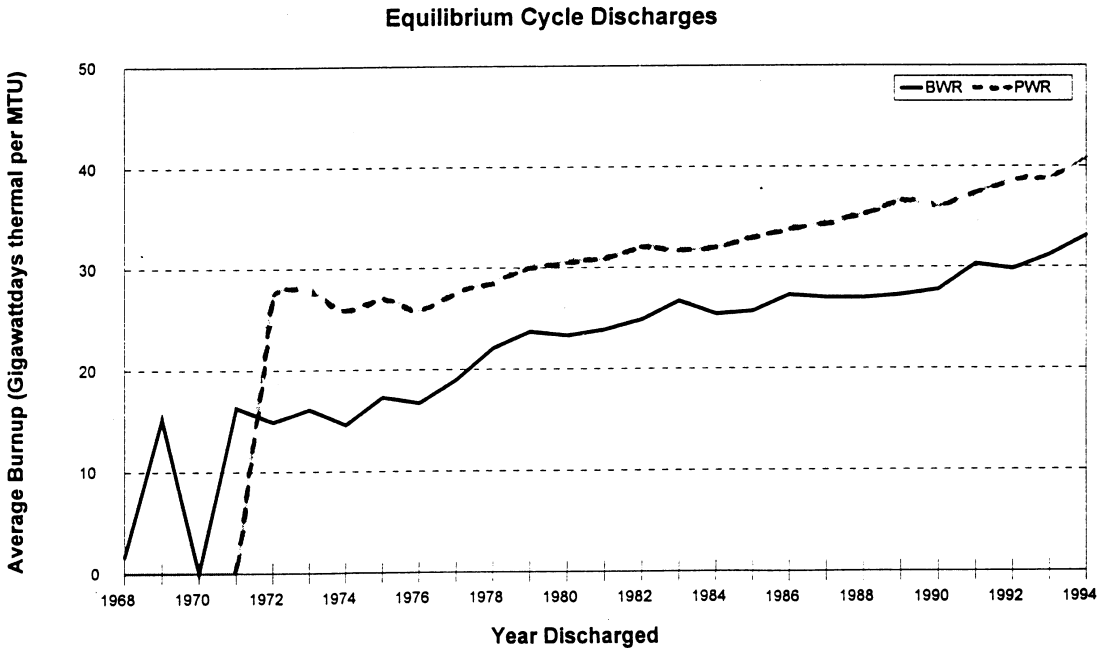

Figure 1. Equilibrium Cycle Discharge vs. Calendar Year (from DOE 1996)

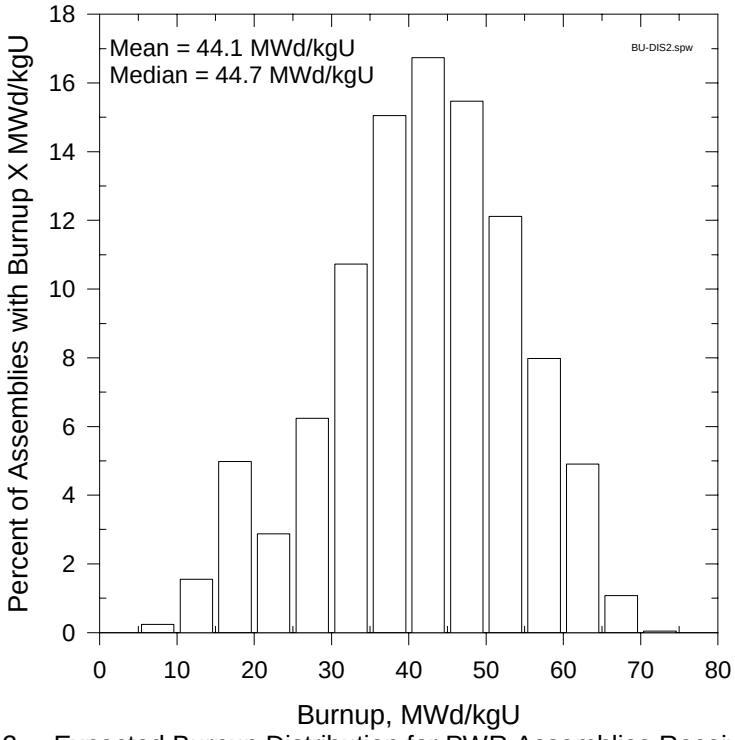

Figure 2. Expected Burnup Distribution for PWR Assemblies Received at YMP

DTN: MO0001SPAICC48.037

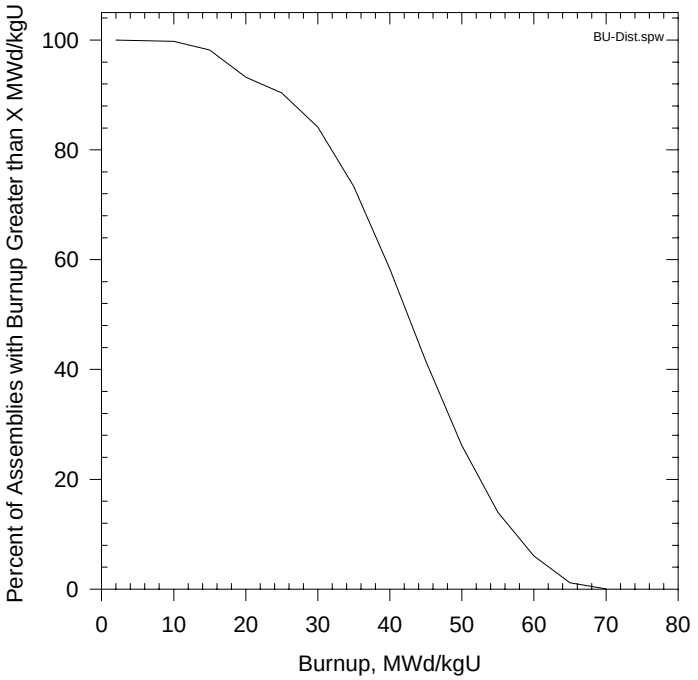

Figure 3. CCDF of Assembly Burnup for Fuel Received at YMP

DTN: MO0001SPAICC48.037

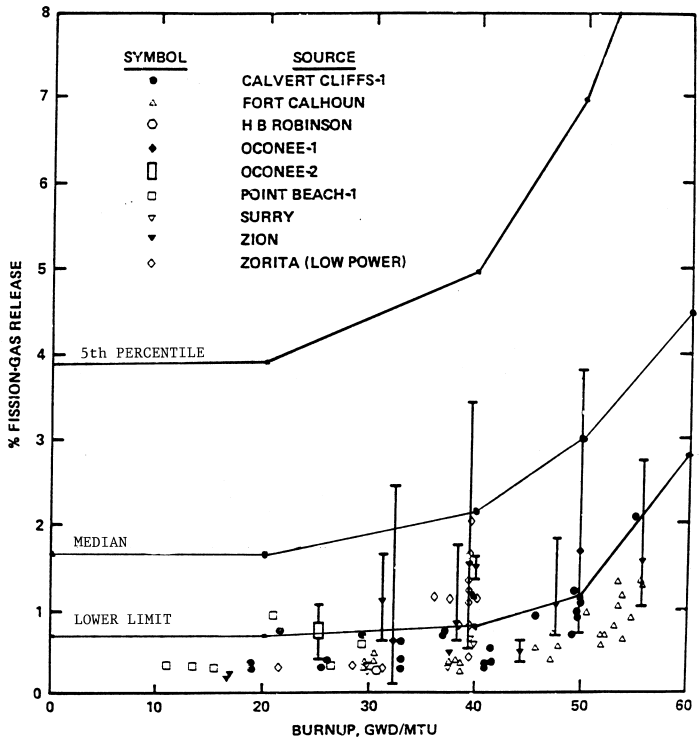

Figure 4. Fission Gas Release for U.S. PWR Fuel Rods (from Garde 1986)

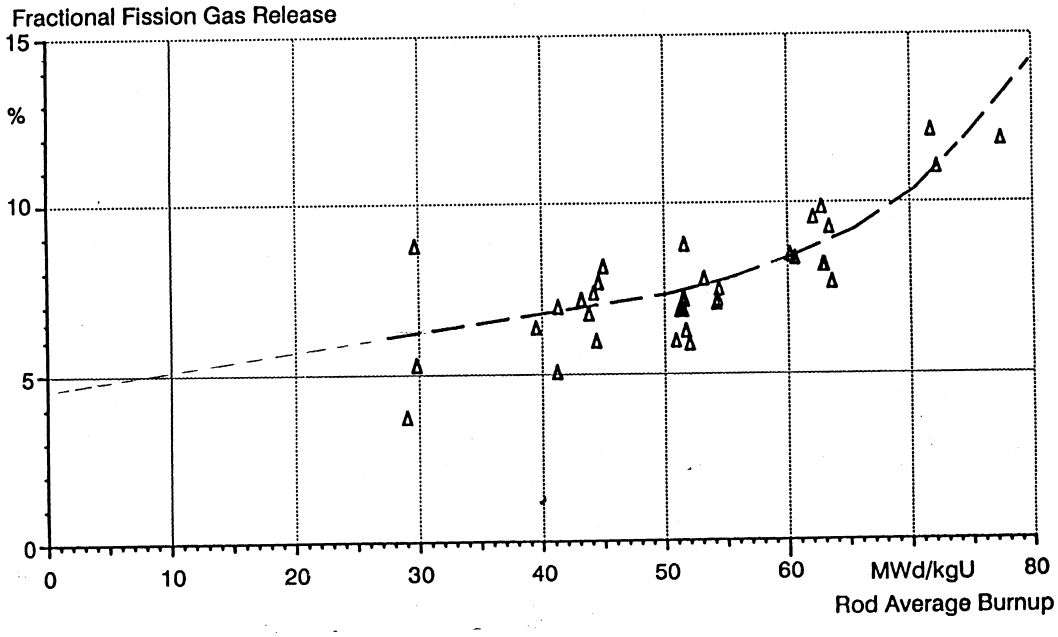

Figure 5. Fission Gas Release vs. Burnup (from Manzel and Coquerelle 1997)

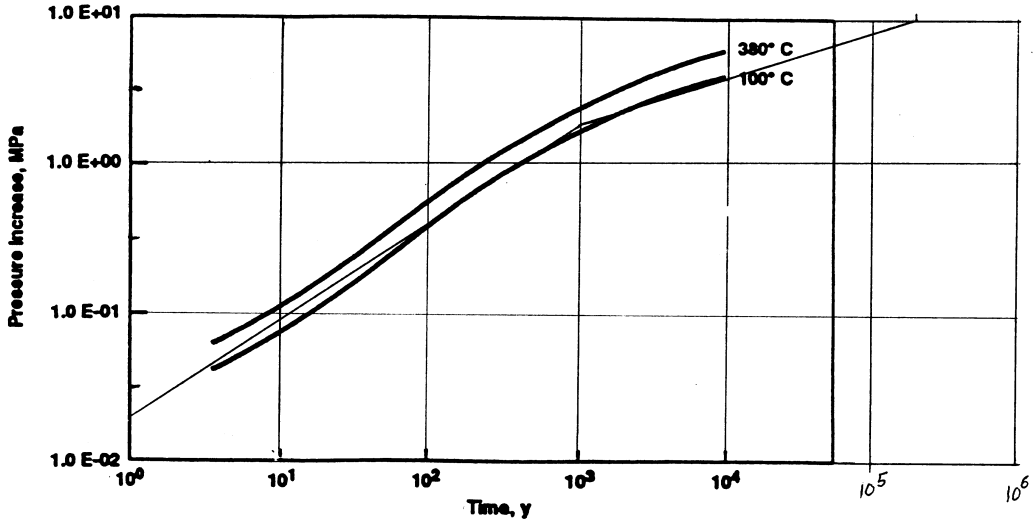

Figure 6. Helium Pressure from Alpha Decay (from Manaktala 1993)

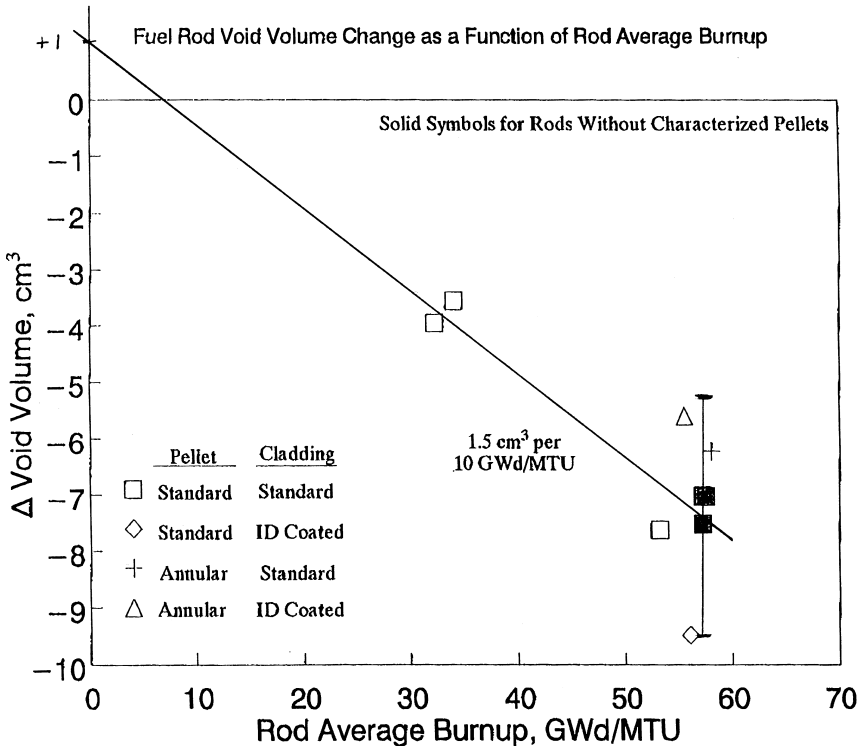

Figure 7. Fuel Rod Void Volume Change as a Function of Rod Average Burnup (from Smith et al. 1994)

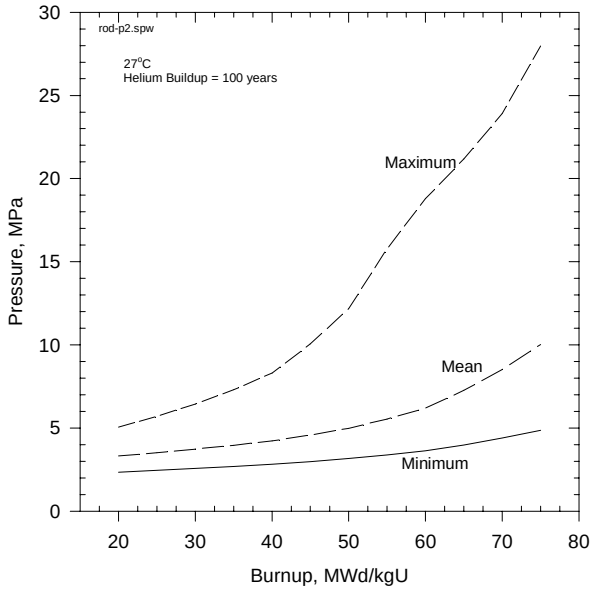

Figure 8. Rod Internal Pressure vs. Burnup

DTN: MO0001SPAICC48.037

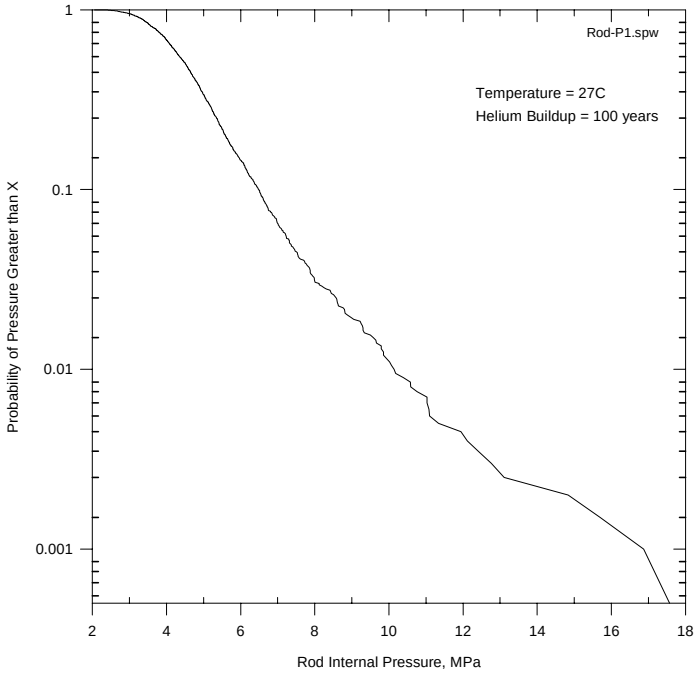

Figure 9. CCDF for Rod Internal Pressure

DTN: MO0001SPAICC48.037

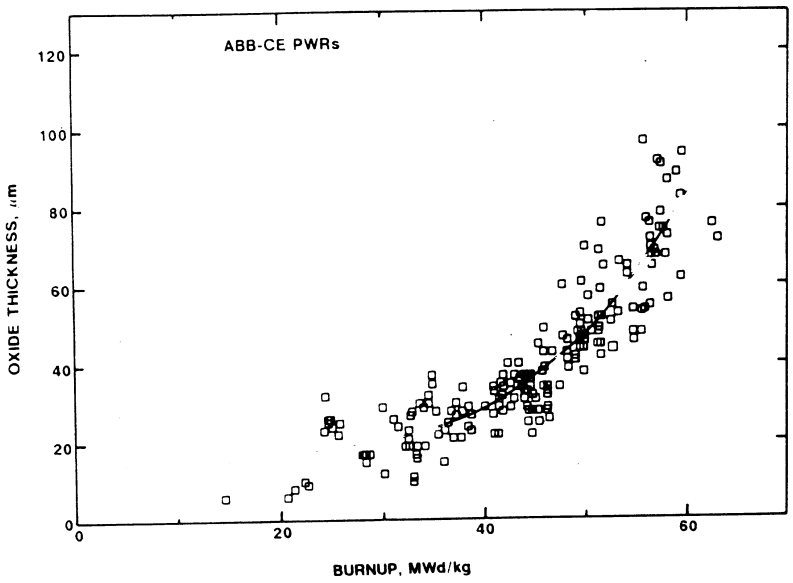

Figure 10. Cladding Oxide Thickness vs. Burnup Reported by Garde (1991)

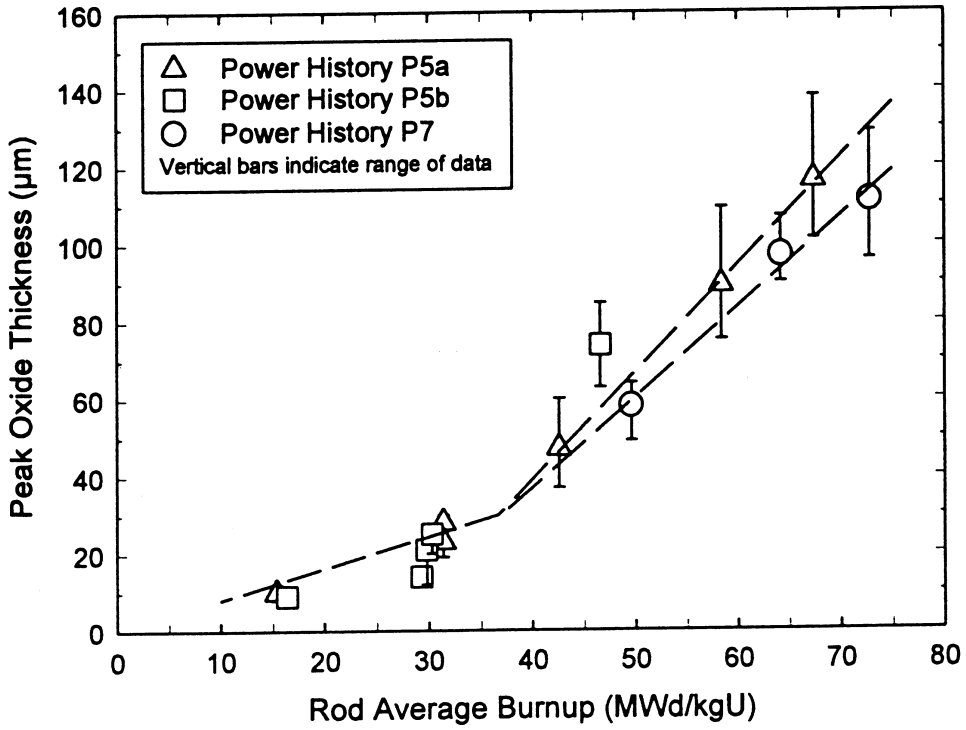

Figure 11. PWR Fuel Rod Oxide Thickness for High Burnup Fuels (from Van Swam et al. 1997a)

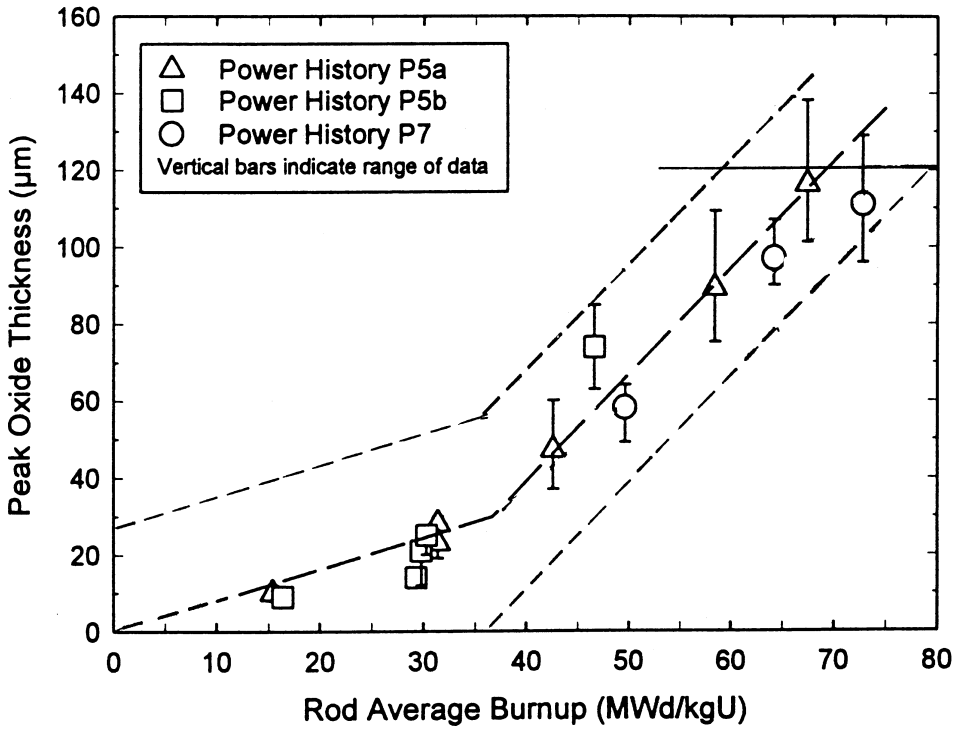

Figure 12. Mean Oxide Thickness and Range vs. Burnup

DTN: MO0001SPAICC48.037

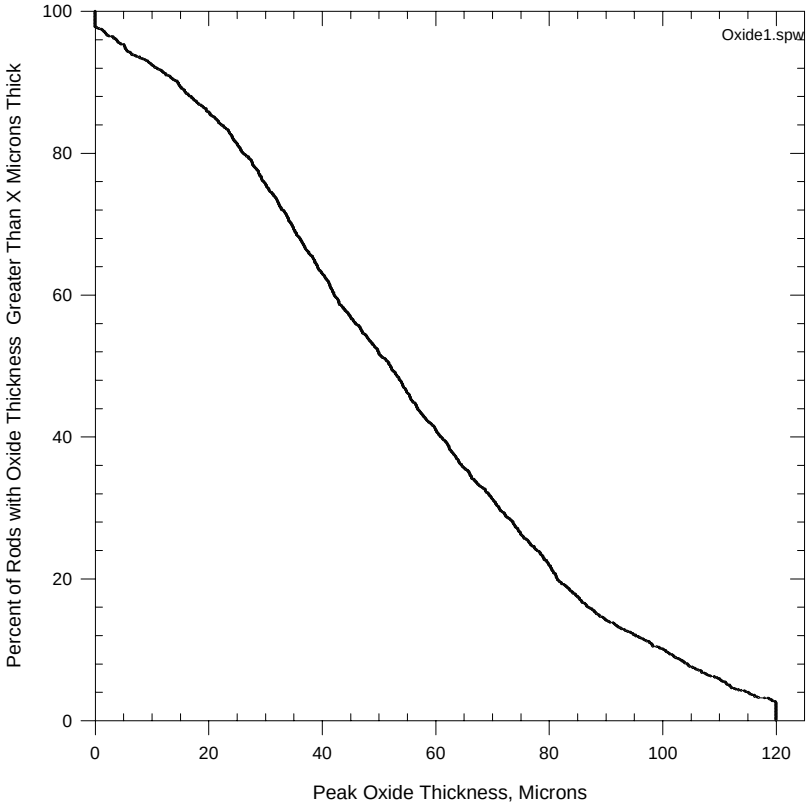

Figure 13. CCDF for Peak Rod Oxide Thickness

DTN: MO0001SPAICC48.037

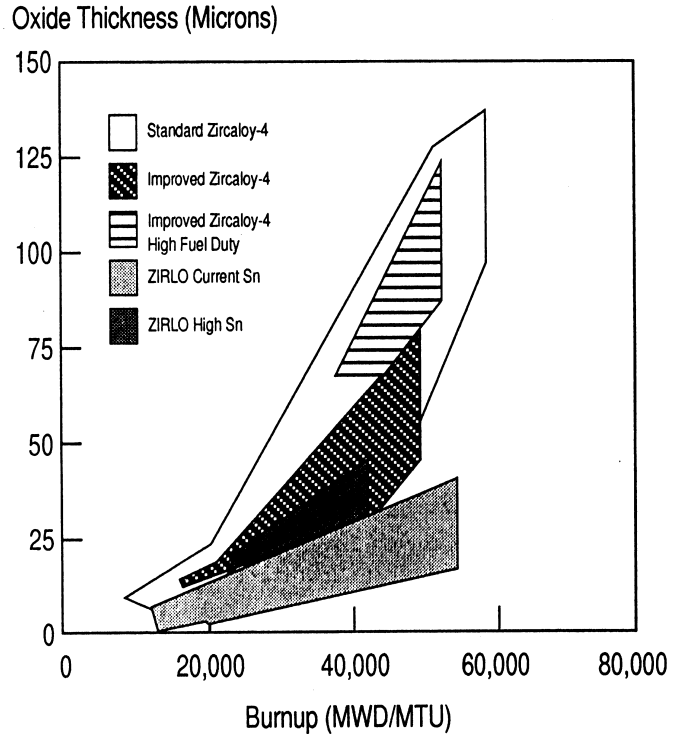

Figure 14. Corrosion: Oxide Thickness vs. Burnup for Alternative Fuel Rod Cladding Materials (from Wilson et al. 1997)

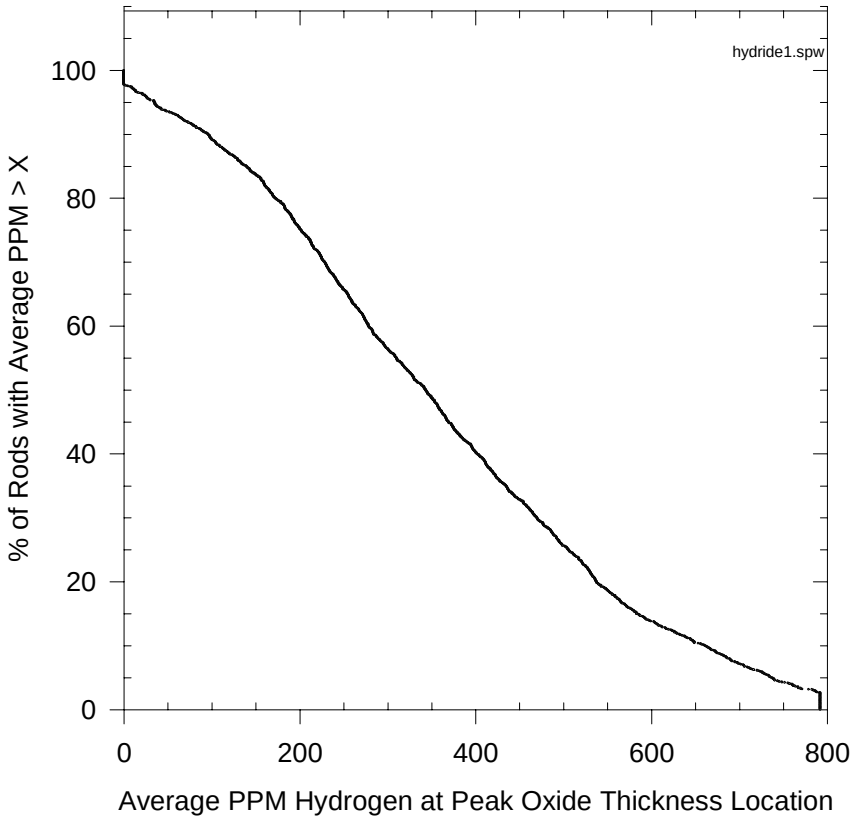

Figure 15. CCDF for Average Hydrogen Concentrations at Locations of Peak Cladding Oxide Thickness in PWR Fuel Rods

DTN: MO0001SPAICC48.037

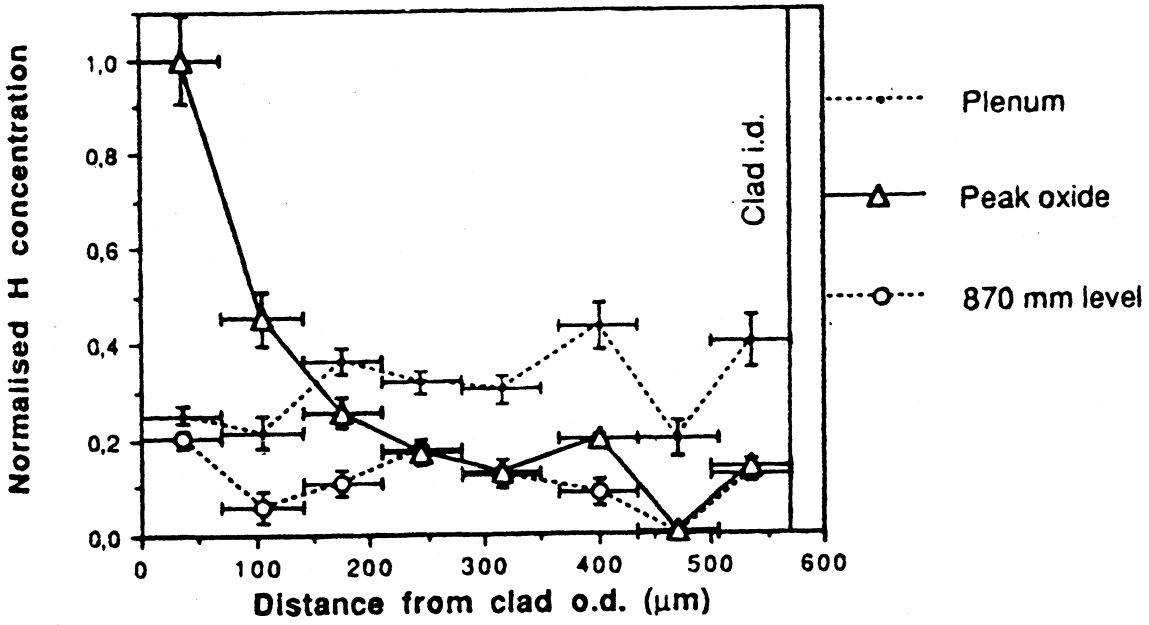

Figure 16. Cladding Radial Hydride Profiles (from Schrire et al. 1994)

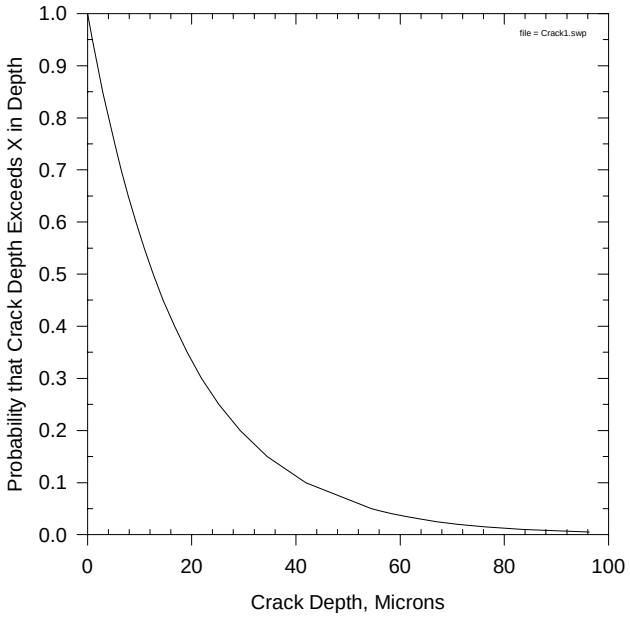

Figure 17. Crack Size Distribution for PWR Rods

DTN: MO0001SPAICC48.037

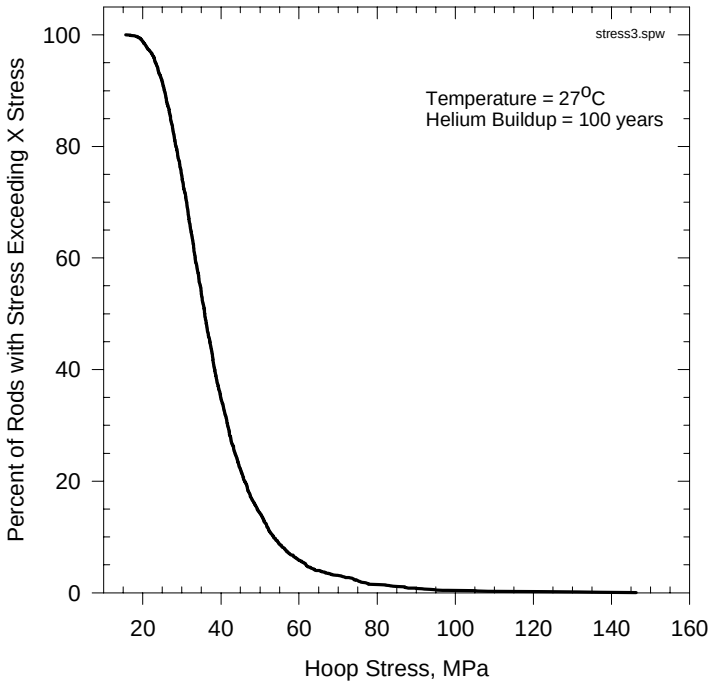

Figure 18. CCDF for Cladding Stress

DTN: MO0001SPAICC48.037

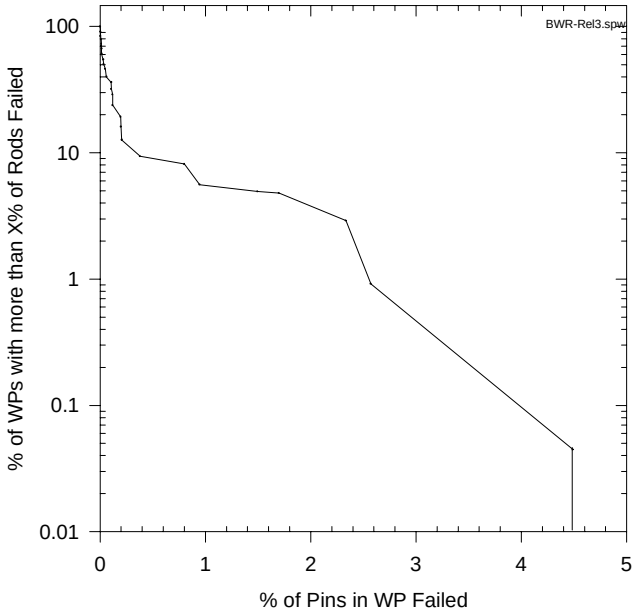

Figure 19. BWR: Distribution of Failed Rods in WPs

DTN: MO0001SPAICC48.037

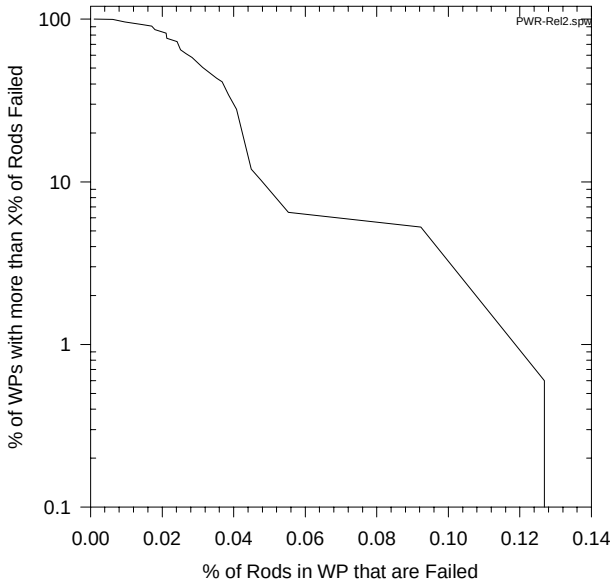

Figure 20. PWR: Distribution of Failed Rods in WPs

DTN: MO0001SPAICC48.037

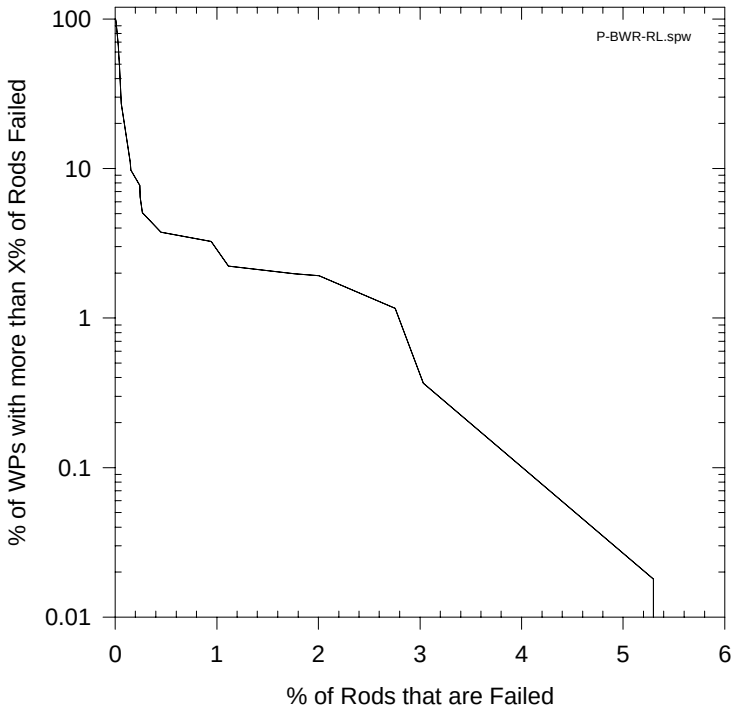

Figure 21. CCDF for Combined BWR & PWR Failed Rods in Waste Package

DTN: MO0001SPAICC48.037

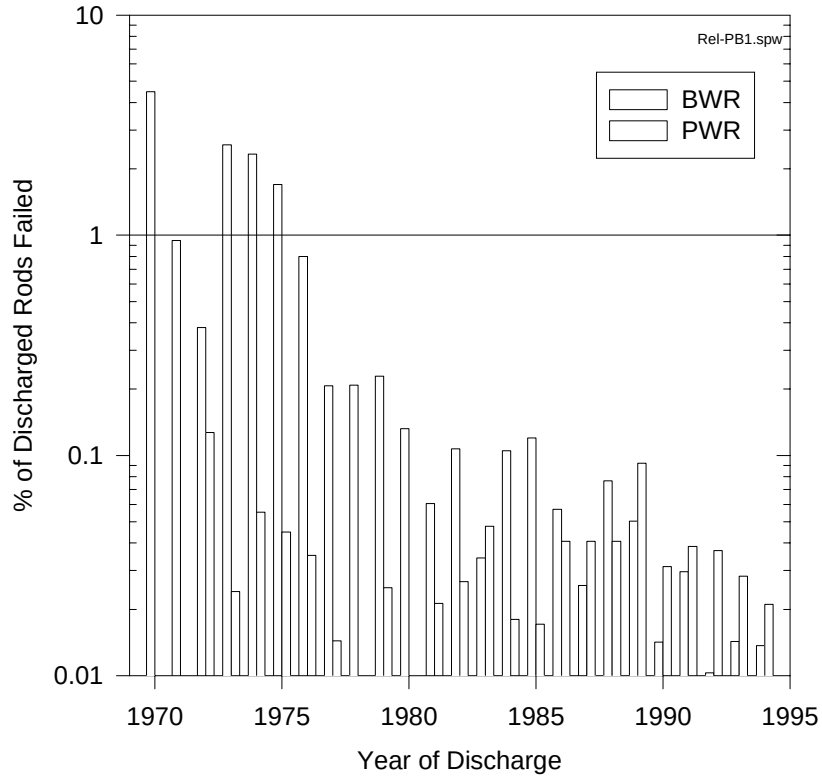

Figure 22. Fuel Reliability as a Function of Calendar Year

DTN: MO0001SPAICC48.037

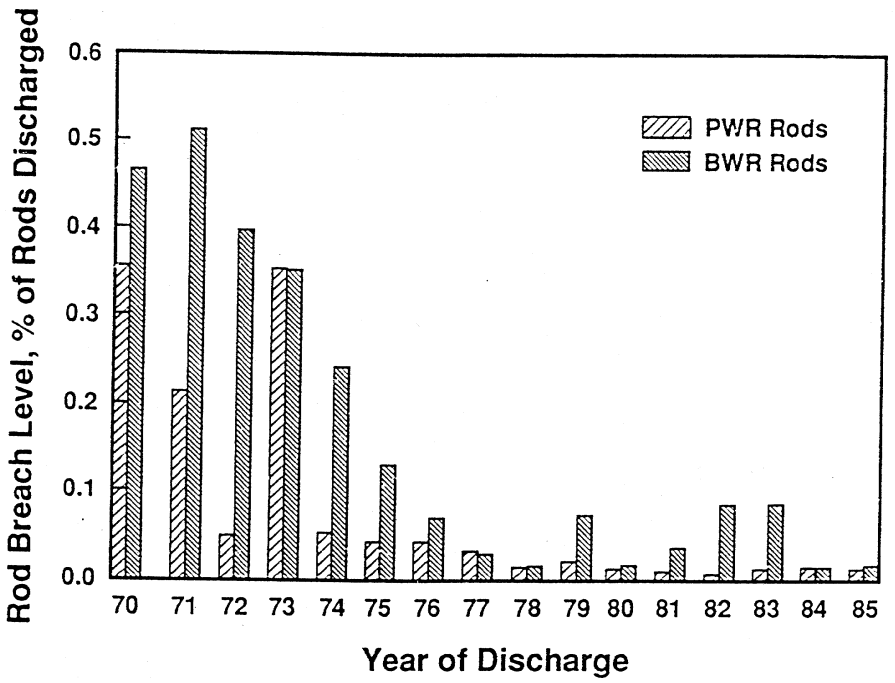

Figure 23. Fuel Rod Reliability Reported by Sanders et al. (1992)

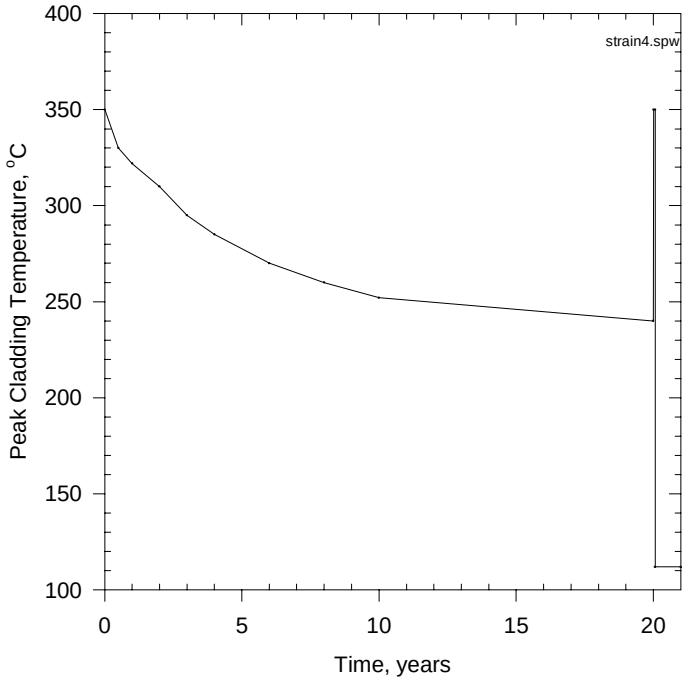

Figure 24. Temperature History Representing Dry Storage and Transportation

DTN: MO0001SPAICC48.037

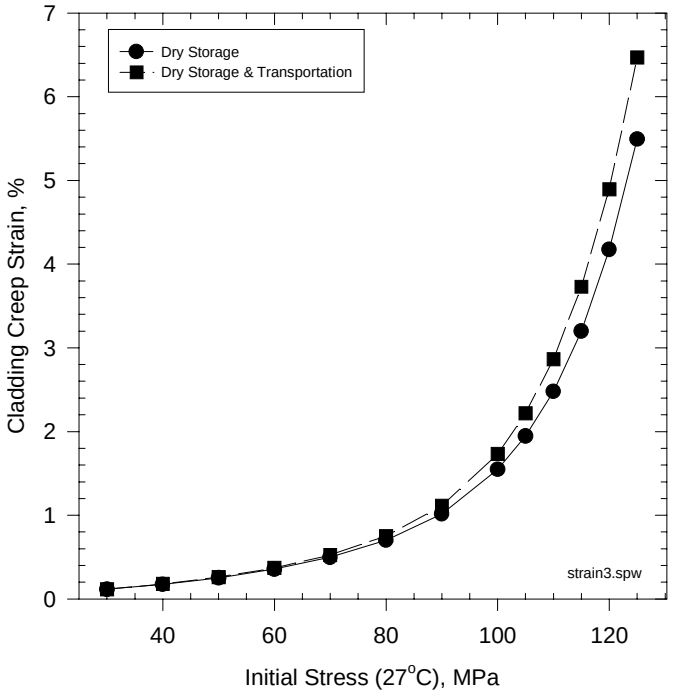

Figure 25. Cladding Creep Strain from Dry Storage and Transportation

DTN: MO0001SPAICC48.037

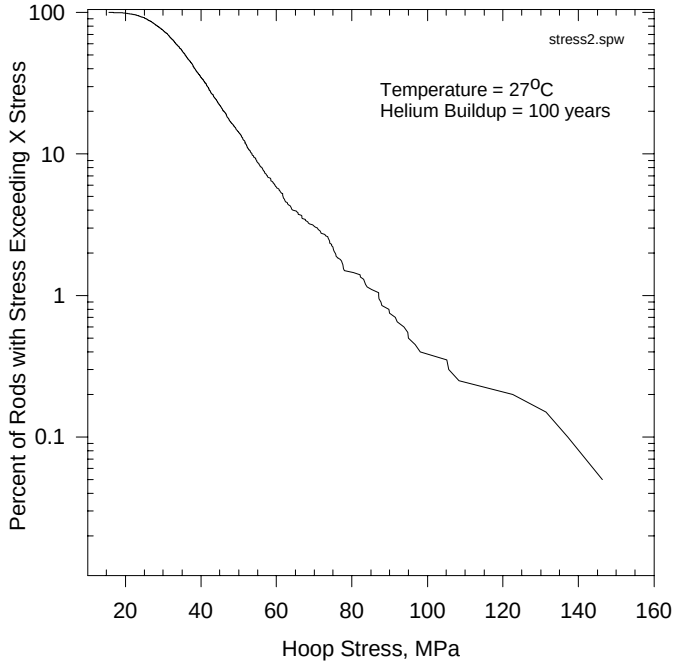

Figure 26. Details of CCDF for High Rod Stresses

DTN: MO0001SPAICC48.037

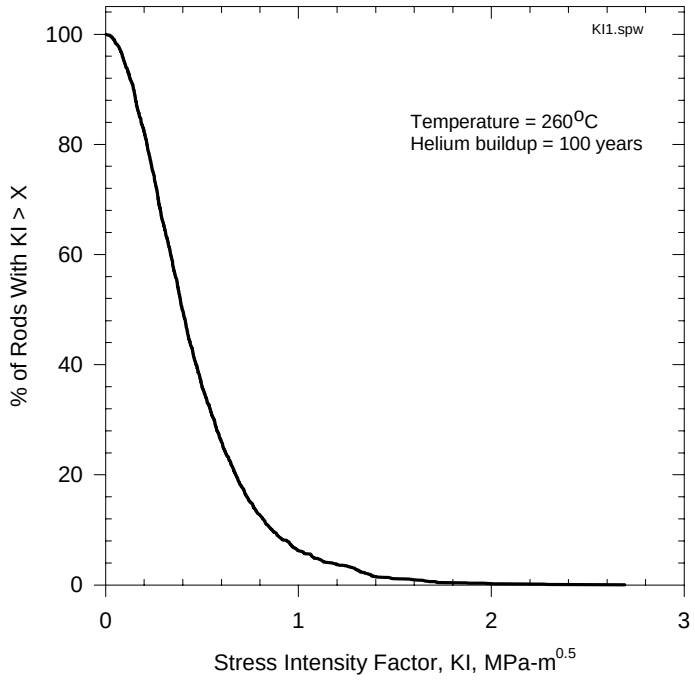

Figure 27. CCDF for Rod Stress Intensity Factors

DTN: MO0001SPAICC48.037

9. ATTACHMENTS

The attachments are listed as follows:

Attachment	Title	Pages
I	Rod Failure during Reactor Operation	5
II	Description of Software Routine: Rod-Initial-C.xls	19
III	NRC IRSR Issues Comparison	4

Attachment I
Rod Failures During Reactor Operation: BWR Data

	A	B	C	D	E	F	G	H	I	J	K	L
1	file = Rod-Initial-C.xls, Sheet = Reactor F							file = Rod-Initial-C.xls			Sheet = Reactor F	
2	**BWR Data**											
3	**YEAR**	**BWR (Total discharged)**	**BWR, Assembly damaged**	**% Assembly Damaged/yr**	**% of Total Assembly Damaged**	**Rods/ Assembly**	**Total Number Rods**	**Failed Rods**	**% FAILED Rods/yr.**	**Number of WPs/yr**	**% of Total BWR WPs**	**Source for Column C**
4	1969	96	32	33.33	0.05	49	4704	70.4	1.497	2.18	0.15	A
5	1970	29	29	100.00	0.04	49	1421	63.8	4.490	0.66	0.04	A
6	1971	413	87	21.07	0.13	49	20237	191.4	0.946	9.39	0.64	A
7	1972	801	68	8.49	0.10	49	39249	149.6	0.381	18.20	1.24	A
8	1973	564	323	57.27	0.50	49	27636	710.6	2.571	12.82	0.87	A
9	1974	1290	671	52.02	1.04	49	63210	1476.2	2.335	29.32	1.99	A
10	1975	1223	463	37.86	0.71	49	59927	1018.6	1.700	27.80	1.89	A
11	1976	1666	297	17.83	0.46	49	81634	653.4	0.800	37.86	2.57	A
12	1977	2047	108	5.28	0.17	56	114632	237.6	0.207	46.52	3.16	A
13	1978	2239	119	5.31	0.18	56	125384	261.8	0.209	50.89	3.46	A
14	1979	2131	124	5.82	0.19	56	119336	272.8	0.229	48.43	3.29	A
15	1980	3330	112	3.36	0.17	56	186480	246.4	0.132	75.68	5.14	A
16	1981	2467	42	1.70	0.06	62	152954	92.4	0.060	56.07	3.81	A
17	1982	1951	59	3.02	0.09	62	120962	129.8	0.107	44.34	3.01	A
18	1983	2698	26	0.96	0.04	62	167276	57.2	0.034	61.32	4.16	A
19	1984	2735	81	2.96	0.13	62	169570	178.2	0.105	62.16	4.22	A
20	1985	2928	99	3.38	0.15	62	181536	217.8	0.120	66.55	4.52	A
21	1986	2551	41	1.61	0.06	62	158162	90.2	0.057	57.98	3.94	B
22	1987	3316	24	0.72	0.04	62	205592	52.8	0.026	75.36	5.12	B
23	1988	2956	64	2.17	0.10	62	183272	140.8	0.077	67.18	4.56	B
24	1989	4020	57	1.42	0.09	62	249240	125.4	0.050	91.36	6.21	C
25	1990	3759	15	0.40	0.02	62	233058	33.0	0.014	85.43	5.80	C
26	1991	2872	24	0.84	0.04	62	178064	52.8	0.030	65.27	4.43	C
27	1992	4150	12	0.29	0.02	62	257300	26.4	0.010	94.32	6.41	C
28	1993	3974	16	0.40	0.02	62	246388	35.2	0.014	90.32	6.13	C
29	1994	3893	15	0.39	0.02	62	241366	33.0	0.014	88.48	6.01	C
30	1995	4684	4	0.09	0.01	62	290408	8.8	0.003	106.45	7.23	C
31												
32	sum	64783	3012		4.65		3878998	6626.4		1472.34	100.00	
33					% Rods failed, all years			0.170828				
34					% Rod failed through 1985			0.37				
35		A: Bailey and Wu 1990, Table 30, B: Potts and Proebste 1994, pTable 2, C: Yang 1997, Table 2										

Rod Failures During Reactor Operation: BWR, PWR, and Combined CCDFs

	A	B	C	D	E	F	G	H	I	J	K	L
38	**BWR CCDF for Rods Failed/WP**			**PWR CCDF for Rods Failed/WP**				**Combined CCDF**				
39	**BWR % FAILED Rods/WP**	**BWR, % WPs**	**BWR, CCDF**	**PWR, % FAILED Rods/WP**	**PWR, % WPs**	**PWR, CCDF**		**% Failed**	**CCDF BWR**	**CCDF PWR**	**CCDF Both**	**% failure incl. Incipient Failures**
40	0.0030	7.230	100.000	0.0000	0.451	100		0.0000	100.0000	100.0000	100.0000	0.000
41	0.0103	6.406	92.770	0.0061	3.098	99.549		0.0030	100.0000	99.7775	99.8658	0.004
42	0.0137	6.009	86.364	0.0095	3.543	96.451		0.0061	96.8879	99.5490	98.4931	0.007
43	0.0142	5.802	80.354	0.0144	2.356	92.908		0.0144	74.5112	92.9080	85.6082	0.017
44	0.0143	6.134	74.552	0.0171	4.332	90.552		0.0257	68.4176	63.6600	65.5478	0.030
45	0.0257	5.119	68.418	0.0180	4.122	86.220		0.0297	63.2990	54.8365	58.1944	0.035
46	0.0297	4.433	63.299	0.0211	5.609	82.099		0.0342	58.8658	45.1312	50.5811	0.040
47	0.0342	4.165	58.866	0.0213	3.373	76.490		0.0503	54.7011	8.9306	27.0923	0.059
48	0.0503	6.205	54.701	0.0241	0.351	73.117		0.0768	40.7499	5.7847	19.6589	0.090
49	0.0570	3.938	48.496	0.0241	7.801	72.766		0.1269	26.3970	0.6001	10.8363	0.148
50	0.0604	3.808	44.558	0.0251	3.536	64.965		0.1321	24.434	0.000	9.695	0.154
51	0.0768	4.563	40.750	0.0267	3.173	61.429		0.2073	19.294	0.000	7.656	0.241
52	0.1051	4.222	36.187	0.028	7.686	58.256		0.2088	16.134	0.000	6.402	0.243
53	0.1073	3.012	31.965	0.0313	7.364	50.570		0.2286	12.678	0.000	5.031	0.266
54	0.1200	4.520	28.954	0.0352	1.981	43.206		0.3812	9.388	0.000	3.725	0.444
55	0.1321	5.140	24.434	0.0370	7.026	41.225		0.8004	8.152	0.000	3.235	0.932
56	0.2073	3.160	19.294	0.0386	6.249	34.199		0.9458	5.580	0.000	2.214	1.102
57	0.2088	3.456	16.134	0.0408	15.978	27.949		1.4966	4.943	0.000	1.961	1.744
58	0.2286	3.289	12.678	0.0449	1.696	11.971		1.6997	4.794	0.000	1.902	1.980
59	0.3812	1.236	9.388	0.0476	3.779	10.275		2.3354	2.907	0.000	1.153	2.721
60	0.8004	2.572	8.152	0.0553	1.224	6.496		2.5713	0.915	0.000	0.363	2.996
61	0.9458	0.638	5.580	0.0923	4.673	5.273		4.4898	0.045	0.000	0.018	5.231
62	1.4966	0.148	4.943	0.1269	0.600	0.600						
63	1.6997	1.888	4.794									
64	2.3354	1.991	2.907									
65	2.5713	0.871	0.915									
66	4.4898	0.045	0.045									Both
67			BWR			PWR						
68		Median =	0.0554		Median =	0.0316					Median=	0.0346
69		Mean=	0.1963		Mean =	0.0298					Mean=	0.109
70		WPs =	1472.34		WPs =	2237.90					WPs =	3710.25
71		% of WPs	39.68		% of WPs	60.32						

Rod Failures During Reactor Operation: PWR Data

	A	B	C	D	E	F	G	H	I	J	K	L
73	**PWR DATA**											
74												
75	**YEAR**	**PWR (Total discharged)**	**PWR, Assembly damaged**	**% Assembly Damaged/yr**	**% of Total Assembly Damaged**	**Rods/ Assembly**	**Total Number Rods**	**Failed Rods**	**%FAILED Rods/yr.**	**Number of WPs/yr**	**% of Total PWR WPs**	**Source for Column C**
76												
77	1970	99	0	0.00	0.00	221.4	21919	0.0	0.0000	4.71	0.21	A
78	1971	113	0	0.00	0.00	221.4	25018	0.0	0.0000	5.38	0.24	A
79	1972	282	36	12.77	0.08	221.4	62435	79.2	0.1269	13.43	0.60	A
80	1973	165	4	2.42	0.01	221.4	36531	8.8	0.0241	7.86	0.35	A
81	1974	575	32	5.57	0.07	221.4	127305	70.4	0.0553	27.38	1.22	A
82	1975	797	36	4.52	0.08	221.4	176456	79.2	0.0449	37.95	1.70	A
83	1976	931	33	3.54	0.07	221.4	206123	72.6	0.0352	44.33	1.98	A
84	1977	1107	16	1.45	0.03	221.4	245090	35.2	0.0144	52.71	2.36	A
85	1978	1665	16	0.96	0.03	221.4	368631	35.2	0.0095	79.29	3.54	A
86	1979	1662	42	2.53	0.09	221.4	367967	92.4	0.0251	79.14	3.54	A
87	1980	1456	9	0.62	0.02	221.4	322358	19.8	0.0061	69.33	3.10	A
88	1981	1585	34	2.15	0.07	221.4	350919	74.8	0.0213	75.48	3.37	A
89	1982	1491	40	2.68	0.09	221.4	330107	88.0	0.0267	71.00	3.17	A
90	1983	1776	85	4.79	0.18	221.4	393206	187.0	0.0476	84.57	3.78	A
91	1984	1937	35	1.81	0.07	221.4	428852	77.0	0.0180	92.24	4.12	A
92	1985	2036	35	1.72	0.07	221.4	450770	77.0	0.0171	96.95	4.33	A
93	1986	2291	94	4.11	0.20	221.4	507227	206.9	0.0408	109.10	4.87	B
94	1987	2593	106	4.11	0.23	221.4	574090	234.2	0.0408	123.48	5.52	B
95	1988	2625	108	4.11	0.23	221.4	581175	237.1	0.0408	125.00	5.59	B
96	1989	2196	204	9.29	0.43	221.4	486194	448.8	0.0923	104.57	4.67	C
97	1990	3461	109	3.15	0.23	221.4	766265	239.8	0.0313	164.81	7.36	C
98	1991	2937	114	3.88	0.24	221.4	650252	250.8	0.0386	139.86	6.25	C
99	1992	3302	123	3.73	0.26	221.4	731063	270.6	0.0370	157.24	7.03	C
100	1993	3612	103	2.85	0.22	221.4	799697	226.6	0.0283	172.00	7.69	C
101	1994	2636	56	2.12	0.12	221.4	583610	123.2	0.0211	125.52	5.61	C
102	1995	3666	89	2.43	0.19	221.4	811652	195.8	0.0241	174.57	7.80	C
103												
104	sum	46996	1559				10404914	3430.4		2237.90	100.00	
105					% rods failed, all yrs =			0.0330				
106					% rods failed, thru 1985=			0.0255				
107					% PWR+BWR rods failed, all yrs			0.070407				
108	A: Bailey and Wu 1990, Table 30, B: Rod failure Rate during this three year perion is average of previous and future 3 years (avg. of 6 yrs).											
109	C: Yang 1997, Table 2											

Rod Failures During Reactor Operation: Final CCDF for Fuel Rods Failed Before Receiving at YMP

	A	B	C	D	E	F	G	H	I	J	K	L
111	**Calculation of Average Number of pins/PWR assembly**						**Table 14 in AMR, used in Total Cladding Abstraction**					
112												
113	**Type**	**Rods/assembly**	**Assemb Discharged**	**Rods * discharge**			**CCDF Both**	**Lower Unc.**	**% failure incl. All**	**Upper Unc**		error factor =
114	W1717	264	14874	3926736			1.0000	0.0138	0.0550	0.2200		4
115	W1515	204	7490	1527960			0.9987	0.0146	0.0585	0.2341		
116	B&W1515	208	5435	1130480			0.9849	0.0155	0.0622	0.2486		
117	CE1414	164	4565	748660			0.8561	0.0179	0.0717	0.2869		
118	W1414	179	4093	732647			0.6555	0.0212	0.0849	0.3397		
119	CE1616	224	2340	524160			0.5819	0.0224	0.0895	0.3582		
120	sum		38797	8590643			0.5058	0.0237	0.0948	0.3793		
121	average =	221.425445					0.2709	0.0284	0.1136	0.4545		
122	rods/WP	4649.93435					0.1966	0.0361	0.1445	0.5780		
123	W1717 Rods	5544					0.1084	0.0507	0.2028	0.8111		
124							0.0970	0.0522	0.2089	0.8357		
125							0.0766	0.0741	0.2965	1.1859		
126							0.0640	0.0746	0.2983	1.1930		
127	Andrews and Matzie						0.0503	0.0803	0.3213	1.2853		
128	799,500	620,100	450,100	109,000	1,978,700	0.010866	0.0373	0.1248	0.4990	1.9962		
129	140	50	25	0	215		0.0323	0.2469	0.9875	3.9499		
130							0.0221	0.2892	1.1568	4.6274		
131							0.0196	0.4496	1.7985	7.1941		
132							0.0190	0.5088	2.0352	8.1408		
133							0.0115	0.6939	2.7757	11.1029		
134							0.0036	0.7626	3.0505	12.2022		
135							0.0002	1.3214	5.2856	21.1424		
136							0.0000	1.3214	5.2856	21.1424		
137												
138												
139												

Interpolation of PWR and BWR CCDFs To Generate Combined CCDF

	A	B	C	D	E	F	G	H	I	J	K	L	M	N	O
141	**PWR interpolation for CCDF**					**Combining of CCDFs**					**BWR Interpolation for CCDF**				
142	PWR	PWR	PWR	PWR	PWR						BWR	BWR	BWR	BWR	BWR
143	% FAILED	CCDF	fail dif	ccdf dif	Interpolate	BOTH, %	BWR	PWR	combined		% FAILED	CCDF	fail dif	ccdf dif	Interpolat
144	0.0000	100	0.0061	-0.4510	99.7775029	0	100	100	100		0	100	0.0030	0.0000	
145	0.0061	99.549	0.0034	-3.0981		0.00303022	100	99.7775	99.86578972		0.0030	100.0000	0.0072	-7.2303	96.88794
146	0.0095	96.45086399	0.0048	-3.5429		0.006142232	96.887938	99.549	98.49309071		0.0103	92.7697	0.0034	-6.4060	
147	0.0144	92.90800928	0.0027	-2.3555		0.0144	74.511	92.90801	85.60816741		0.0137	86.3637	0.0005	-6.0093	
148	0.0171	90.55248966	0.0009	-4.3323		0.0257	68.4176	63.65998	65.54781829		0.0142	80.3544	0.0001	-5.8024	
149	0.0180	86.22020606	0.0032	-4.1216		0.0297	63.2990	54.83645	58.19439822	Median	0.0143	74.5520	0.0114	-6.1343	74.51123
150	0.0211	82.09857869	0.0002	-5.6090		0.0342	58.8658	45.13121	50.58107537	0.0345937	0.0257	68.4176	0.0040	-5.1186	
151	0.0213	76.48959069	0.0028	-3.3726		0.0503	54.7011	8.930604	27.09232858		0.0297	63.2990	0.0045	-4.4333	
152	0.0241	73.11696323	0.0000	-0.3511		0.0768	40.7499	5.78472	19.65889865		0.0342	58.8658	0.0161	-4.1647	
153	0.0241	72.76586952	0.0010	-7.8007		0.126852332	26.396965	0.600109	10.83630146		0.0503	54.7011	0.0067	-6.2053	
154	0.0251	64.96520563	0.0015	-3.5365	63.6599777						0.0570	48.4957	0.0034	-3.9378	
155	0.0267	61.42873445	0.0017	-3.1726							0.0604	44.5580	0.0164	-3.8081	
156	0.0283	58.25612401	0.0030	-7.6858	54.8364549	Median					0.0768	40.7499	0.0283	-4.5629	
157	0.0313	50.57036352	0.0039	-7.3645	45.1312086	0.031598777					0.1051	36.1870	0.0022	-4.2218	
158	0.0352	43.20590697	0.0018	-1.9810							0.1073	31.9652	0.0127	-3.0116	
159	0.0370	41.22488731	0.0016	-7.0261							0.1200	28.9536	0.0122	-4.5197	26.39697
160	0.0386	34.19875743	0.0022	-6.2495							0.1321	24.4339	0.0751	-5.1402	
161	0.0408	27.94928939	0.0041	-15.9780							0.2073	19.2936	0.0015	-3.1598	
162	0.0449	11.97128939	0.0027	-1.6959							0.2088	16.1339	0.0198	-3.4562	
163	0.0476	10.27540037	0.0077	-3.7790	8.93060417						0.2286	12.6777	0.1526	-3.2894	
164	0.0553	6.496355349	0.0370	-1.2235	5.78471992						0.3812	9.3883	0.4192	-1.2364	
165	0.0923	5.272846966	0.0345	-4.6727							0.8004	8.1518	0.1454	-2.5717	
166	0.1269	0.60010886									0.9458	5.5802	0.5508	-0.6375	
167											1.4966	4.9427	0.2031	-0.1482	
168											1.6997	4.7945	0.6357	-1.8878	
169											2.3354	2.9066	0.2359	-1.9913	
170											2.5713	0.9154	1.9185	-0.8706	
171											4.4898	0.0448	-4.4898	-0.0448	
172															

Attachment II

Description of Software Routine: Rod-Initial-C.xls

The statistical analysis of the rod initial conditions is performed in the routine "Rod-Initial-C.xls" (Version is file date, 1/25/00) which is included in the DTN file: MO0001SPAICC48.037. Microsoft Excel for Windows Version 4.0 was used for the analysis and the analysis is documented in this AMR as a software routine. The analysis was performed on a Dell Pentium personal computer (CPU number 111920) with a WINDOWS 95 operating system. This attachment describes the various sheets that compose this routine, including a listing of the top of each sheet of the file, and correlates the various equations presented in the text of this report to the routine.

The routine (spreadsheet) contains 12 sheets, many of which are linked. Each sheet addresses a specific aspect of cladding condition. Table II-1 summarizes the different sheets.

Table II-1. Description of Sheets in Rod-Initial-C.xls

Sheet Title	Subject	Equations	Dependencies
Burnup	Burnup distribution	Initial distribution	BU, sheet: WP-BU-A
Corrosion	Oxide thickness and hydride formation	6.4-1	Burnup (BU)
Crack	Crack size	6.6-4	None
Crack	Stress	6.7-1	Pressure, Crack Size, Oxide thickness
Crack	Stress intensity, K_I	6.10-2	Stress, Crack Size
Creep	Creep in dry storage and transportation	6.10-1	Stress, Temperature, Time
FGR	Fission gas release	Table 4	BU
Free Vol.	Rod free volume	6.3-5	BU
He Pres.	Helium pressure, alpha particles	6.3-4	Time, BU, Temperature
Pressure	Pressure Distribution	6.3-2, 6.3-3, 6.3-4, 6.3-5	BU, He, FGR, F Vol.,T, Pfill
P vs BU	Rod pressure distribution for fixed BU	6.3-2, 6.3-3, 6.3-4, 6.3-5	BU, He, FGR, F Vol.,T, Pfill,
Rand #	Table of random numbers	None	Used in all sampling
Reactor F	Reliability of Rods in Reactor Operation	None	Listed in Attachment I
WP-BU-A	Distribution of burnup	None	Burnup (BU)

The first 30 to 40 lines of each sheet are included (in alphabetical order) in this attachment (Table II-3 to II-14). Many of the sheets have 2000 lines of statistical sampling and only the first few rows are included. A brief description of each sheet follows including the testing and test results.

This analysis is based on observed fuel performance for PWR fuel and therefore there are constraints, caveats and limitations to this analysis. This analysis is only applicable to

U.S. commercial pressurized water reactor fuel with Zircaloy cladding. It is also limited to fuel exposed to normal operation and anticipated operational occurrences (AOOs) and not fuel that has been exposed to severe accidents. Fuel burnup projections have been limited to the current commercial power licensing environment with restrictions on fuel enrichment, oxide coating thickness and rod plenum pressures. The ranges of applicability are:

1. Temperature: 27°C to 420°C. The upper temperature limit is the highest temperatures of Matsuo's experiments. This is also the approximate temperature of the ID of the cladding during normal operation in a PWR (340°C to 370°C, (Pescatore et al. 1990, Table 3, p. 7)). The lower limit is not important since the cladding degradation rates become negligible at these temperatures.

2. Stress: 0 to 314 MPa. The lower limit is not important because low stress does not cause damage. The upper limit is the upper limit of Matsuo's tests for which the creep equation was derived.

3. Burnup: 2 to 80 MWd/kgU, the approximate range of experiments reported in this AMR.

The analysis itself addresses the uncertainties of the various parameters. Uncertainty ranges are defined for each parameter based on experimental observations reported in the literature. These uncertainties are statistically combined in the sampling routine. The range for each parameter is defined and justified in the body of this AMR.

Burnup Sheet

The burnup distribution is developed in Section 6.2 and shown in Figure 3. The raw data is presented in sheet "WP-BU-A." The BU distribution is reproduced in cells A2 through G17 and rows 20 and 21. Column A, Rows 29 through 2028 are two thousand (2000) random samplings of the burnup distribution described in Rows 2 through 16. The random number is given in Column B and taken from the sheet "Rand #", Column A. The sample case number (Column C) is generated so that the characteristics of a specific sampling can be identified.

This sheet can be tested through inspection and comparison. The BU distribution has a median of 44.7 and a mean of 44.1, in good agreement with the original data abstraction (Rows 2-16) which has a median of 45.0 and a mean of 41.8. Visual inspection of the interpolation of the random number (Column B) with the burnup distribution (Rows 20 and 21) shows that the interpolation is correct.

Corrosion Sheet

The first 25 rows of this sheet contain the fitting of the linear equations to Figure 12 and the derivation of Equation 6.4-1. For testing, Rows 13, 17, and 22 demonstrate that the equation confirms the fit is correct (oxide thickness same as Cells B8, B9, and B10). Rows 27 through 2026 contain the 2000 samples of oxide thickness (Column C) and

hydride formations (Column H) for the case number (Column A) and burnups (Column B). Again, the random number for the uncertainty in oxide thickness is taken from sheet "Rand#", Column G. This analysis can be further tested by comparing the results (Column C for specific burnups (Column B) against the desired results shown in Figure 12. Oxide thickness are used in calculating stress.

Crack Sheet

This sheet contains the calculation of crack size, cladding stress, and crack stress intensity factor distributions. Column A contains the sample ID number. The crack depth is evaluated using Equation 6.6-4 and given in Column B of rows 16 through 2015. This can be tested by a hand calculation using the equation given in Row 9 and the random number given in Column D (value from sheet "Rand #", Column F). Using the pressure from the "Pressure" sheet for each sample, the stress (Column G, using Eq. 6.7-1) and stress intensity factor (Column F, using Eq. 6.10-2) are calculated. The wall thickness for each sample is given in Column I where the metal loss from general corrosion (sheet "Corrosion", Column C for each sample) is subtracted off after adjusting for the difference between metal and oxide thickness. Column M contains the CCDF (ordered values of stress) that will be used in the *Clad Damage – Summary and Abstraction* AMR and is plotted as Figures 18 and 26. Column L contains the CCDF for the stress intensity factor, shown as Figure 27. Column N contains the CCDF for the crack length and is shown as Figure 17. This sheet can be tested by a hand calculation for any row of samples since the random number and all equations are given.

Creep Sheet

This sheet calculated the creep strain for a given initial room temperature stress. The results of this analysis are given in Cells H4 through J20 and plotted in Figure 25. Equation 6.10-1 is used to calculate the creep strain. The actual calculations are performed in Rows 25 through 39. The room temperature stress is specified as an input in Cell H24 and the resulting strains are shown in cells I24 and J24. The room temperature stress is varied and the resulting strain is copied and saved in the Cells H4 through J20. The details of the creep analysis are as follows:

Rows 25 through 39

Column	Description
A	Not used
B	Time, years
C	Gives the cladding temperatures, ^{o}C, at that time
D	The average temperature over the time interval (in Kelvin)
E	Stress, adjusted for the average temperature in time interval using ideal gas law for the fission gas in the gas plenum, MPa
F	Time duration of the time step in hours
G	Total running sum of creep (both types, all previous time steps)
H	Sum of primary and secondary creep for time interval

I Running sum of primary creep, all time intervals
J Potential primary creep for time interval (amount of saturated primary creep that is possible in time interval)
K Actual primary creep for time interval (amount of primary creep you could get above previous time step)
L Secondary creep for time interval (rate * time interval)
M Secondary creep rate (slope of secondary term)
N Saturated primary creep, maximum amount of primary creep possible
O Youngs module, E
P Temperature coefficient for Arrhenius term
Q Ec term

The creep correlation developed by Matsuo (1987, pp. 23, 26) was used and is given below:

$$Ec = 3.62E12*(E/T)*\exp(2.4E3*stress/E)*\exp(-2.72E5/(RT)) \quad \text{(Eq. 6.10-1)}$$
$$Es = 1.57E13*(E/T)*[\sinh(1.13E3*stress/E)]^{2.1}*\exp(-2.72E5/RT),,$$
$$Esp = 2.16E\text{-}2*Ec^{0.109},$$
$$Strain = esp*(1-\exp(-52*(Es*t)^{0.5})) + Es*t$$

Where

Strain	=	Total Creep Strain, %
Ec, Es, esp	=	Strain Components
Ec	=	Calculated creep rate component
Es	=	Steady state creep rate, units = %
esp	=	Saturated primary (transient) creep strain, units = %

Inputs:

stress	=	Stress, MPa
t	=	Time, hrs
T	=	Temperature, Kelvin
E	=	114800-59.9*T, Young's modulus, MPa
R	=	8.3169, gas constant, j/mole-T_k

Test Case: In Rows 43 through 47 of the sheet Creep is a test case. This case is presented in CRWMS M&O 2000a and is an analysis of three experiments reported by Matsuo. The test conditions are: time duration = 960 hours, temperature = 360^{o}C, stress = 118 MPa at 360^{o}C (55.9 MPa at 27^{o}C). The measured strains (three tests) were 0.33, 0.40, and 0.44%. CRWMS M&O (2000a), reports a calculated creep of 0.38%, the same result as shown in Row 47 and Cell G47. This demonstrated that the equations were programmed correctly. Visual inspection and hand calculations were also performed.

FGR Sheet

The FGR sheet calculates the Fission Gas Release (FGR) for the 2000 realizations (Rows 39 through 2038). FGR is a function of burnup as represented in Table 4 and is reproduced in Cells A25 through G31 and Rows 36 and 37. For each burnup sample (Column A, taken from the sheet "Burnup", Column A), the FGR (excluding uncertainty) is calculated (Column J) by performing a linear interpolation of the BU and FGR values listed in Rows 36 and 37, Columns K through P. This linear interpolation can be tested by visual inspection and hand calculation. A random number is taken from sheet "Rand #", Column B and listed in Column C, after converting to percents. The uncertainty is then calculated by performing a linear interpolation on the uncertainty CCDF given in Cells C36 through I37. This interpolation is shown in Columns D through H and the final uncertainty multiplier is given in Column I. Again a visual inspection and hand calculation of the linear interpolation are the test. The final FGR is given in Column B and is the product of the uncertainty multiplier (Column I) and the burnup dependent median FGR (Column J), limited to 50% FGR maximum. This can be tested by visual inspection and hand calculation of any row of the sampling.

Free Volume Sheet

The free volume inside the rod is calculated using Equation 6.3-5 and is used to calculate the pressure and therefore the stress. The free volume is dependent on the burnup (Column B, taken from the "Burnup" sheet). Rows 4 through 24 calculate various characteristics of the CE 16 x 16 and W1717WL rods. Rows 28 through 2027 contain the free volume (Column C) for each realization. Column E contains the random number from sheet "Rand #", Column D and is used to calculate the volume lost (Column F) using the equation given on Row 21. This sheet is tested by visual inspection and hand calculation. A second test can be performed by comparing the lost free volume with Figure 7 for the specific burnup in Column B.

Helium Pressure (He Pres.) Sheet

The derivation of Equation 6.3-4 is given in Rows 2 through 24. These are linear fits to the straight lines shown in Figure 6. Rows 14 through 24 gives the tests of these fitted equations and show that they predict the points that were used to generate the fits. Table 7 is calculated in Rows 26 through 35 for a initial fill and fission gas pressure of 4 MPa and 27^{o}C. Column C of Rows 40 through 2039 contain the helium pressures for the 2000 realizations (identified in Column A) and burnups (Column B, from sheet "Burnup", Column A). Column D gives the random number for the release fraction uncertainty given in Column E. Columns G and H calculated the helium production for time periods less than or greater than 1000 years. This realization is performed for the time and temperature specified in the "Pressure" sheet (Cell B3 and B4) and repeated in Cell D38 and Cell F38. The helium pressure is included in calculating the total pressure. This sheet is tested by a hand calculation of any row in the sampling.

Pressure Sheet

The pressure for the 2000 samples is calculated in Rows 22 through 2021. Table II-2 identifies the contents of the columns. The resulting pressure distribution is listed in Columns A and B and plotted as Figure 9. This pressure distribution is used to generate the stress distribution used in the Clad Degradation – Summary and Abstraction AMR. The analysis is performed for the temperature specified in Cell B3 and the time (for helium production) specified in Cell B4. The equations used are given in Rows 7 through 10. The uncertainty used for the fill gas pressure uses the random number from sheet "Rand #", Column C. For testing, Columns D, G, H, and J can be verified by hand calculations of any sample row. In addition Section 6.3.6 compares the resulting pressure distribution with pressures reported in the literature.

Table II-2
Column Description for Pressure Sheet

Column	Description	Source
A	CCDF for ordered pressures (Col. B)	Index from 100% to zero
B	Ordered pressure, MPa	Col. D, Fixed for 27^{o}C
C	Sample Number	BU sheet
D	Pressure for sample	Sum, Columns G + H + J.
E	Burnup	BU sheet
F	Free volume	Free volume sheet
G	Fill pressure	Calculated, Eq. 6.3-1
H	Fission gas pressure	Calculated, Eq. 6.3-2
I	FGR %	FGR sheet
J	Helium pressure	Helium sheet

P vs. BU Sheet

This sheet is used to generate Figure 8, Rod Internal Pressure vs. Burnup. It is identical to the pressure sheet except all 2000 realizations are performed at the same burnup (Column E), specified in Cell F3. The region F5 Through J17 is the resulting pressures and is used to generate Figure 8. This sheet is tested in the same fashion as the Pressure sheet.

Rand # Sheet (Random Number Sheet)

This sheet contains 2000 rows of random numbers that were fixed after they were generated. This has the same effect as using a fixed seed in a random number generator and is needed if the user is to get the same answer each time the user accesses the routine (spreadsheet). Row 4 identifies which calculation uses each column. Column J contains the sample number, which is available for tracking the results for any specific sample. This sheet is tested by inspection. As a test, the calculated mean for cells A5 through I2004 is 0.5005 and the median is 0.5017, both very close to the theoretical center of the distribution, 0.5.

Reactor F Sheet

Page 1 of this sheet is included and this page sheet describes the fraction of BWR fuel rods damaged during reactor operation that could be loaded into a WP. The complete sheet is described in Section 6.8, and listed as Attachment I and also contains information for PWR fuel rods.

WP-BU-A Sheet

This sheet contains the initial estimate of the PWR assemblies expected to be received at YMP from DTN: MO0001SPASRW41.001. The BWR deliveries were removed and the PWR deliveries were ordered by increasing BU. The number of assemblies in each group of BU (grouped in increments of 5 MWT/kgU) was then summed in Column A (the first value is in Row 67 but not shown in the page II-19 listing which only shows through Line 32). As a test, the sum of the groups was compared with the sum of the individual deliveries. The resulting BU distribution is given in Cells Q3 through T19 and used to generate Figure 2. This distribution is used to generate the 2000 samples of BU given in the sheet: "Burnup".

Table II-3. Listing of Top Rows of Sheet: Burnup

	A	B	C	D	E	F	G	H	I	J	K	L	M	N	O	P	Q	R
1	file = Rod-Initial-C.xls			**Sheet = Burnup**														
2	BU	BU range	Number assemb.		% of Tot	CCDF	BU											
3	2	BU 2-10	295	1770	0.24	100.00	2											
4	10	BU 10-15	1936	24200	1.55	99.76	12.5											
5	15	BU 15-20	6213	108727.5	4.98	98.21	17.5											
6	20	BU 20-25	3597	80932.5	2.88	93.23	22.5											
7	25	BU 25-30	7783	214032.5	6.24	90.35	27.5											
8	30	BU 30-35	13382	434915	10.73	84.11	32.5											
9	35	BU 35-40	18782	704325	15.05	73.38	37.5	median=										
10	40	BU 40-45	20873	887102.5	16.73	58.33	42.5	44.98946										
11	45	BU 45-50	19306	917035	15.47	41.60	47.5											
12	50	BU 50-55	15124	794010	12.12	26.13	52.5											
13	55	BU 55-60	9959	572642.5	7.98	14.00	57.5											
14	60	BU 60-65	6115	382187.5	4.90	6.02	62.5											
15	65	BU 65-70	1342	90585	1.08	1.12	67.5											
16	70	BU 70 - 75	54	3915	0.04	0.04	72.5											
17	75					0	75											
18		SUM	124761	5216380	100													
19			avg.+	41.81098														
20			**CCDF**	100	99.76355	98.21178	93.23186	90.34875	84.11042	73.38431	58.32993	41.59954	26.12515	14.00277	6.020311	1.118939	0.043283	0
21			**BU**	2	12.5	17.5	22.5	27.5	32.5	37.5	42.5	47.5	52.5	57.5	62.5	67.5	72.5	75
22																		
23	**Test of random calculation of burnup below**																	
24		**BU**	**rand #**															
25	median	44.72	50.90	tests of sheet below		Max bu=	72.50											
26	mean	44.12	50.44			min bu=	4.98											
27																		
28	**BU**	**Rand #**	Case num.															
29	53.70	23.21	1	0.00	0.00	0.00	0.00	0.00	0.00	0.00	0.00	0.00	53.70	0.00	0.00	0.00	0.00	
30	52.52	26.08	2	0.00	0.00	0.00	0.00	0.00	0.00	0.00	0.00	0.00	52.52	0.00	0.00	0.00	0.00	
31	41.56	61.16	3	0.00	0.00	0.00	0.00	0.00	0.00	41.56	0.00	0.00	0.00	0.00	0.00	0.00	0.00	
32	25.28	91.63	4	0.00	0.00	0.00	25.28	0.00	0.00	0.00	0.00	0.00	0.00	0.00	0.00	0.00	0.00	
33	51.15	30.32	5	0.00	0.00	0.00	0.00	0.00	0.00	0.00	0.00	51.15	0.00	0.00	0.00	0.00	0.00	
34	41.67	60.83	6	0.00	0.00	0.00	0.00	0.00	0.00	41.67	0.00	0.00	0.00	0.00	0.00	0.00	0.00	
35	44.22	52.56	7	0.00	0.00	0.00	0.00	0.00	0.00	0.00	44.22	0.00	0.00	0.00	0.00	0.00	0.00	
36	33.76	81.41	8	0.00	0.00	0.00	0.00	0.00	33.76	0.00	0.00	0.00	0.00	0.00	0.00	0.00	0.00	

Table II-4. Listing of Top Rows of Sheet: Corrosion

	A	B	C	D	E	F	G	H	I	J	K	L	M	N	O	P
1	file = Rod-Initial-C.xls			**Sheet = Corrosion**												
2	Corrosion during reactor operation						y = 0.81081*x									
3	Sheet = Corrosion						y = 2.7907*x -73.256									
4	Fit to Van Swam, 1997, Figure 8				y-y1 = slope*(x-x1)		**Range = -28um to +28um**									
5	Data for fit				low BU		**Maximum = 120 um**									
6	**BU**	**Peak Thickness**			y = (30/37) * x		**Maximum = 20 um above NRC limits**									
7	**MWd/kgU**	**um**			y = 0.81081*x		**Minimum = 0, no negative**									
8	0	0			High BU		Linear fit to Fig. 12									
9	37	30			y-30 = (120/43)*(x-37)		Pilling-Bedworth factor		1.75	from Literature				**Hydride absorption**		
10	80	150			y = 2.7907*x -73.256		below Calculations checks Pilling -Bedworth value									
11	**Test equation**	**Oxide thickness**	**Low BU**	**High BU**	**Single Equation**		Material	gm/cc	Atm. Wt	Mol/cc	ratio of moles	Calculated inverse		zr +2 h2o = zrO2 + 4H, 4 moles H per Zr n		
12	**BU**	**microns**	**microns**	**microns**	**microns**		Zr	6.56	91.2	0.07193	0.568736142	1.758285		Calculation per micron of oxide thickness		
13	0	0.00	0.00	-73.26	0.00		ZrO2	5.60	123.20	0.045455				metal loss,cm	5.71429E-05	
14	10	8.11	8.11	-45.35	8.11		90% ZrO2	5.04	123.20	0.040909	1cc			moles loss/cm2	4.11028E-06	
15	20	16.22	16.22	-17.44	16.22		0.90	5.06		0.04	0.571428571	1.75		Mole H/moleZr	4	
16	30	24.32	24.32	10.47	24.32									absorb fr.	0.15	
17	37	30.00	30.00	30.00	30.00									clad thickness,c	0.057	
18	40	38.37	32.43	38.37	38.37									H absorbed	2.46617E-06	
19	50	66.28	40.54	66.28	66.28		Min =	0.00		Min =	0.00			PPM H clad	6.595435958	
20	60	94.19	48.65	94.19	94.19		Max =	120.00		Max =	792.00			PPM per 1 micron oxide thickness		
21	70	122.09	56.76	122.09	122.09		mean=	54.23		mean=	357.91					
22	80	150.00	64.86	150.00	150.00		median=	52.04		median=	343.48					
23	90	177.91	72.97	177.91	177.91		5%-95%	5.28 to 112		5%-95%	35-738					
24	100	205.81	81.08	205.81	205.81											
25									Fig. 13,15	Fig. 13	Fig. 15					
26	**Sample #**	**BU**	**Oxide thickness**	**Before negative check**	**thickness with range**	**Uncertainty correction**	**median oxide thickness**	**PPM hydrogen**	**CCDF**	**ordered thickness**	**Ordered PPM hydrogen**					
27	1	53.70	81.25	81.25	81.25	4.65	76.61	535.91	100.00	0	0					
28	2	52.52	100.22	100.22	100.22	26.91	73.31	660.98	99.95	0	0					
29	3	41.56	54.18	54.18	54.18	11.45	42.73	357.37	99.90	0	0					
30	4	25.28	47.09	47.09	47.09	26.59	20.50	310.57	99.85	0	0					
31	5	51.15	65.63	65.63	65.63	-3.85	69.48	432.87	99.80	0	0					
32	6	41.67	30.08	30.08	30.08	-12.95	43.03	198.38	99.75	0	0					
33	7	44.22	34.08	34.08	34.08	-16.08	50.16	224.74	99.70	0	0					
34	8	33.76	52.90	52.90	52.90	25.52	27.37	348.88	99.65	0	0					
35	9	56.91	110.72	110.72	110.72	25.17	85.55	730.26	99.60	0	0					
36	10	43.86	69.94	69.94	69.94	20.80	49.14	461.27	99.55	0	0					
37	11	67.33	110.02	110.02	110.02	-4.62	114.63	725.62	99.50	0	0					

Table II-5. Listing of Top Rows of Sheet: Crack

	A	B	C	D	E	F	G	H	I	J	K	L	M	N
1	file = rod-initial-C.xls			**Sheet = Crack**										
2	Crack size distribution				stress=P*ID/[2*(Th-Ox-w)]									
3					Initial wall thickness=		571.5	(calculated, Free vol sheet)			**Note: CCDF for stress**			
4	F(w) = e^-B*w				KI=st*(w*pi)^0.5						**(boxed values) are used**			
5	Where w = crack depth				ID, cm =		0.83566				**in the total cladding**			
6	F(W) probability that crack is larger than w microns										**cladding abstraction AMR**			
7	B=	5.50E-02										**KI at 260C**	**Stress, 27C**	
8											"95%	0.0966732	23.21846	
9	Reverse equation, w = -ln(rand())/B										"5%	1.0781574	61.76155	
10											Max	2.6926	146.3432	
11	max=	1.19E+02			Max	1.5155	146.3432	17.5688			min	1.61E-03	1.56E+01	
12	min=	4.19E-04			min	9.08E-04	1.56E+01	2.06E+00			mean	0.4675	38.4179	
13	mean=	1.86E+01			mean	0.2631	38.4135	4.7561			median	0.3975	35.8445	
14	median=	1.30E+01			median	0.2237	35.8445	4.5074			Fig.17,18	Fig. 27	Fig. 18, 26	Fig.17
15	**Sample ID**	**Crack Depth, microns**		**Rand. Num**		**KI**	**Stress**	**Pressure**	**Wall thickness**		**CCDF**	**KI at 260C**	**Stress, 27C**	**Crack Length**
16	1	1.22E+01		0.511765		2.82E-01	45.65	5.60	5.13E+02		100.00	0.0016138	15.60166	0.0004187
17	2	4.59E+01		0.080065		7.55E-01	62.88	7.05	4.68E+02		99.95	0.0036567	16.84212	0.0007165
18	3	1.14E+01		0.532937		2.27E-01	37.88	4.80	5.29E+02		99.90	0.0054046	16.86978	0.002912
19	4	1.59E+01		0.417997		2.36E-01	33.40	4.23	5.29E+02		99.85	0.0123518	17.96101	0.0111781
20	5	2.55E+01		0.245376		3.20E-01	35.76	4.35	5.08E+02		99.80	0.0236145	18.09328	0.0371494
21	6	5.04E+00		0.758004		1.49E-01	37.57	4.94	5.49E+02		99.75	0.0237965	18.22731	0.0440847
22	7	1.67E+01		0.398187		2.55E-01	35.17	4.51	5.35E+02		99.70	0.0242072	18.55339	0.0552382
23	8	4.04E+01		0.108182		4.08E-01	36.16	4.33	5.01E+02		99.65	0.0247777	18.62807	0.0637964
24	9	2.69E+01		0.228251		3.29E-01	35.81	4.13	4.81E+02		99.60	0.025851	18.74939	0.0756253
25	10	1.55E+00		0.918156		8.79E-02	39.81	5.05	5.30E+02		99.55	0.0274925	18.75517	0.0763945
26	11	2.12E+01		0.311268		6.01E-01	73.58	8.58	4.87E+02		99.50	0.0324051	18.95559	0.076478

Table II-6. Listing of Top Rows of Sheet: Creep

	A	B	C	D	E	F	G	H	I	J	K	L	M	N
1		file = Rod-Initial-C.xls												
2		**Sheet = Creep**							R =	8.32E+00				
3								**Room Temp.**	**Strain**	**Strain**				
4								**Stress**	**Dry Storage**	**Trans.&dry stor.**				
5								Mpa	% strain	% strain				
6								30.00	0.114	0.115				
7								40.00	0.173	0.177				
8								50.00	0.250	0.258				
9								60.00	0.352	0.368				
10								70.00	0.490	0.521				
11								80.00	0.688	0.747				
12								90.00	0.993	1.105				
13								100.00	1.501	1.726				
14								105.00	1.882	2.202				
15								110.00	2.391	2.834				
16								**112.94**	2.769	**3.301**				
17								115.00	3.075	3.680				
18								**116.40**	**3.306**	3.965				
19								120.00	3.997	4.817				
20								125.00	5.243	6.354				
21								Above Table used for Fig. 25						
22								**Room Temp.**	**Strain**	**Strain**				
23								**Stress**	**Dry Storage**	**Trans.**				
24								**136**	**9.754**	**11.933**				
25		**Total Time, yrs**	**T,C**	Average Temp,K over inteval	Average Stress in Interval, Mpa	Interval Duration,hr	Total Creep, new method	Creep interval, new method	Sum of Primary Creep Components	Potential Prim. Creep, for interval	Actual Prim. Creep in Interval	Secondary Creep, Interval	Secondary Creep Rate, fract./hr	Saturated primary strain, esp
26		Yrs	C	K	Mpa	hrs	%	%	%	%	%	%	Es	%
27		0	350				0		0					
28		0.50	330	613.0	277.89	4.38E+03	7.07E+00	7.07E+00	6.48E-01	6.48E-01	6.48E-01	6.42E+00	1.47E-05	6.48E-01
29		1	322	599.0	271.55	4.38E+03	8.51E+00	1.44E+00	6.48E-01	5.49E-01	0.00E+00	1.44E+00	3.29E-06	5.50E-01
30		2	310	589.0	267.01	8.76E+03	9.47E+00	9.60E-01	6.48E-01	4.85E-01	0.00E+00	9.60E-01	1.10E-06	4.88E-01
31		3	295	575.5	260.89	8.76E+03	9.68E+00	2.08E-01	6.48E-01	3.74E-01	0.00E+00	2.08E-01	2.37E-07	4.13E-01
32		4	285	563.0	255.23	8.76E+03	9.73E+00	4.79E-02	6.48E-01	2.39E-01	0.00E+00	4.79E-02	5.47E-08	3.52E-01
33		6	270	550.5	249.56	1.75E+04	9.75E+00	2.09E-02	6.48E-01	1.58E-01	0.00E+00	2.09E-02	1.19E-08	2.98E-01
34		8	260	538.0	243.89	1.75E+04	9.75E+00	4.32E-03	6.48E-01	7.27E-02	0.00E+00	4.32E-03	2.47E-09	2.51E-01
35		10	252	529.0	239.81	1.75E+04	9.75E+00	1.34E-03	6.48E-01	3.82E-02	0.00E+00	1.34E-03	7.63E-10	2.21E-01
36		20.000	240	519.0	235.28	8.76E+04	**9.75E+00**	1.75E-03	6.48E-01	3.72E-02	0.00E+00	1.75E-03	1.99E-10	1.91E-01
37		20.0100	350	568.0	257.49	8.76E+01	9.76E+00	8.66E-04	6.48E-01	5.33E-02	0.00E+00	8.66E-04	9.89E-08	3.75E-01
38		20.0680	350	623.0	282.43	5.08E+02	1.19E+01	2.18E+00	7.25E-01	7.25E-01	7.73E-02	2.10E+00	4.13E-05	7.26E-01
39		20.07	112	504.0	228.48	1.75E+01	**1.19E+01**	4.28E-08	7.25E-01	1.63E-04	0.00E+00	4.28E-08	2.45E-11	1.52E-01
40														
41		**Time and Temperatures for Fig. 24**												
42														
43		**Test Calculation**				Checks with CRWMS M&O 2000a , P. Macheret								
44		**total Time, yrs**	**T,C**	Average Temp,K over inteval	Average Stress in Interval, Mpa	Interval Duration,hr	Total Creep, new method	Creep interval, new method	Sum of Primary Creep Components	Potential Prim. Creep, for interval	Actual Prim. Creep in Interval	Secondary Creep, Interval	Secondary Creep Rate, fract./hr	Saturated primary strain, esp
45		Yrs	C	K	Mpa	hrs	%	%	%	%	%	%	Es	%
46		0	360				0		0					
47		0.11	360	633	118.00	9.60E+02	3.80E-01	3.80E-01	3.24E-01	3.24E-01	3.24E-01	5.63E-02	5.86E-07	4.57E-01

Table II-7. Listing of Top Rows of Sheet: FGR (Fission Gas Release)

	A	B	C	D	E	F	G	H	I	J	K	L	M	N
1	file = Rod-Initial-C.xls		**sheet = FGR (fission Gas Release)**											
2	**Burnup**		**20**	**40**	**50**	**60**	**80**		*Column1*					
3	Garde 86, Fig 4		0.5	0.8	1	2								
4	Garde, Fig.4, High		1	3.3	3.8	4.5			Mean	4.201091				
5	Garde, 86, Table 4, avg of 12 tests				0.94				Standard Error	0.099986				
6	Manzet et al. 97, Fig 6-9		6	6.6	7.5	8.6	14		Median	3.078865				
7	Manzet, High			8	9	10			Mode	50				
8	Morel, 94, Fig. 4		0.3	0.8	1.8	3			Standard Deviation	4.471513				
9	VanSwam et al. Fig.9, Best est.			1	3	4.5	8		Sample Variance	19.99443				
10	VanSwam, High				3.2	5	9		Kurtosis	30.93212				
11	Bain et al.85, Fig 4			1.5	1.6				Skewness	4.623178				
12	Bain et al.High			3.4	3.8				Range	49.30436				
13	Median for CCDF		**1.69**	**2.14**	**2.98**	**4.53**	**11.00**		Minimum	0.695637				
14	Average highs			4.90	4.95	6.50			Maximum	50				
15	Avg. High/Median			2.29	1.66	1.44		1.80	Sum	8402.182				
16	Manaktala, 93, Fig.3-5, Maine Yankee		12 to15						Count	2000				
17									Largest(100)	10.84228				
18	ATM-101, p. 4.9 (10 pins)		.15-.27						Smallest(100)	1.091504				
19	ATM-103, p. 4.15		0.25 (30 MWd/kgU)						Confidence Level(95.0%)	0.196088				
20	ATM-104, p. 8.7			0.38, 0.62, 1.10										
21	ATM-106, p.2.1			1.4,7.4,11.2					Above supports Table 5 in AMR					
22														
23	Lanning et al. 97, Transients, Tbl. 2.1, 2.2		3.5-38	3.5-44	13-14.4	22-34								
24	Note, Above supports Table 3 in AMR													
25	**CCDF**	**FGR Multiplier**	**20**	**40**	**50**	**60**	**80**							
26	100	0.4	0.68	0.86	1.19	1.81	4.40							
27	50	1	1.69	2.14	2.98	4.53	11.00							
28	5	2.3	3.89	4.92	6.85	10.41	25.30							
29	1	6	10.14	12.84	17.88	27.15	50.00							
30	0.22	15	25.35	32.10	44.70	50.00	50.00							
31	0	15	25.35	32.10	44.70	50.00	50.00							
32	**Statistics on sampling below**			Above supports Table 4 in AMR										
33	Max FGR	50.00												
34	Min FGR	0.70												
35	Mean FGR	4.20												
36	Median FGR	3.08	**Uncert.**	100	50	5	1	0.22	0	**BU**	0	20	40	50
37			**FGR Mult.**	0.40	1.00	2.3	6	15	15	**FGR**	1.69	1.69	2.14	2.98
38	**BU**	**FGR**	rand, fg mult.						Uncertainty Multiplier					
39	53.70	3.48	51.6955585	0.98	0.00	0.00	0.00	0.00	0.98	3.55	0.00	0.00	0.00	3.55
40	52.52	19.17	1.33438015	0.00	0.00	5.69	0.00	0.00	5.69	3.37	0.00	0.00	0.00	3.37
41	41.56	3.84	26.0706672	0.00	1.69	0.00	0.00	0.00	1.69	2.27	0.00	0.00	2.27	0.00
42	25.28	0.85	94.2134709	0.47	0.00	0.00	0.00	0.00	0.47	1.81	0.00	1.81	0.00	0.00
43	51.15	2.65	63.3244255	0.84	0.00	0.00	0.00	0.00	0.84	3.16	0.00	0.00	0.00	3.16

Table II-8. Listing of Top Rows of Sheet: Free Volume

	A	B	C	D	E	F	G	H	I	J	K	L
1	file = Rod-Initial-C.xls		**Sheet = Free Vol.**									
2	**Free Volume for Fission Gasses**											
3	**CE 16X16 pin**						**Westinghouse W1717WL**					
4		inches	cm	areas,cm2	Volume,cc		inches	cm	areas,cm2	Volume,cc		
5	plenim in	9.527	24.199		13.515	plenim in	6.300	16.0020		8.777		
6	rod dia	0.382	0.970			rod dia	0.374	0.9500				
7	thickness	0.025	0.064			thickness	0.023	0.0572				
8	rod ID	0.332	0.843	0.559		rod ID	0.329	0.8357	0.548			
9	pellet dia	0.325	0.826	0.535		pellet dia	0.323	0.8192	0.527			
10	pellet dens	0.950				pellet dens	0.950					
11	rod length	161.000	408.940		228.399	rod length	151.600	385.0640		211.195		
12	fuel length	150.000	381.000		203.915	fuel length	144.000	365.7600		192.759		
13												
14	pore volume				10.196	pore volume				9.638		
15	rod-fuel vol.				34.679	rod-fuel vol.				28.074		
16	Calc. free vol				29.939	Calc. free vol				**23.334**		
17	published Free Vol				25.690	Estm. Free vol.				23.334		
18												
19												
20		cc/cu in=	16.390									
21		cu in	cc			**FV, cc = FV0 - (Uncer * (0.15*bu - 1))**						
22	spring Vol	0.236	3.868			**uncert range = 0.75 - 1.25**						
23	Alumina Vol	0.040	0.659									
24	end cap v	0.013	0.213									
25												
26				Initial Free Vol.=		**23.334**						
27	**Run Number**	**burnup**	**Free Volume**	**Uncert coef.**	**Rand Number**	**Vol. Loss**						
28	1	53.701	16.839	0.921	0.341	7.055201994		16.839				
29	2	52.519	17.055	0.913	0.326	6.877785683						
30	3	41.562	16.893	1.231	0.961	5.234254441						
31	4	25.278	20.045	1.178	0.856	2.791629898						
32	5	51.146	17.283	0.907	0.314	6.671916805						
33	6	41.668	17.116	1.184	0.869	5.250216088						
34	7	44.223	17.299	1.071	0.643	5.633465004						
35	8	33.760	20.041	0.810	0.121	4.064037143						
36	9	56.906	16.894	0.855	0.209	7.535845751						

Table II-9. Listing of Top Rows of Sheet: Helium (He) Pressure

	A	B	C	D	E	F	G	H	I	J
1	file = Rod-Initial-C.xls		**Sheet = He Pres.**							
2	Calculation of He pressure from Manaktala, 3-4									
3										
4	**Time, yrs**	**log10(time)**	**Log10(P)**	**Pressure, Mpa**		**Pressure at 100C**				
5	**(pionts used for fit)**	X	Y			**Early time period**				
6	1	0	-1.7	0.02		y-y1 = slope*(x-x1)				
7	1000	3	0.25	1.78		y+1.7 = (1.95/3) * (x)				
8	177827.941	5.25	1	10.00		y=0.65 * x -1.7				
9	**(test early time equation**					constant =	0.019953			
10	1	0	-1.7	0.02		**P(MPa) = 0.019953*time^0.65**				
11	10	1	-1.05	0.09						
12	100	2	-0.4	0.40		**Late time period**				
13	1000	3	0.25	1.78		y-y1 = slope*(x-x1)				
14	**Test converted equation, early time period**					y-0.25 = (0.75/2.25) * (x-3)				
15	1			0.02		y=0.3333 * x -1 +0.25				
16	10			0.09		y = 0.3333 * x -0.75				
17	100			0.40		constant=	0.177828			
18	1000			1.78		**P(MPa)=0.17783 time^0.3333**				
19	**Test converted equation, Late time period**									
20	1000			1.78						
21	10000			3.83						
22	177827.941			10.00						
23	500000			14.11						
24	1000000			17.78						
25										
26		Pressure Effect from Helium Production								
27	Time	Temp.	Helium Pressure	Fission Gas Pressure	Total Pressure	He % of total Pres.		P,He, 100C	temp, K	
28	yrs	C	MPa	MPa	MPa	%		MPa	T, k	
29	1	210	0.03	6.44	6.5	0.40		0.02	483	
30	10	240	0.12	6.84	7.0	1.76		0.09	513	
31	100	150	0.45	5.64	6.1	7.41		0.40	423	
32	1000	104	1.80	5.03	6.8	26.34		1.78	377	
33	10000	79	3.62	4.69	8.3	43.51		3.83	352	
34	100000	27	6.64	4.00	10.6	62.40		8.25	300	
35	1000000	27	14.30	4.00	18.3	78.15		17.78	300	
36		Above Table is reproduced as Table 7 in AMR								
37	Fission and fill gas pres. (27C) =			4	MPa	timee fct=	19.95262	4.641517583		
38			**Time=**	**100**	**Temperature=**	27		Tk=	300	
39	**Run Number**	**burnup**	**He Pressure**	**Rand. Num**	**He gas release fraction**	**He Max pres.**	**Press., time<1000**	**Press., time>1000**		
40	1	53.70	0.299126792	0.2525333	0.626267	0.477635	0.477635	0.990268148		
41	2	52.52	0.356676666	0.5271474	0.763574	0.467115	0.467115	0.968457432		
42	3	41.56	0.218984192	0.1847826	0.592391	0.369661	0.369661	0.766409533		
43	4	25.28	0.153191342	0.3627579	0.681379	0.224825	0.224825	0.466124911		

Table II-10. Listing of Top Rows of Sheet: Pressure

	A	B	C	D	E	F	G	H	I	J	K	L	M	N	O
1	file = Rod-Initial-C.xls		**Sheet = Pressure**												
2	Assumptions:														
3	temperature=	27	300			normally used 27 for room temp									
4	Time =	100													
5	rod Wt, kg =	1.76									*Statistics*				
6	free volume=	23.333966													
7	FVol = FVol0 – [Unc * (0.15 * BU – 1.0)]				unc = 0.75 - 1.25, uniform distrib						Mean	4.761098			
8	fill gas Pf(0)=2 to 3.5 MPa .			Pf(i) = Pf (0) * (FVol(0)/FVol(i)) * (Tk(i)/Tk(0))							Standard Error	0.033386			
9	fission gas pres= 31.0* BU * Mkg * 0.1MPa* Tk(i) * FGR / (FVol(i)*273oK) =										Median	4.512135			
10	PHe(MPa) = 1.4859E-6 * BU * Tk * HGR * t**0.65 ,HGR 0.5 - 1.0										Standard Deviation	1.493069			
11											Sample Variance	2.229254			
12											Kurtosis	10.00848			
13											Skewness	2.199956			
14											Range	15.50433			
15		Room Temp.									Minimum	2.064444			
16	5% value=	7.34	min=	2.06							Maximum	17.56877			
17	95% value=	3.03	maximum=	17.57							Count	2000			
18			Mean=	4.76							Confidence Level(95.0%)	0.065475			
19			Median=	4.51											
20	**Pressure CCDF, Ordered %**	**Ordered Pressure**	**Iteration Number**	**Random Total Pressure**	**Burnup**	**Free Volume**	**Fill Pressure**	**Fission Gas Pressure**	**FGR %**	**He Pressure**					
21	none	MPa	none	MPa	MWd/kgU	MPa	MPa	MPa	%	MPa					
22	100.00	2.06	1	5.60	53.70	16.84	4.64	0.67	3.48	0.30					
23	99.95	2.25	2	7.05	52.52	17.06	3.15	3.54	19.17	0.36					
24	99.90	2.28	3	4.80	41.56	16.89	4.01	0.57	3.84	0.22					
25	99.85	2.29	4	4.23	25.28	20.04	4.01	0.06	0.85	0.15					
26	99.80	2.35	5	4.35	51.15	17.28	3.64	0.47	2.65	0.24					
27	99.75	2.39	6	4.94	41.67	17.12	4.49	0.16	1.11	0.29					
28	99.70	2.41	7	4.51	44.22	17.30	3.83	0.32	2.06	0.36					
29	99.65	2.42	8	4.33	33.76	20.04	3.97	0.11	1.09	0.25					
30	99.60	2.42	9	4.13	56.91	16.89	3.19	0.47	2.32	0.47					
31	99.55	2.47	10	5.05	43.86	17.64	4.49	0.28	1.88	0.28					
32	99.50	2.47	11	8.58	67.33	13.97	4.65	3.58	12.38	0.35					
33	99.45	2.48	12	5.36	52.14	17.91	4.32	0.78	4.46	0.27					
34	99.40	2.49	13	5.56	56.14	15.64	3.85	1.38	6.40	0.33					
35	99.35	2.51	14	3.60	46.32	18.07	3.01	0.23	1.52	0.36					
36	99.30	2.52	15	4.17	52.47	16.95	3.60	0.27	1.45	0.30					

Table II-11. Listing of Top Rows of Sheet: P vs BU

	A	B	C	D	E	F	G	H	I	J	K	L	M	N	O	P	Q	R
1	file = Rod-Initial-C.xls			**Sheet = P vs BU**				Sheet for doing burnup studies										
2	Assumptions:					BU	min=	Median=	Mean=	max=								
3	temperatur	27	300		**Fixed BU =**	**45**	2.97	4.52	4.57	10.05								
4	Time =	100																
5	rod Wt, kg	1.76				BU	min=	Median=	Mean=	max=								
6	free volum	23.3				20	2.329419	3.322285	3.317787	5.05								
7						25	2.442418	3.505861	3.515321	5.69								
8						30	2.562607	3.724797	3.729535	6.44								
9						35	2.681852	3.952835	3.962492	7.3								
10						40	2.808487	4.19735	4.216616	8.3								
11						45	2.976284	4.522454	4.572838	10.05								
12						50	3.162785	4.89266	4.981752	12.18								
13						55	3.388929	5.378968	5.540326	15.77373								
14						60	3.62745	5.953015	6.187576	18.78717								
15						65	3.983298	6.872592	7.254082	21.17792								
16						70	4.391269	7.988242	8.519825	23.90417								
17						75	4.857681	9.287376	10.0175	27.97911								
18						Above table used to generate Figure 8													
19																		
20	Supports	Supports												**CCDF**	100	50	5	1
21	Fig.9	Fig.9												**FGR Mult.**	0.40	1.00	2.3	6
22	**Pressure CCDF,Ordered %**	**Ordered Pressure**	**Iteration Number**	**Random Total Pressure**	**Burnup**	**Free Volume**	**Fill Pressure**	**Fission Gas Pressure**	**FGR %**	**He Pressure**		**BU**	**FGR**	rand, fg mult.				
23	none	Mpa	none	Mpa	MWd/kgU	Mpa	Mpa	Mpa	%	Mpa,t<1000								
24	100.00	2.56	1	4.96	45.00	18.006	4.33	0.38	2.51	0.25		45.00	2.51	51.69556	0.98	0.00	0.00	0.00
25	99.95	2.57	2	5.46	45.00	18.051	2.97	2.18	14.57	0.31		45.00	14.57	1.33438	0.00	0.00	5.69	0.00
26	99.90	2.60	3	5.13	45.00	16.225	4.17	0.72	4.33	0.24		45.00	4.33	26.07067	0.00	1.69	0.00	0.00
27	99.85	2.60	4	5.32	45.00	16.525	4.86	0.20	1.20	0.27		45.00	1.20	94.21347	0.47	0.00	0.00	0.00
28	99.80	2.64	5	4.01	45.00	18.085	3.48	0.32	2.15	0.21		45.00	2.15	63.32443	0.84	0.00	0.00	0.00
29	99.75	2.64	6	5.17	45.00	16.490	4.65	0.20	1.24	0.31		45.00	1.24	92.89682	0.49	0.00	0.00	0.00
30	99.70	2.65	7	4.56	45.00	17.140	3.86	0.33	2.11	0.36		45.00	2.11	64.57911	0.83	0.00	0.00	0.00
31	99.65	2.66	8	4.80	45.00	18.640	4.27	0.20	1.40	0.33		45.00	1.40	87.80779	0.55	0.00	0.00	0.00
32	99.60	2.66	9	3.51	45.00	18.387	2.92	0.22	1.47	0.37		45.00	1.47	85.59152	0.57	0.00	0.00	0.00
33	99.55	2.66	10	5.13	45.00	17.430	4.54	0.30	1.95	0.28		45.00	1.95	69.74164	0.76	0.00	0.00	0.00
34	99.50	2.66	11	4.68	45.00	17.381	3.73	0.71	4.60	0.24		45.00	4.60	22.48041	0.00	1.80	0.00	0.00
35	99.45	2.67	12	4.85	45.00	18.732	4.12	0.50	3.45	0.23		45.00	3.45	38.03137	0.00	1.35	0.00	0.00
36	99.40	2.67	13	4.38	45.00	17.338	3.46	0.65	4.17	0.27		45.00	4.17	28.24521	0.00	1.63	0.00	0.00

Table II-12. Listing of Top Rows of Sheet: Rand # (Random Numbers)

	A	B	C	D	E	F	G	H	I	J	K	L
1	file = Rod-Initial-C.xls			**Sheet = Rand #**								
2	This sheet contains columns of random numbers used for the Fuel Rod Characteristics analysis.									colm.A-I	mean=	0.50050014
3	Each column is used for the calculation noted at the column title.										median=	0.50173504
4	**BU Distribution**	**FGR calc**	**Fill Gas**	**free Volume**	**He Prod.**	**Crack size**	**Corrosion**	**Currently not used**	**Currently not used**	**Sample Number**	**Currently not used**	**Currently not used**
5	0.232125157	0.516956	0.898514	0.341278	0.252533	0.511765	0.582965119	0.37240318	0.77488658	1	0.565084663	0.78631033
6	0.260801258	0.013344	0.202301	0.325831	0.527147	0.080065	0.980538513	0.48373579	0.82774386	2	0.15648822	0.47754253
7	0.611550437	0.260707	0.60249	0.961042	0.184783	0.532937	0.704543489	0.81473304	0.99782134	3	0.795878952	0.49776851
8	0.916302715	0.942135	0.962604	0.856405	0.362758	0.417997	0.974870855	0.90477177	0.6584557	4	0.642173886	0.04545676
9	0.303152686	0.633244	0.464965	0.313843	0.050209	0.245376	0.431324106	0.9023745	0.70773761	5	0.800444078	0.4164127
10	0.608346534	0.928968	0.860576	0.868715	0.571496	0.758004	0.268765571	0.10529044	0.14152265	6	0.531166899	0.69446287
11	0.525643003	0.645791	0.562003	0.642536	0.809432	0.398187	0.212828313	0.91182176	0.72942679	7	0.837232745	0.22376804
12	0.814069086	0.878078	0.942233	0.120734	0.667336	0.108182	0.955798478	0.71599068	0.9856944	8	0.14738858	0.52712922
13	0.154437886	0.855915	0.204424	0.209041	0.862437	0.228251	0.949497701	0.87503698	0.52781425	9	0.100435613	0.04112505
14	0.537888612	0.697416	0.931116	0.541668	0.418117	0.918156	0.871469996	0.73115366	0.60976681	10	0.347364541	0.24265717
15	0.012881751	0.224804	0.523471	0.558834	0.174458	0.311268	0.417584761	0.35965851	0.8771152	11	0.939072313	0.99203011
16	0.272310328	0.380314	0.877117	0.088857	0.152823	0.872308	0.021348231	0.82168924	0.66750946	12	0.327253479	0.37777374
17	0.173095511	0.282452	0.385406	0.57389	0.332895	0.299575	0.646073541	0.84965225	0.2390427	13	0.393850552	0.96886086
18	0.455396338	0.860426	0.220105	0.270136	0.729667	0.643266	0.809024737	0.14108519	0.46124934	14	0.471333072	0.04818858
19	0.262097141	0.974244	0.411747	0.358742	0.282369	0.384184	0.696891646	0.92398794	0.06452629	15	0.370052754	0.26801331
20	0.104180317	0.415629	0.817962	0.885715	0.273157	0.154268	0.381727211	0.741897	0.30450367	16	0.165100401	0.38071009
21	0.523601867	0.770218	0.7902	0.472109	0.191046	0.330107	0.383985213	0.28522275	0.92883351	17	0.519091341	0.06071762
22	0.03158437	0.814461	0.486774	0.96999	0.683511	0.071018	0.416643895	0.65097295	0.86390792	18	0.415849222	0.02720747
23	0.882318223	0.148933	0.428463	0.786398	0.801301	0.79784	0.850787752	0.40002438	0.00551764	19	0.354816725	0.84422599
24	0.884378554	0.140584	0.059966	0.288652	0.727938	0.848031	0.614564373	0.94495502	0.37977127	20	0.288672592	0.69688192
25	0.051703482	0.605217	0.459057	0.59192	0.056347	0.954266	0.779018729	0.05819852	0.62303705	21	0.431408755	0.2853294
26	0.201558558	0.772629	0.859033	0.338219	0.679984	0.080997	0.069327937	0.07808349	0.10231817	22	0.600412369	0.25408707
27	0.226445835	0.141331	0.059152	0.853156	0.680851	0.907389	0.927980456	0.3728456	0.73181565	23	0.847845512	0.52333128
28	0.617316359	0.474331	0.226888	0.000613	0.242927	0.373387	0.522875681	0.51087583	0.32657566	24	0.553833015	0.13433892
29	0.39518612	0.25315	0.135734	0.505745	0.398258	0.205293	0.907035329	0.80620056	0.2859785	25	0.742133094	0.16215567
30	0.476381941	0.622672	0.753326	0.573011	0.439503	0.925896	0.98266109	0.73717252	0.65731859	26	0.577850053	0.74609169
31	0.788442292	0.684409	0.262751	0.63772	0.094331	0.253119	0.599943162	0.12976159	0.49658064	27	0.674795496	0.60568817
32	0.553292172	0.835082	0.720968	0.003514	0.768129	0.329453	0.153764192	0.09845662	0.25189768	28	0.031788292	0.85233891
33	0.662464615	0.56007	0.257341	0.857962	0.114005	0.657153	0.656699504	0.0952495	0.95477894	29	0.343865873	0.52490913
34	0.168922185	0.294365	0.197952	0.122797	0.274607	0.762047	0.020318778	0.93145392	0.36470015	30	0.178207797	0.20720567
35	0.489717156	0.302747	0.641695	0.527485	0.612699	0.013991	0.951410515	0.88959781	0.13009656	31	0.66516201	0.8654367
36	0.970456976	0.746844	0.990076	0.555013	0.714524	0.854649	0.934491734	0.2150212	0.9123311	32	0.871176155	0.93143874

Table II-13. Listing of Top Rows of Sheet: Reactor F (Failure)

	A	B	C	D	E	F	G	H	I	J	K	L
1	file = Rod-Initial-C.xls, Sheet = Reactor F							file = Rod-Initial-C.xls			Sheet = Reactor F	
2	**BWR Data**											
3	**YEAR**	**BWR (Total discharged)**	**BWR, Assembly damaged**	**% Assembly Damaged/yr**	**% of Total assem damaged**	**RODS/ ASSEMB**	**Total Number Rods**	**Failed Rods**	**% FAILED Rods/yr.**	**Number of WPs/yr**	**% of Total BWR WPs**	**Source for Column C**
4	1969	96	32	33.33	0.05	49	4704	70.4	1.497	2.18	0.15	A
5	1970	29	29	100.00	0.04	49	1421	63.8	4.490	0.66	0.04	A
6	1971	413	87	21.07	0.13	49	20237	191.4	0.946	9.39	0.64	A
7	1972	801	68	8.49	0.10	49	39249	149.6	0.381	18.20	1.24	A
8	1973	564	323	57.27	0.50	49	27636	710.6	2.571	12.82	0.87	A
9	1974	1290	671	52.02	1.04	49	63210	1476.2	2.335	29.32	1.99	A
10	1975	1223	463	37.86	0.71	49	59927	1018.6	1.700	27.80	1.89	A
11	1976	1666	297	17.83	0.46	49	81634	653.4	0.800	37.86	2.57	A
12	1977	2047	108	5.28	0.17	56	114632	237.6	0.207	46.52	3.16	A
13	1978	2239	119	5.31	0.18	56	125384	261.8	0.209	50.89	3.46	A
14	1979	2131	124	5.82	0.19	56	119336	272.8	0.229	48.43	3.29	A
15	1980	3330	112	3.36	0.17	56	186480	246.4	0.132	75.68	5.14	A
16	1981	2467	42	1.70	0.06	62	152954	92.4	0.060	56.07	3.81	A
17	1982	1951	59	3.02	0.09	62	120962	129.8	0.107	44.34	3.01	A
18	1983	2698	26	0.96	0.04	62	167276	57.2	0.034	61.32	4.16	A
19	1984	2735	81	2.96	0.13	62	169570	178.2	0.105	62.16	4.22	A
20	1985	2928	99	3.38	0.15	62	181536	217.8	0.120	66.55	4.52	A
21	1986	2551	41	1.61	0.06	62	158162	90.2	0.057	57.98	3.94	B
22	1987	3316	24	0.72	0.04	62	205592	52.8	0.026	75.36	5.12	B
23	1988	2956	64	2.17	0.10	62	183272	140.8	0.077	67.18	4.56	B
24	1989	4020	57	1.42	0.09	62	249240	125.4	0.050	91.36	6.21	C
25	1990	3759	15	0.40	0.02	62	233058	33.0	0.014	85.43	5.80	C
26	1991	2872	24	0.84	0.04	62	178064	52.8	0.030	65.27	4.43	C
27	1992	4150	12	0.29	0.02	62	257300	26.4	0.010	94.32	6.41	C
28	1993	3974	16	0.40	0.02	62	246388	35.2	0.014	90.32	6.13	C
29	1994	3893	15	0.39	0.02	62	241366	33.0	0.014	88.48	6.01	C
30	1995	4684	4	0.09	0.01	62	290408	8.8	0.003	106.45	7.23	C
31												
32	sum	64783	3012		4.65		3878998	6626.4		1472.34	100.00	
33					% Rods failed, all years			0.170828				
34					% Rod failed through 1985			0.37				
35		A: Bailey and Wu 1990, Table 30, B: Potts and Proebste 1994, pTable 2, C: Yang 1997, Table 2										
36												

Table II-14. Listing of Top Rows of Sheet: WP-BU-A

	A	B	C	D	E	F	G	H	I	J	K	L	M	N	O	P	Q	R
1	file = Rod-Initial-C.xls			**Sheet = WP-BU-A**														
2																		
3	**Sum, each group**	**Burnup (MWD/MTU)**	**Assem**	**ID**	**Cask Load**	**RX Name**		**MTU**	**Enrich**	**Disch Yr**	**Fuel Type**	**Fuel Type**	**SS**	**MGR Arrival**	**MOX/UOX**	**MODE(T,R,C)**	**Bu Range**	**Numb. Assemblies**
4		2000	2	6878	2901	ST LUCIE 1		0.800	0.30	1994	1	PWR		2018	UOX	T		
5		2000	4	6878	2902	ST LUCIE 1		1.600	0.30	1994	1	PWR		2018	UOX	T	BU 70+	54
6	(first sum	2000	2	6878	2903	ST LUCIE 1		0.800	0.30	1994	1	PWR		2018	UOX	T	BU 2-10	295
7	row 67)	2769	1	603	5013	MAINE YANKEE		0.396	1.93	1975	1	PWR		2024	UOX	C	BU 65-70	1342
8		2769	1	600	5014	MAINE YANKEE		0.395	2.95	1975	1	PWR		2024	UOX	C	BU 10-15	1936
9		3713	2	501	112	INDIAN PT 1		0.350	4.36	1974	1	PWR	SS	2011	UOX	T	BU 20-25	3597
10		3713	4	501	113	INDIAN PT 1		0.701	4.36	1974	1	PWR	SS	2011	UOX	T	BU 60-65	6115
11		3713	2	501	114	INDIAN PT 1		0.350	4.36	1974	1	PWR	SS	2011	UOX	T	BU 15-20	6213
12		4239	4	495	128	INDIAN PT 1		0.701	4.36	1974	1	PWR	SS	2011	UOX	T	BU 25-30	7783
13		4239	4	495	129	INDIAN PT 1		0.701	4.36	1974	1	PWR	SS	2011	UOX	T	BU 55-60	9959
14		4244	1	429	3364	YANKEE-ROWE 1		0.238	3.70	1974	1	PWR		2019	UOX	C	BU 30-35	13382
15		4316	2	599	5014	MAINE YANKEE		0.791	1.93	1975	1	PWR		2024	UOX	C	BU 50-55	15124
16		4321	4	508	100	INDIAN PT 1		0.780	4.08	1974	1	PWR	SS	2011	UOX	T	BU 35-40	18782
17		4536	4	497	124	INDIAN PT 1		0.701	4.36	1974	1	PWR	SS	2011	UOX	T	BU 45-50	19306
18		4536	4	497	125	INDIAN PT 1		0.701	4.36	1974	1	PWR	SS	2011	UOX	T	BU 40-45	20873
19		5000	4	6211	1207	TROJAN		1.800	3.60	1992	1	PWR		2014	UOX	C	SUM	124761
20		5058	2	602	5013	MAINE YANKEE		0.772	1.93	1975	1	PWR		2024	UOX	C		
21		5139	1	790	1080	PALISADES		0.412	2.43	1975	1	PWR		2014	UOX	C		
22		5150	1	598	5014	MAINE YANKEE		0.380	1.93	1975	1	PWR		2024	UOX	C		
23		5856	4	47	63	WEST VALLEY (440		1.529	3.47	1971	1	PWR		2010	UOX	R		
24		5941	2	502	110	INDIAN PT 1		0.350	4.36	1974	1	PWR	SS	2011	UOX	T		
25		5941	4	502	111	INDIAN PT 1		0.700	4.36	1974	1	PWR	SS	2011	UOX	T		
26		5941	2	502	112	INDIAN PT 1		0.350	4.36	1974	1	PWR	SS	2011	UOX	T		
27		5980	2	498	123	INDIAN PT 1		0.399	2.83	1974	1	PWR	SS	2011	UOX	T		
28		6343	7	781	599	PALISADES		2.881	3.05	1975	1	PWR		2013	UOX	C		
29		6343	1	782	599	PALISADES		0.409	3.05	1975	1	PWR		2013	UOX	C		
30		6355	2	503	110	INDIAN PT 1		0.398	3.28	1974	1	PWR	SS	2011	UOX	T		
31		6522	2	437	5019	MAINE YANKEE		0.790	2.95	1974	1	PWR		2024	UOX	C		
32		7000	12	6197	2143	TROJAN		5.400	3.60	1992	1	PWR		2016	UOX	C		

Attachment III

NRC IRSR Issues Comparison

Background

Issues associated with the NRC IRSR, and its subsequent Revisions 1 and 2, have been compared to those of the cladding degradation issues addressed in this report, or in lower tier AMRs which form the basis of this assessment. General administrative methodology are addressed in the sections which immediately follow, while specific technical issues to be resolved are summarized in the final section of this attachment.

NRC Issue Resolution

Both expectations of the Commission and strategic planning activities by the NRC call for the early identification and resolution of licensing issues, prior to the receipt of a potential license application to construct a geologic repository. The objective is to reduce the number of and to better define the issues that may be in dispute. NRC regulations and a 1993 agreement between NRC and DOE expand on this initiative by allowing staff-level issue resolution to be achieved during the pre-licensing consultation period. Such resolution, however, would not preclude the issue being raised and considered during licensing proceedings.

Staff-Level Issue Resolution

To structure staff-level interactions, NRC has focused on the topics most critical to post-closure performance of the proposed geologic repository. At present, NRC staff has developed 10 Key Technical Issues (KTIs), nine of which (Table III-1) relate to post-closure performance assessment.

Table III-1. Key Technical Issues Related to Post-Closure Performance Assessment

Number	Issue
1	Total System Performance Assessment and Integration
2	Container Lifetime and Source Term
3	Evolution of the Near Field
4	Radionuclide Transport
5	Unsaturated and Saturated Flow Under Isothermal Conditions
6	Thermal Effects on Flow
7	Repository Design and Thermal Mechanical (TM) Effects
8	Structural Deformation and Seismicity
9	Igneous Activity

Each KTI is fully configured with sub-issues, sub-issue components, and acceptance criteria, thus facilitating the Issue Resolution Status Reports (IRSRs). An important part of the staff-level interaction process, the IRSR provides the primary mechanism that NRC staff will use to provide feedback to DOE.

Staff-level issue resolution is achieved during pre-licensing whenever the NRC staff has no further questions or comments regarding how the DOE program is addressing the issue. Furthermore, there may be some cases in which resolution at staff level may be limited to documenting a common understanding regarding differences in NRC and DOE technical positions.

Cross-Reference Between FEPS Related to Cladding Degradation and NRC Key Technical Issues

The following tables contain cross-references between NRC technical issues and the cladding degradation FEPS.

Table III-2 Cross-Reference Between FEPS Related to Cladding Degradation and Container Life and Source Terms Issues

CLST Sub-Issue	Acceptance Criteria	FEPs	
		Number	Title
3. The rate at which radionuclides in SNF are released from the EBS through the oxidation and dissolution of spent fuel	4. DOE has identified and considered likely processes for SNF degradation and the release of radionuclides from the EBS, as follows: dissolution of the irradiated UO2 matrix, with the consequent formation of secondary minerals and colloids; prompt release of radionuclides; degradation in the dry air environment; degradation and failure of fuel cladding; preferential dissolution of intermetallics in DOE SNF; and release of radionuclides from the WP emplacement drifts.	2.1.02.11.00	Waterlogged rods
		2.1.02.12.00	Cladding degradation before YMP receives it
		2.1.02.13.00	General corrosion of cladding
		2.1.02.14.00	Microbial corrosion (MIC) of cladding
		2.1.02.15.00	Acid corrosion of cladding from radiolysis
		2.1.02.16.00	Localized corrosion (pitting) of cladding
		2.1.02.17.00	Localized corrosion (crevice corrosion) of cladding
		2.1.02.18.00	High dissolved silica content of waters enhances corrosion of cladding
		2.1.02.19.00	Creep rupture of cladding
		2.1.02.20.00	Pressurization from He production causes cladding failure
		2.1.02.21.00	Stress corrosion cracking (SCC) of cladding
		2.1.02.22.00	Hydride embrittlement of cladding
		2.1.02.23.00	Cladding unzipping
		2.1.02.24.00	Mechanical failure of cladding

Table III-3 Cross-Reference Between FEPS Related to Cladding Degradation and Total System Performance Assessment and Integration Issues

TSPAI Sub-Issue	Acceptance Criteria	FEPs	
		Number	Title
4) Scenario Analysis			
1) Identification of an Initial Set of Processes and Events	Criterion T1: DOE has identified a comprehensive list of processes and events that: (1) are present or might occur in the Yucca Mountain region and (2) includes those processes and events that have the potential to influence repository performance.	2.1.02.11.00	Waterlogged rods
		2.1.02.12.00	Cladding degradation before YMP receives it
		2.1.02.13.00	General corrosion of cladding
		2.1.02.14.00	Microbial corrosion (MIC) of cladding
		2.1.02.15.00	Acid corrosion of cladding from radiolysis
		2.1.02.16.00	Localized corrosion (pitting) of cladding
		2.1.02.17.00	Localized corrosion (crevice corrosion) of cladding
		2.1.02.18.00	High dissolved silica content of waters enhances corrosion of cladding
		2.1.02.19.00	Creep rupture of cladding
		2.1.02.20.00	Pressurization from He production causes cladding failure
		2.1.02.21.00	Stress corrosion cracking (SCC) of cladding
		2.1.02.22.00	Hydride embrittlement of cladding
		2.1.02.23.00	Cladding unzipping
		2.1.02.24.00	Mechanical failure of cladding

Technical Issues Specific to the Effect of Cladding on the Release of Radionuclides

The following table contains a listing of specific technical issues addressed in Revision 2 of the NRC IRSR, for Container Life and Source Term (IRSR-CLST) dated September 1999, and the status of their resolution.

Table III –4
Resolution of IRSR-CLST Issues

Technical Issue	Resolution Status
Evaluate the processes of pitting corrosion and Stress Corrosion Cracking in the presence of oxidizing chloride solutions. Evaluate the effects on cladding integrity within the WC.	Pitting is addressed in F0035 SCC is addressed in F0155 Localized corrosion by fluorides addressed in F0155
Evaluate and assess creep rupture models and the validity of extrapolation to lower temperatures. Resolve issues relating to the DCCG model of creep.	Creep Rupture addressed in F0048 and F0155
Further qualify the DHC analysis with the use of a crack-size distribution in the cladding. Assess hydrogen embrittlement in the cladding as a function of cladding temperature and assess the possibility of hydride reorientation.	DHC is quantified in this AMR, F0048 and F0040 Hydride embrittlement is addressed in F0050 Hydride reorientation is addressed in F0040
Develop models for clad splitting for repository storage temperatures in dry air and aqueous environments.	Clad dry splitting is addressed in F0030 Wet splitting is addressed in F0025 and F0155
Assess the possibility of cladding mechanical failure during rock fall and seismic events using a fracture mechanics model.	Addressed in F0020 and F0155
Evaluate the damage introduced during reactor operation and deterioration during transportation and dry storage that may affect the behavior under disposal conditions.	Addressed in this AMR, F0048 and F0155